Transport measurements on NdCeCuO thin films

by

Andreas Kussmaul

Submitted to the Department of Physics
in partial fulfillment of the requirements for the degree of

Doctor of Philosophy

at the

MASSACHUSETTS INSTITUTE OF TECHNOLOGY

May 1992

Author .....
Department of Physics
May 4, 1992

Certified by .....
Marc A. Kastner
Professor, Department of Physics
Thesis Supervisor

Accepted by ....
George F. Koster
Chairman, Departmental Committee on Graduate Students

Transport measurements on NdCeCuO thin films

by

Andreas Kussmaul

Submitted to the Department of Physics
on May 4, 1992, in partial fulfillment of the
requirements for the degree of
Doctor of Philosophy

Abstract

This work describes the synthesis and the study of the transport properties of thin films of $Nd_{1.85}Ce_{.15}CuO_{4-\delta}$ carried out respectively at the IBM T. J. Watson Research Center in collaboration with Dr. A. Gupta, and at the Francis Bitter National Magnet Laboratory under the direction of Dr. P. M. Tedrow. The thin films were prepared by laser ablation of a stoichiometric target on heated substrates in a reactive ambient. The influence of the deposition parameters was studied, and the use of a nitreous oxide ambient was found to yield a clear improvement of the sample quality. The transport properties of the films were measured at low temperatures and in high magnetic fields. Non superconducting samples showed a strong, highly anisotropic, negative magnetoresistance that is consistent with two dimensional weak-localization. Superconducting samples show two dimensional fluctuation effects above T_c. The theory of fluctuations in a magnetic field was used to extract the position of H_{c2} (in the perpendicular direction) in the broad and almost featureless resistive transition, and the extracted values were fit to the theory of dirty superconductors. The angular dependence of the resistive transition was studied close to T_c and found to be somewhat better described by a two-dimensional model.

Thesis Supervisor: Marc A. Kastner
Title: Professor, Department of Physics

Acknowledgments

It is a pleasure to thank Paul Tedrow for his guidance through this four and a half year long journey. He was always available to give advice and encouragement, while leaving me enough freedom to pursue my own ideas and to learn how to become an independent researcher.

I am grateful to Jagadeesh Moodera, who was always willing to help and to give his time selflessly, and who has taught me most of the skills that I needed in order to carry out my experiments.

Working with Arunava Gupta has meant a lot to me. He showed me that film deposition is not just a trial and error process, but that working in a systematic and scientific way will be rewarded by the long-term results. His deep knowledge of materials science and his intuition have often helped when nothing seemed to work.

I would also like to express my appreciation for the work of the people who run the facilities that I needed to use: Joe Adario for X-ray diffraction, John Chervinsky and Grant Coleman for RBS, Chris Feild for the ac-susceptibility, and of course Larry Rubin, Bruce Brandt, Scott Hannahs, and their team at the high field facility. Mike Blaho and Dick MacNabb have provided our research group with reliable technical support. Brian Hussey did a great job in Arunava Gupta's lab, helping us to get things to work on many occasions.

I am forever endebted to my parents, who have made many sacrifices to give me the privilege of a good education, and who have always supported me in my endeavors. My fiancee Julita Pomorska also had an important role in this work: she brought romance into my workaholic life and helped me put things into perspective, for which I want to thank her. I further thank Jari Kinaret and Louis Marville for their friendship and for the many interesting conversations about physics and other important matters that we had over lunch or coffee. Rabia, Gordon and Cindy were around in the lab during most of the duration of my thesis research, and were always there to help me and to support me morally as well. Finally, I wish to express my gratitude to my roommates Jacques Demael, Olivier Herbelot, and Manfred Dahl, for

remaining good friends despite the mess that I sometimes (often, they claim) created.

I thank the AFOSR and especially the Consortium for Superconducting Electronics for the funding of the projects I worked on. I am grateful for the financial help from Groupe Saint-Gobain, without which I would not have been able to come to MIT.

Contents

List of Figures

List of Tables

Chapter 1

Introduction

1.1 About this thesis

The following thesis represents roughly four years of work on thin films of high-T_c superconductors. When I started in Spring 1988, a good year after the beginning of the era of high-T_c, very little was still known about film making: most groups, including ours, were still depositing at room-temperature and post-annealing their films. Laser ablation was just starting to become an established technique. It was also the era where any result could be published, and there was an abundance of often contradictory and irreproducible discoveries and recipes. Especially in the field of tunneling, any glitch in a dI/dV curve was used to yield a new and higher value of the energy gap. Today, the pace has become more reasonable, and systematic work has become fashionable again. It has become clear that many "discoveries" were in fact artefacts due to the low sample quality, and researchers have become more careful in the characterization of their samples. However, the problem remains that almost every measurement that one can think of has already been done a few times, but unfortunately on samples of unknown quality. Our goal was to carefully measure (and remeasure) transport properties of thin films of the electron-doped superconductor $Nd_{1.85}Ce_{.15}CuO_{4-\delta}$, which is an interesting compound for the study of the particle-hole symmetry in high-T_c superconductors. We have made an effort to make our own thin films by following the evolution of the preparation techniques, and to characterize

them with the tools that were available. The Consortium for Superconducting Electronics has helped us in this task by funding my numerous trips to Arunava Gupta's laboratory at the IBM T.J.Watson Research Center, where I learned the technique of laser ablation and made all of the $Nd_{1.85}Ce_{.15}CuO_{4-\delta}$ films used in the measurements. Our efforts to measure the superconducting properties in high magnetic fields were considerably slowed by the difficulty of producing good superconducting samples, and by the breadth of the resistive transitions in field, common to most high-T_c compounds. The former problem was solved by our discovery that the use of nitreous oxide during the deposition yields samples of higher quality, while the latter problem was tackled by carefully analysing the fluctuations in the conductance at the approach of the mean-field transition, and extracting in this way the value of the upper critical field. A major theme of this work is the two-dimensional character of the conduction, revealed by the analysis of weak-localization in the normal state, and later by the form of the fluctuation conductance above T_c. The fact that $Nd_{1.85}Ce_{.15}CuO_{4-\delta}$ apparently behaves like a 2D metal is probably the most interesting finding of this work.

The work is organized as follows: we will continue this first chapter with a short introduction to the superconductor $Nd_{1.85}Ce_{.15}CuO_{4-\delta}$ (which we will often call NCCO), since this compound is much less studied than $(La,Sr)_2CuO_4$ (LSCO), $YBa_2Cu_3O_7$ (YBCO) or the Bi-system (BSCCO in short). In the following chapter, we will discuss the thin film preparation and characterization, followed by a short chapter on the experimental methods used in our experiments. Chapter 4 starts the discussion of the transport measurements which constitute the heart of the thesis, and discusses two-dimensional weak localization effects first seen in non-superconducting samples. It is followed by a chapter on measurements above T_c, where the analysis of superconducting fluctuations above the critical temperature is addressed. The use of the fluctuations to extract the value of the critical field H_{c2} from the broad resistive transition is explained in the next chapter. The temperature dependence of H_{c2} is fitted to the theory of dirty superconductors. Chapter 7 is on a slightly different subject, namely the study of thin film tunnel junctions on high temperature superconductors.

Since we have been more succesful on Bi-Sr-Ca-Cu-O than on $Nd_{1.85}Ce_{.15}CuO_{4-\delta}$, most of the chapter is concerned with the Bi-compound. A recapitulation of our main findings will follow.

1.2 The compound $Nd_{1.85}Ce_{.15}CuO_{4-\delta}$

The compound $Nd_{1.85}Ce_{.15}CuO_{4-\delta}$ is just one member of a large family of superconducting copper oxides whose unusual properties have excited the physics community since the discovery of superconductivity in $(La,Sr)_2CuO_4$ by Müller and Bednorz in 1986. Other commonly studied members are Y-Ba-Cu-O, Bi-Sr-Ca-Cu-O (with many different phases), the Tl compounds, and the most recently discovered $SrCuO_2$. In this section, we will give a short description of the fundamental properties of these materials.

1.2.1 Crystal Structures

Figure 1-1 shows the crystal structures of some representative cuprates. $SrCuO_2$ has the simplest structure: simple square planar sheets of CuO_2 separated by simple cations. This compound can only be synthesized under high pressures and temperatures. Nd_2CuO_4, whose structure (called the T' structure) was discovered in 1977[61], is just slightly more complicated, the CuO_2 sheets being separated by layers of Nd-O. La_2CuO_4, although it has an almost identical formula, has a different structure, the T structure, where Cu is bound to 6 oxygen atoms: 4 in the plane and 2 so-called apical oxygen atoms out of the plane. The Y-Ba-Cu-O structure is called the T* structure; each Cu atom in the sheets is bound to 5 O atoms. Both the Bi and Tl compounds also have the T* structure. The study of these systems is complicated by the existence of many phases which contain the same elements with different stacking sequences in the c-direction (the direction perpendicular to the planes).

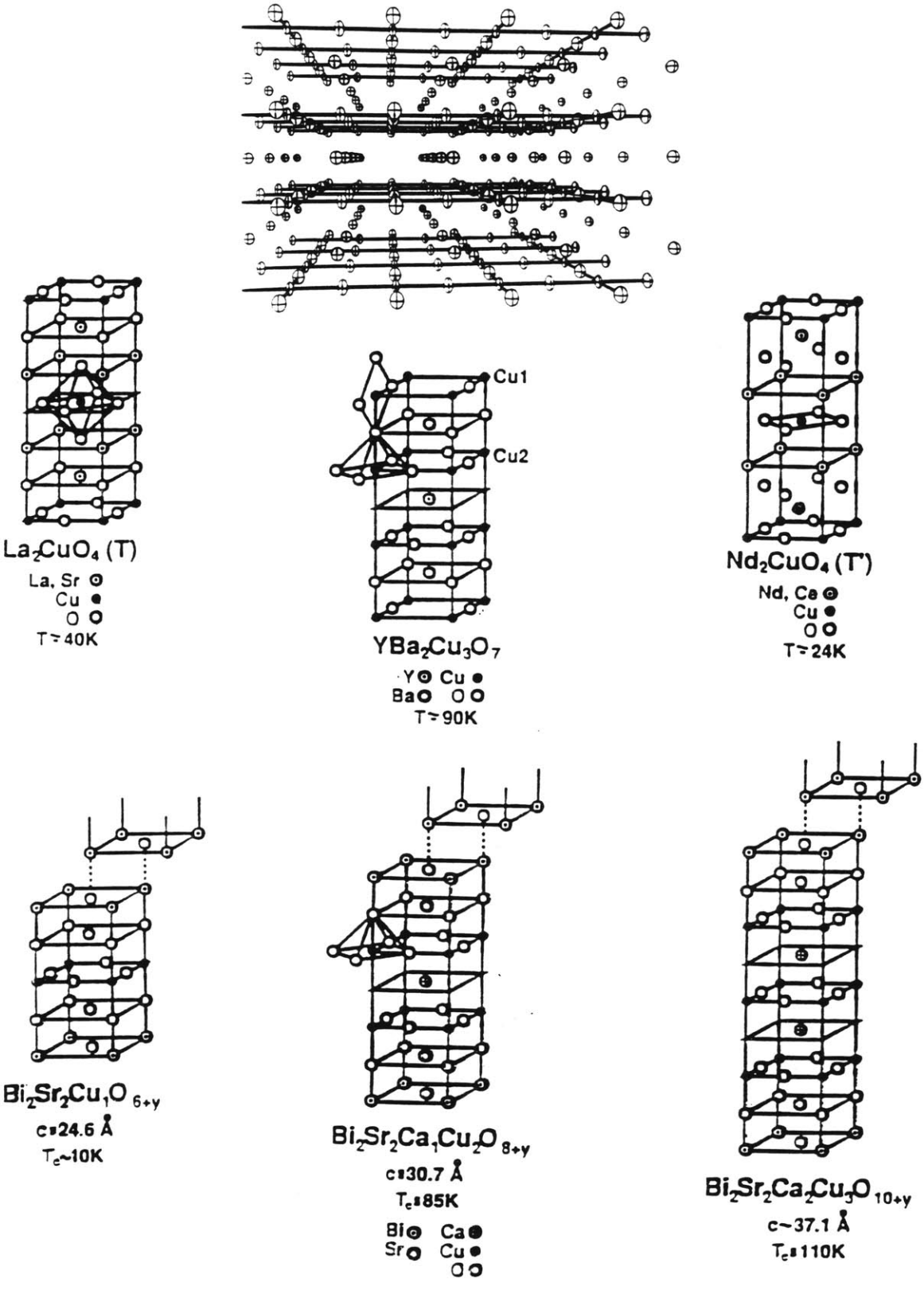

Figure 1-1: Crystal structures of some cuprates.

1.3 Doping and electronic properties

Müller and Bednorz found that one can dope the insulating parent compound La_2CuO_4 by substituting Sr for La, and it is now well known that for 15% Sr, one observes a superconducting transition around 40K. All the high T_c materials found to this day can be doped easily, and undergo an insulator-superconductor transition as the doping is varied; this can be achieved by cation substitution and/or oxygen stoichiometry changes. However, most of the high-T_c systems can only be doped with holes. No electron-doped cuprate superconductor was known until 1989, when Tokura, Takagi, and Uchida[89] announced the discovery of superconductivity in the system $(Nd,Ce)_2CuO_4$. The parent compound Nd_2CuO_4 is an antiferromagnetic insulator[52], as is La_2CuO_4. One can add electrons to the system by substituting Ce for Nd. One electron is available for each tetravalent Ce[1] substituted for the trivalent Nd. Reducing the compound at high temperature (T> 400°C) also has the result of making the compound more metallic. Removal of O-atoms liberates electrons that were bound in the O 2p shells. A negative Hall coefficient consistent with the formal valence was reported in the initial publication[89], but positive coefficients were seen as well by some groups; however, recent data on better samples[44] clearly show that the Hall coefficient is negative for superconducting samples, and only changes sign for over-doped crystals (17-18% Ce) . As one increases x in $Nd_{2-x}Ce_xCuO_4$, the antiferromagnetic fluctuations become weaker[52, 77], the conductance increases, and for x between .14 and .17, one observes a superconducting transition (T_c=23K), strongly peaked at about x=.15.

However, many questions still wait for a definite answer. For instance, it is not known why this compound can only be made superconducting in such a narrow range of Ce doping, and why one cannot compensate slight differences from the optimum Ce content by adjusting the oxygen concentration. It is also not clear whether the Ce is distributed randomly on Nd sites, or whether one has in fact a line compound

[1] Ce is known to have two possible valences, 3 or 4. However Ce and Th doping yield very similar properties [10]. Since Th only occurs in the 4+ state, one may conclude that Ce is also in the 4+ state when in the Nd_2CuO_4 lattice.

with an ordering of the substituted cations. Many other facts about the doping are puzzling when one starts to look into the details: into which states do the electrons go, and what happens to the lattice? The situation is made difficult by the fact that the reduction necessary to achieve superconductivity is usually very quickly followed by the irreversible decomposition of the samples[69], revealed by Cu loss or migration, and the appearance of foreign phases (usually $NdCeO_x$). One can observe some of these changes happen under an electron microscope when the electron beam heats up the sample[2]. When one adds the obvious observation that it is difficult to ensure a narrow Ce and O distribution through a macroscopic sample, one can doubt almost every experimental result obtained so far, and especially those obtained on reduced samples. Some groups found evidence for phase separation[38] except for 0% Ce and for 16.5% Ce, where the diamagnetic signal peaks. If this is true, there might not even be continuity from the antiferromagnetic phase to the superconducting phase. More work is clearly needed in the understanding of the crystal chemistry and synthesis of this compound.

Keeping in mind these caveats, let us now proceed to review some of the work done on the electronic structure.

1.3.1 Electronic structure

The simple theory of formal valence tells us that O is in the -II state, Nd is in the III state, and Cu is thus in the II state in Nd_2CuO_4 (same valence as in CuO). Thus one expects Cu to be in the Cu $3d^9$ configuration, and O to have full O 2p orbitals. Band structure calculations for Nd_2CuO_4 show that the important bands (those close to the Fermi surface) arise from the Cu and the planar O-orbitals. Guo *et al.*[31], using a linear muffin tin calculation with a local density approximation to include exchange and correlation effects, find that the Fermi energy E_F is close to the midpoint of a dispersive (i.e., itinerant) antibonding Cu-O_{planar} band. Upon Ce doping, electrons are predicted to enter this band, raising the Fermi level. They also note the appearance of Ce-like levels above the Fermi level, crossing it at higher doping. A band-structure calculation by Massidda *et al.*[56] (using a Full Potential

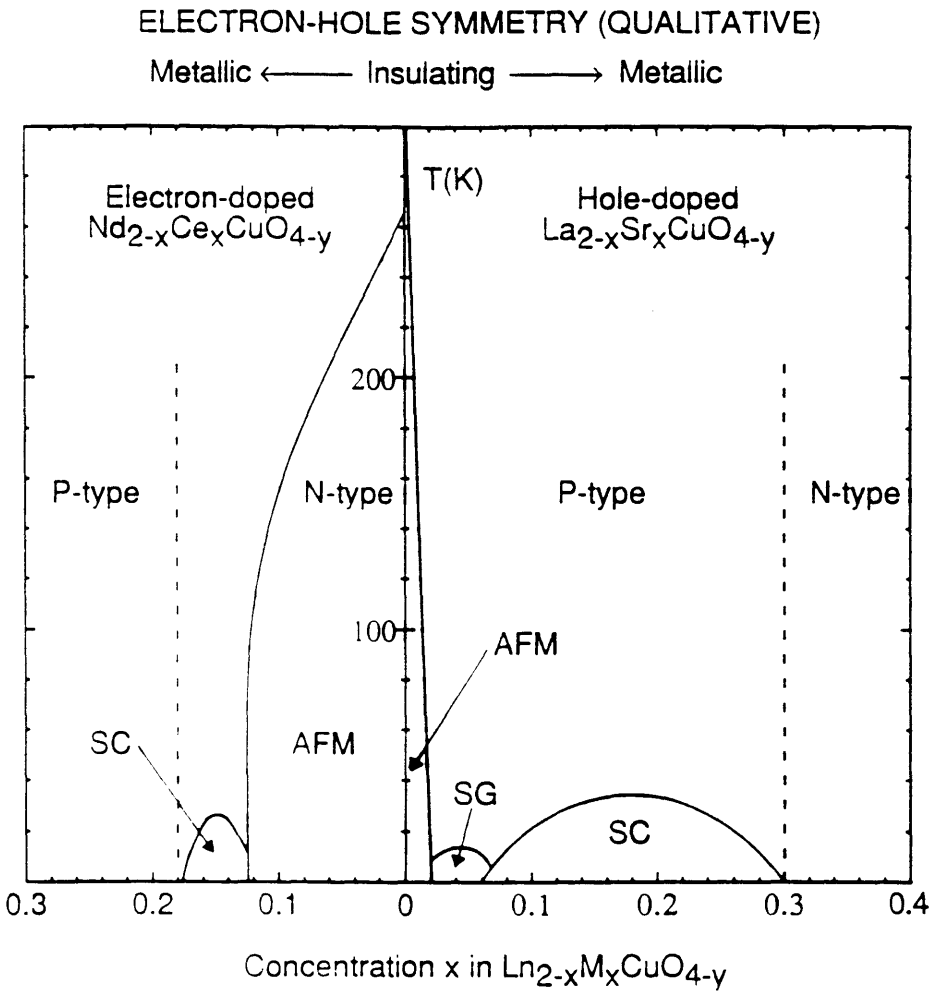

Figure 1-2: The observed properties of the hole-doped and electron-doped superconducting cuprates seem to be symmetric with respect to the AFM (antiferromagnetic) phase. SG stands for spin-glass, and SC for superconductor.

Augmented Plane Wave Method) arrives at similar conclusions, stressing the strongly two-dimensional character of the conduction bands and Fermi surface, which is in addition found to be nested, as in the case of La_2CuO_4, albeit in a different direction. The nesting should lead to a Peierls instability and to the opening of a semiconducting band.

An often discussed issue is the electron-hole symmetry, which is qualitatively observed in the phase-diagram of the electronic properties (figure 1-2); it has important implications for possible theories of high-T_c superconductivity. If the band picture

is right, one expects the electron and hole doped compounds to behave symmetrically, since the half-filled p-dσ conduction band has a natural symmetry for electrons and holes. There is, however, a problem: band structure by construction assumes independent electrons, and the only correlations included are due to the exchange interaction. But it is a fact that both $La_2CuO_4$and Nd_2CuO_4 are antiferromagnets, i.e., have a highly correlated ground state, so the band picture cannot really be expected to hold in the undoped case (though it might well apply in the doped case where the electrons are itinerant). An alternative way to describe the insulating state is the Mott-Hubbard model, where electrons are localized and highly correlated. In the simplest version of this model, one considers only the Cu $3d^9$ orbitals. Each orbital can accomodate zero, one or two electrons, but having two electrons costs an energy U because of the Coulomb repulsion. There is also a hopping probability from each site to neighboring sites, expressed by an overlap energy t. If t is much larger than U, one gets an itinerant band of width t; if U is very large, electrons are localized, and the band is split into two bands separated by U. The effect of t is to order the spins of the electrons. In the CuO superconductors, the planar-oxygen band has to be included (two band model), and its position is usually assumed to be between the two Hubbard bands. If one looks at the doping, one realizes that this model is not symmetric for electrons and holes: the latter go into the O 2p orbitals, while the former can only go on the Cu atoms. If this holds, and the electrons occupy the empty Cu 3d state in a correlated fashion, one should see some Cu(2+) change into Cu(+). So a detailed study of the electron-doped superconductors might be an important step in order to understand which theoretical model is relevant.

Quite a few experimental studies have been done, and the following is a brief review of some selected work. An important experimental technique to measure the electronic structure is photoemission spectroscopy (PES), where one shines photons of known frequency (in the UV or X-ray range) onto the material and analyzes the energy distribution of the emitted electrons (photoelectric effect). By comparison to spectra of known elements and compounds, one can deduce the ground state (or ionization) of the elements. Satellite peaks or small shifts in energy can give information on the

hybridization. A useful variation is resonant PES, where one studies the change in intensity of the features as one approaches a resonance in an elemental cross-section. If the intensity of the feature is strongly varying, one concludes that it is closely related to the atomic orbital that has the particular resonance (for instance, the Cu 3d-4s transition has a resonance at around 75 eV). A closely related technique is Inverse PES (IPES), which gives information on the addition of quasiparticles. A drawback of these methods is that they are surface sensitive, because the mean-free path of electrons out of the material is only a few tens of Å, so that one has to be careful about the state of the surface. Studies on $Nd_{1.85}Ce_{.15}CuO_{4-\delta}$[3] have shown that the valence band has clear Cu 3d character. There is a gap of about 2 eV, lower than the repulsive energy U of the one-band Hubbard model (due to on-site repulsion, or energy difference between Cu $3d^9$ and Cu $3d^8$), a clear indication that the O 2p band is important and leads to screening of the Cu holes through hybridization: instead of Cu $3d^8$ as the final state of the photoemission, one has a mixture of $Cu3d^9L^{-1}$ (L^{-1} represents a delocalized hole in the surrounding O 2p orbitals) and $Cu3d^{10}L^{-2}$ states. Upon doping, states start appearing in the gap at the Fermi surface[3], while the rest of the spectrum does not change much. The first published experiments had actually missed these Fermi surface states, probably due to a degraded surface (cf. the discussion by Vasquez[92] on surface preparation of our films). Remarkably enough, the main features, including the position of the Fermi edge between the two bands, are the same as in La_2CuO_4. The origin of these states is not well understood in the Hubbard model; band theory, on the other hand, agrees quite well with the general features revealed by an angle-resolved study of the Fermi surface[70], except that the observed dispersion of .2 eV is about a factor 10 too small. PES has also established that Ce is in the (4+) state[41], although there is some hybridization with O that gives a valence of about 3.5; but this is different from a mixed valence state where one has both Ce(3+) and Ce(4+) in the same crystal. It also seems that there is no Cu^+ appearing[26] with the introduction of electrons, as an analysis in terms of a simple Hubbard model would predict. Another common observation is that there is very little change in the spectra of Ce doped samples upon reducing. This strongly

suggests that the role of reduction is not just to bring in more carriers. Kohiki et al.[41], however, see a change in the relative intensities of two Cu $2p_{3/2}$ peaks that indicates an increase in covalency of the Cu-O bond. Of course, extreme caution is required when analyzing spectra of reduced samples because of the deterioration of the surface.

Thus, striking similarities are seen between the electron-doped and the hole-doped compounds. It seems that the band picture is more consistent with the data taken on carefully characterized samples. However, it is fair to say that the exact mechanism of the doping is not yet understood.

1.3.2 Resistivity: temperature dependence and anisotropy

As mentioned earlier, undoped samples are insulating; Ce doping and reduction of the oxygen content increases the metallic character. The resistivities of the best available crystals are on the order of 10-100$\mu\Omega$cm[35, 66]. Let us first talk about the in-plane resistance. In contrast with $YBa_2Cu_3O_7$ (YBCO from now on) or the Bi-Sr-Ca-Cu-O compounds (BSCCO), where the resistivity is linear in temperature for superconducting samples (until T_c is reached), $Nd_{1.85}Ce_{.15}CuO_{4-\delta}$ displays a quadratic temperature dependence[91]. This behavior is seen in single crystals as well as in thin films, and has not disappeared with the improvement of sample quality, a strong indication that it is an intrinsic phenemenon. One explanation for this unusual (that is, among high-T_c compounds) behavior is based on an enhancement of the electron-electron interactions (attractive or repulsive) due to the stronger anisotropy of the Fermi surface[91].

The conductivity in the c-direction has been measured by several groups. The results are quite inconsistent: while some groups[35] observe an anisotropy of 1000 at low temperature and a residual resistance below T_c, other groups observe a more isotropic behavior[66]. This is clearly related to sample quality. Some recent reports suggest that the high anisotropy results are right, but that the resistivity in the c-axis direction does go to zero below T_c, suggesting that there is transport between the layers. Altogether, it seems that $Nd_{1.85}Ce_{.15}CuO_{4-\delta}$ is not quite as anisotropic as

the Bi-compounds, but clearly more so than YBCO.

1.3.3 Conclusion

Little is known with certainty about $Nd_{1.85}Ce_{.15}CuO_{4-\delta}$. It is a difficult material to synthesize, and the poor availability of good samples has slowed down the exploration of its basic properties. But the material presents us with a few unique opportunities. It allows us to study the important question of electron-hole symmetry. The low T_c also makes it possible to measure the critical fields down to the lowest temperatures and to compare their temperature dependence to the theory. The longer coherence length in the ab plane (estimated to be around 70Å from the perpendicular critical fields[35]) makes $Nd_{1.85}Ce_{.15}CuO_{4-\delta}$ a potential candidate for tunnel structures, if one can learn to make structures in that direction. Thin films clearly have an important role to play in the exploration of these various directions. So let us turn now to our efforts to grow and characterize $Nd_{1.85}Ce_{.15}CuO_{4-\delta}$ films of high enough quality to be used for meaningful experiments.

Chapter 2

Thin film preparation and characterization

2.1 Why laser ablation?

There is an abundance of methods for thin film deposition that can roughly be divided into two categories: the physical processes (such as evaporation and sputtering) and the chemical processes (e.g., MOCVD and MBE). Evaporation and sputtering are the simplest of these methods, and require little equipment as well as easily obtainable starting materials (metals, or simple chemical compounds), which makes them very versatile. As a consequence, these two processes are the most widely used among research laboratories, and the initial efforts in high-T_c films in our group were carried out using these two approaches. The principle of evaporation is extremely simple: a starting compound, usually an element or a mixture of a few elements, is heated in a good vacuum (at least 10^{-6}Torr for a sufficient mean free path) until the vapor pressure is high enough to obtain a coating on a substrate facing the source at a distance of usually a few inches. Several problems make the use of this method difficult for the new superconductors: firstly, one usually needs several metallic targets because a single target combining several elements will emit fluxes of the various elements according to their equilibrium vapor pressures, and not according to the proportions in the target. Secondly, the best films are obtained by deposition on heated substrates

in a reactive environment (oxidizing), which is a serious limitation to the use of heated metallic targets (the oxides formed are usually much more difficult to evaporate). On the other hand, the use of several independent targets makes the control of the film stoichiometry more difficult.

Sputtering is the most popular deposition method in industry. Since it is the deposition method that I used for more than a year to produce BiSrCaCuO films, I will explain its advantages and drawbacks in more detail. The principle is the following: the target is attached to an electrode usually facing the substrates, and a negative bias of a few hundred volts is applied in the presence of a few mTorr of gas (typically Ar) between target and substrate. The gas is ionized into a plasma of electrons and Ar^+ ions. The positive ions are attracted to the target and impinge with considerable kinetic energy, causing some of the atoms in the target to be "knocked out" and to move towards the substrate. In the case of an insulating target, a positive charge will build up, until Ar ions are repelled and the process stops. To avoid this, one uses a rf-frequency bias between the target and the (grounded) substrates; because of the much higher mobility of the electrons, this will cause more negative charge to be built up in the positive cycle than can be cancelled in the nagative part, so that one has a negative dc-biasing superposed on the rf-signal after a very short time[17]. In the stationary state, Ar ions are attracted and the process goes on as in the dc-case. This technique allows the use of virtually any mixture of metals, oxides, carbonates and other compounds in the sputtering target and makes sputtering an extremely versatile technique. Unfortunately, the sputtering yields depend on the mass of the elements, so that the various elements are emitted with different probabilities. One makes up for this by presputtering for one or two hours: elements with high sputtering probability are depleted faster, so that in the stationary state one gets back more or less the right stoichiometry. In the case of high-T_c compounds, a further problem is the presence of oxygen in the target, which ionizes easily to O^- and hits the substrate with high energy due to the repulsion from the negatively charged target. This causes preferential resputtering of those atoms already deposited which have an atomic mass similar to oxygen, which a detrimental effect on both rate, stoichiometry

and smoothness. A solution to this problem was found by turning the substrate by 90 degrees, so that it is out of the direct path of the oxygen anions (and also of the other emitted species). If one then goes to higher pressures, many collisions will allow the particles to thermalize before reaching the target, i.e., they aquire an almost isotropic velocity distribution. This greatly inhibits the destructive effect of the oxygen and has allowed the deposition of films of extremely high quality of the different high-T_c materials[27]. But even the most fervent supporters of sputtering admit that although their best samples have excellent characteristics, many low quality samples come out as well without any obvious reason. We also have had to face the problem of irreproducibilities, and sometimes no good sample came out for several weeks. In a way, this is not too surprising since the transport of the elements from the target to the substrate is obviously a very complex problem and is poorly understood. Slight changes in geometry can affect the flow drastically, and change the distribution of species arriving at the substrate.

Although laser ablation (or pulsed laser deposition, PLD) had been around as a somewhat esoteric thin film deposition method since 1965[73], its potential was not recognized until 1987, when a group of researchers at Bellcore discovered that it allowed the deposition of very high quality films of YBCO, starting from a stoichiometric sintered target[20]. This was the starting point of a synergy which allowed fast progress in hi-T_c film deposition as well as in the field of laser ablation: the number of workers in the field has rapidly grown to several hundred in the world. Laser ablation has proved to be the method of choice for the deposition of complex compounds in reactive environments; it allows the faithful reproduction of the target stoichiometry, and the high energy of the impinging species (velocities of 10^6cm/s are reported[64]) promotes the reaction of the species and the formation of crystal structures. Furthermore, it is relatively simple to use: all one needs is a standard vacuum chamber with a window for the laser beam, and the laser itself. UV lasers with a few hundred mW power at a repetition rate of a few Hz (i.e., about 100 mJ per pulse) produce the best results, because of the high absorption of UV radiation in most compounds. The beam is focussed on the target (the spot size is about 1 mm^2), where it allows the

extremely fast heating of a small thickness of material. This is believed [4] to cause the formation of a molten layer and the quick emission of vapor. The resulting high pressure in the liquid and the recoil from the solid cause the subsequent emission of more material in mostly atomic form (ionic or neutral), constituting the plume. The plume absorbs part of the energy still coming in, so that the phenemenon becomes self limiting until the end of the pulse. However, a detailed model is not available, due to the complicated nature of the laser beam-solid interaction and the higher order interactions taking place in the plume. For a good overview of laser ablation and its applications, the reader is referred to [60].

Most of the development in laser deposition has thus been empirical. Above a certain laser fluence, the target stoichiometry is faithfully reproduced[73]. This is a clear indication that it is not an equilibrium process like evaporation, where the vapor pressures are important; rather, a certain thickness of material is simply blasted. This can only work if the power density per volume is above a certain threshold, which requires the use of high power pulses of short duration and at a wavelength where the penetration into the material is not deep (hence the use of UV for oxide targets; IR and visible light penetrates more deeply). The ablated material moves away in a so-called plume, a luminous cone-shaped plasma characterized by a highly peaked distribution $\cos^n(\theta)$, $8 < n < 12$[72]. Reaction of the ablated species with the ambient takes place during the expansion of the plume, forming metal-oxides[65], and this is important for the in-situ formation of the crystal structures of the various high-T_c compounds. A common problem of laser ablation is the splattering of molten material and the subsequent deposition of particulates on the film surface. Reducing the density of these particulates is an important outstanding problem, but for many applications (especially transport measurements), the presence of these particulates does not seem to pose great problems, since the underlying film is smooth and of high quality.

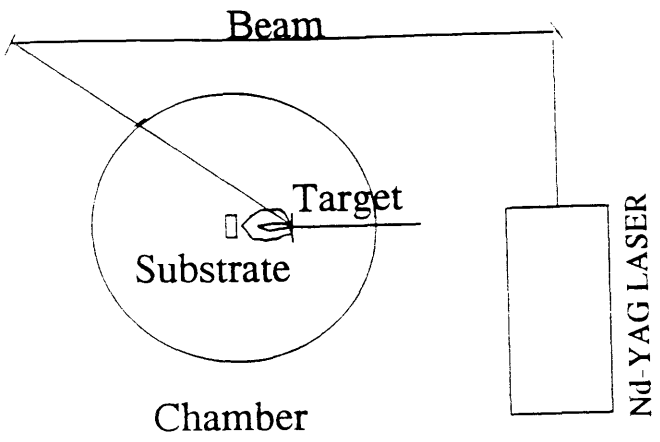

Figure 2-1: Laser Ablation set-up

2.2 Experimental techniques for film preparation

Shortly after the discovery of superconductivity in $Nd_{1.85}Ce_{.15}CuO_{4-\delta}$[89], superconducting thin films were prepared by laser ablation by G.Koren and A.Gupta[42]. Because of the ability to reliably reproduce the target stoichiometry, laser deposition is particularly adapted for $Nd_{1.85}Ce_{.15}CuO_{4-\delta}$, where the range of admissible Ce concentrations is extremely narrow. In our experimental setup (Figure 2-1) a Nd-YAG laser was used with a frequency tripling crystal, so that the beam was in the near UV-range (355nm). The power was between 350 and 500mW (measured before and after each run), the frequency was 4Hz, and the beam was focussed on the target to a spot of size $1mm^2$. The focussing lens was scanned in the vertical plane, making the point of impact describe a $6x6mm^2$ square for better uniformity on the substrate, and also to avoid drilling a hole into the target. It was recognized very early that one needed to deposit onto heated substrates to make high quality films. The elevated temperature allows the crystal structure to form as the material is deposited, causing epitaxial growth (ie, the film structure is a continuation of the substrate structure). Depositing on room-temperature substrates followed by ex-situ annealing produces

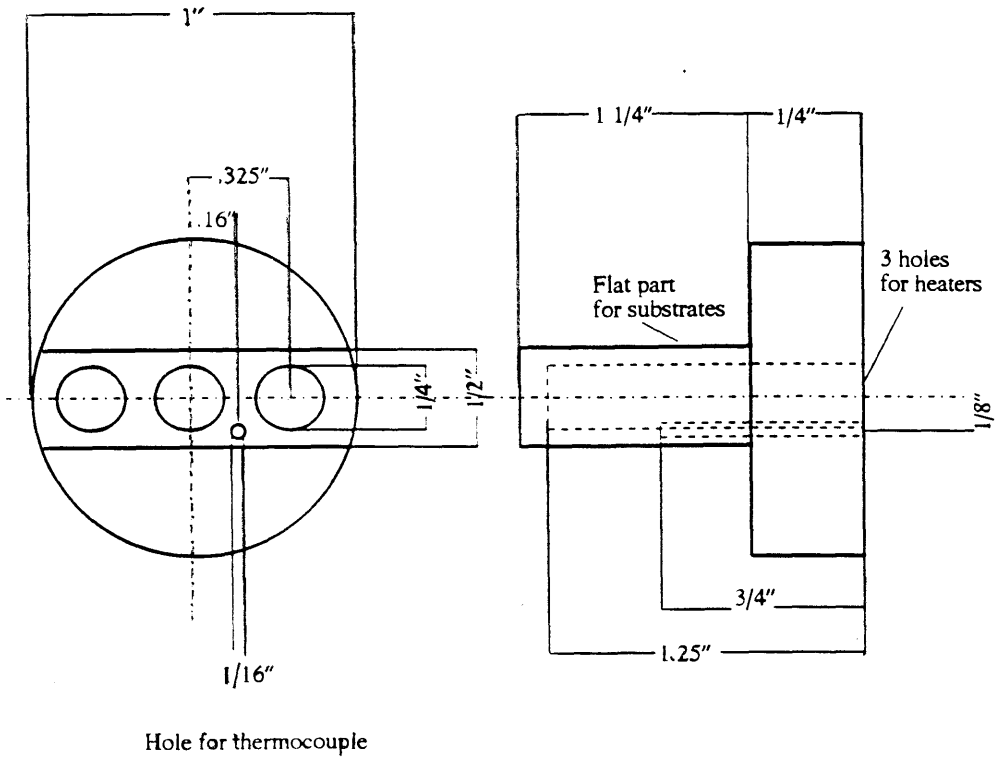

Figure 2-2: Simplified drawing of the substrate heater head. The welding grooves necessary to weld the head to a stainless tubing of wall size 20 mil were left out for simplicity. The three 1/4" holes contain the cartridge heaters.

films with c-axis orientation but with more disordered structure in the ab plane (granular structure). In fact, one would like to work at temperatures as high as possible to perfect the crystalline order; a limiting factor is the thermodynamic stability of the phase with respect to other phases and with respect to melting. Decomposition can only be avoided by having a minimum partial pressure of O_2 which was found to be a few hundred mTorr for most high-T_c compounds at temperatures around 750-800°C where the best films are made. The substrates were attached with silver-paint (Micro-circuits Co., diluted with ethanol) onto a home-made heater with an internal thermocouple (shown in Figure 2-2). Three 1/4" heaters (Chromalox) of nominal power 100W were fit snugly into the three cylindrical holes. This ensures a fairly uniform temperature over the upper half of the flat piece where the substrates are glued. For even better uniformity, it would be good to use a metal with high heat conductivity such as copper. But copper corrodes because of the high temperatures

and the oxydizing environment used in our experiment, so stainless steel with inferior thermal properties had to be used. The biggest question-mark is the real temperature of the substrate surface: attaching a thermocouple on the surface is difficult and contaminates the film. We tried using an infrared pyrometer, but the problem here is the transparency of the substrate in the IR, so that one measures mostly the heater surface, rather than the substrate; and even this temperature is difficult to calibrate because the emissivity of the stainless steal composing the heater is low and difficult to determine precisely. As a consequence, most groups involved in Hi-T_c film preparation have resorted to simply measuring the temperature inside the heater with an integrated thermocouple. The danger of measuring the temperature somewhere else than on the surface is that the "boundary conditions" (such as emissivity of the heater and substrate surfaces, heat conductivity of the heater, and, most of all, the thermal contact between the substrate and the heater) can change from run to run or over the long term. However, if one pays attention to the details explained below, this procedure appeared to yield reproducible results (this is not true for our work on BSCCO thin films where the exact control of the temperature to within 2°C is important). Some attention has to be given to the fact that the dilution of the silver paint changes with time because of the volatility of the organic solvents, so that it has to be carefully rediluted every few weeks. A first layer of paint was applied to both the backside of the substrate and the heater surface. After 10 minutes, a second layer was applied to both surfaces and the substrate was applied on the heater surface and pressed down with a clean Q-tip. At least an hour drying time was allowed before the heater was introduced into the chamber and heated first to 150°C; the chamber was then slowly pumped out and the substrates were heated to the deposition temperature (usually 820°C) in 40 minutes. The heater and the substrates have an intense red glow at this temperature. One then waits for the pressure to come down to the 10^{-6} range, and lets the laser warm up for 10 minutes. The gas used during the ablation (O_2 or N_2O in our experiments) is let in at this point, and one starts the pre-ablation of the target, i.e., the target surface is ablated while the substrates are turned away, so that no film is deposited. This is a cautionary procedure to remove

possible contaminants from the target surface (CO_2, H_2O). Then one starts the actual deposition: the focussed laser beam ablates the surface of the target, resulting in a large plume of ejected material. The target-substrate distance is fixed so that the tip of this plume barely touches the substrate. There was no thickness monitor present in-situ, but the number of pulses shot was recorded by a HP Universal Counter and used as a measure of the thickness. A certain number of samples were later analyzed by Rutherford Backscattering Spectroscopy (RBS), and it was found that the deposition rate was about 1/3 Å per pulse and fairly reproducible from run to run. After completion of the preset number of pulses (a few thousand), films can be either submitted to one or several annealing steps, or can be cooled down fairly quickly be simply shutting the substrate heater off. It takes less than 10 minutes for the internal thermocouple to go from 800 to 400°C, and 100°C is reached in about 25 minutes.

2.3 First work on NCCO

Films cooled down in an oxygen atmosphere were found to have semiconducting behavior at low temperatures: the resistance increases with decreasing temperature below about 150-200K. In order to get superconducting samples, it was found necessary to have the deposition followed by a vacuum-anneal at the deposition temperature. Vacuum anneals were tried at lower temperatures (400°C) but did not yield good samples in reasonable times. Indeed, the time necessary to yield superconducting samples depends strongly on the temperature and on the thickness, as discussed in the initial publication[42]. Figure 2.3 shows the change in the sample resistance vs temperature curve after a vacuum anneal of 30 minutes. As the annealing time is increased, the minimum in resistance is shifted to lower temperatures. After about 15-30 minutes, the resistive transition appears. For the right annealing time, a sharp resitive transition around 20K was observed. For longer times, the superconducting properties deteriorate again. It was observed fairly quickly that the vacuum anneal causes a decomposition at the film surface: Auger spectroscopy revealed a Cu-loss close to the surface. Work on single crystals done at the same time in C.C.Tsuei's

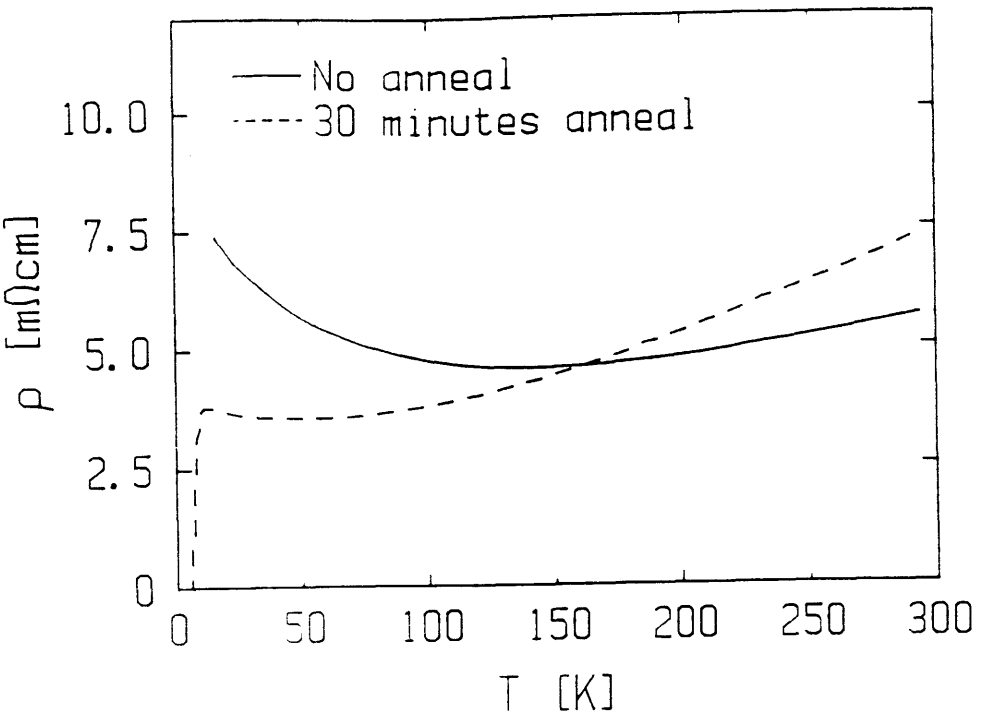

Figure 2-3: Comparison of R(T) for two samples deposited at 820°C in O_2, one as-deposited and one after 30 minutes vacuum anneal.

laboratory showed that after long annealing times at high temperature (the best transitions were seen after overnight anneals at 900°C), one could see a thin Cu coating on the cool parts of the furnace tube.

This was the state of the knowledge when our collaboration started.

2.4 Samples prepared in O_2 environment

The initial idea for my work at IBM was to optimize the vacuum annealing procedure for samples prepared in oxygen by G.Koren and A.Gupta's method, and then try to improve the method in order to produce samples with the right oxygen content as-deposited. One of the projects was to use very low oxygen pressure during deposition, and make up for the Cu loss by having a Cu-rich target.

Unfortunately, it turned out to be extremely difficult to reproduce the high T_c's obtained by my predecessors, presumably because of the very narrow window of tem-

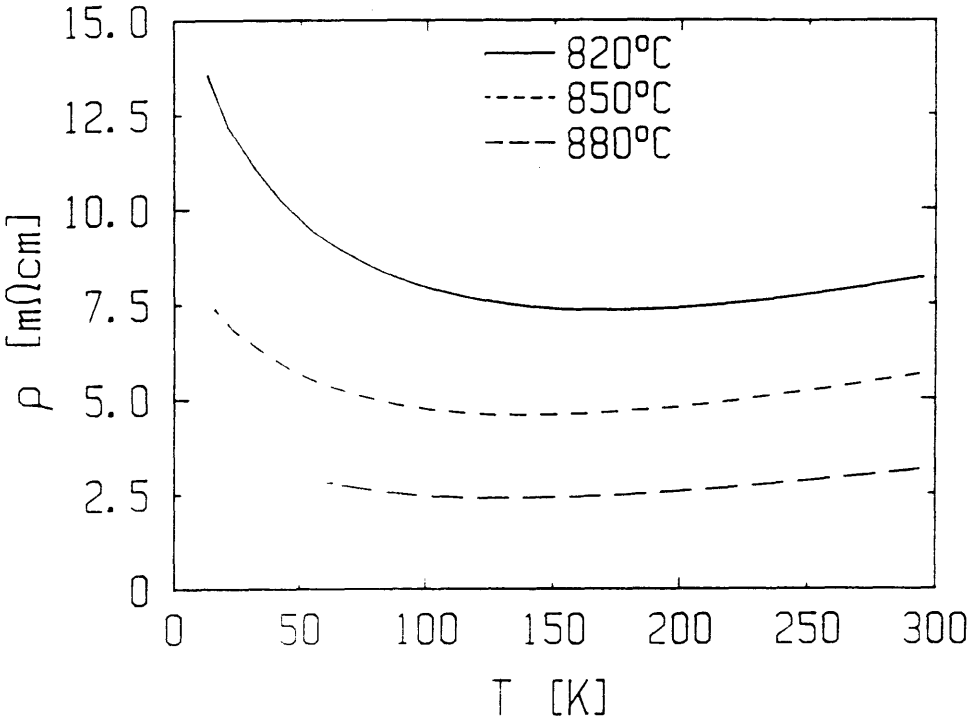

Figure 2-4: Influence of the deposition temperature on the sample resistance. The temperatures quoted are those read on the internal thermocouple; when we switched to a new heater, the same nominal temperature corresponded to a higher substrate temperature.

perature, thickness and time where the best samples could be obtained. After getting films with low or no T_c and having tried various thicknesses, we realized that we would have to do some very systematic work on non-annealed samples to understand what the problem was. We first noticed that the temperature where the metallic behavior of the resistance changed over to semiconducting (T_m) was a strong function of the deposition temperature, everything else being fixed (Figure 2-4). Films deposited at higher temperatures remained metallic down to lower temperatures. It seemed reasonable to assume that the more metallic the film was without anneal, the easier it would be to make it superconducting subsequently. We switched to a new heater that allowed somewhat higher temperatures, but films made at higher temperatures (850°C) and vacuum annealed did still not have good superconducting properties. The only parameter that had never been changed so far was the pressure during deposition, which was always kept at 150 mTorr, and we thus studied the influence of

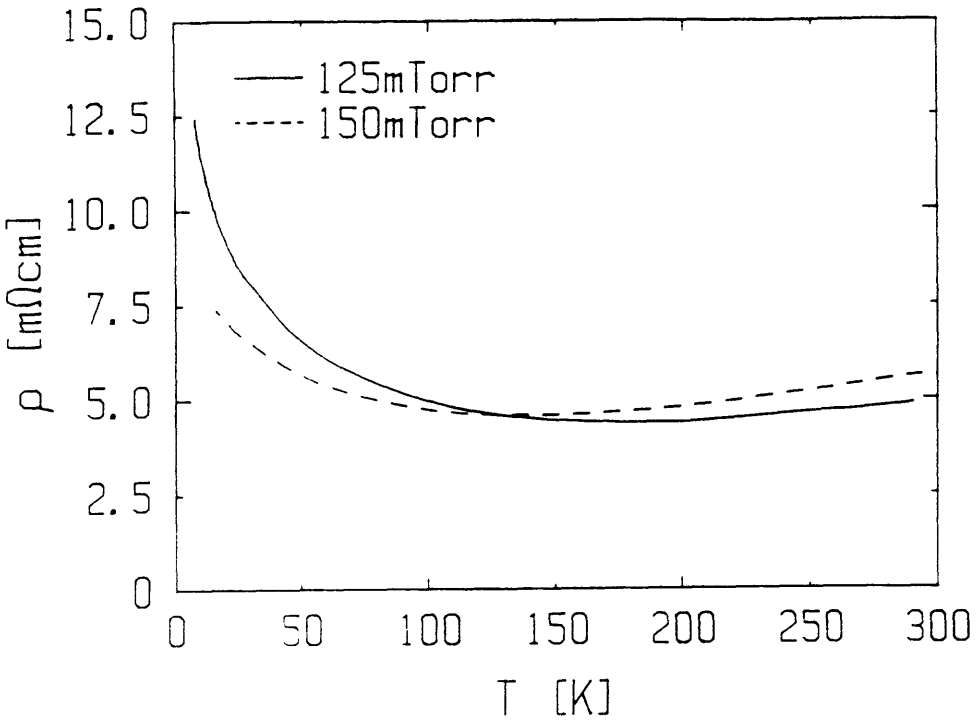

Figure 2-5: Two films deposited at 850°C at two different oxygen pressures. The number of pulses was the same (6000), and RBS showed that the thickness was the same for the two samples despite the slightly different pressure.

the oxygen pressure on the films. The surprising fact was that films made in 230 mTorr O_2 were more metallic than those prepared in 150 mTorr. In Figure 2-5, one can see that the minimum in resistance of the latter is at higher temperatures, and the resistivity is higher. Moreover, films made with higher oxygen pressure became superconducting after shorter vacuum-annealing times. This seems paradoxical since on the contrary, oxygen has to be removed to make the compound more metallic. The point is to realize that two quite different factors enter the resistance: the carrier density and the scattering time (i.e., the disorder). As we will see later, the semiconducting behavior at lower temperatures is also a disorder effect. The role of oxygen in this compound is twofold: it is a reaction product in the formation of the compound from the intial elements, but it also adjusts the carrier concentration (or mobility; this is not quite clear as described in the first chapter) in the final crystal structure. Thus, a lack of oxygen during formation might lead to a disordered crystal strucure,

with less metallic properties (higher resistivity, semiconducting behavior), and presumably degraded T_c. Samples prepared in 100 mTorr O_2 were even less metallic, and the annealing time necessary to see some kind of transition became longer. This indicated clearly that to get better quality samples, one actually needed to have more, and not less, oxygen in the system during the deposition. This recognition finally enabled us to make a film with a fairly good T_c (around 18K). How my predecessors got apparently good films in 150 mTorr is not clear; there might have been a slight difference in target composition (the Ce content was never systematically varied). Another possibility is a difference in laser power, or focus, that might have influenced the growth.

These systematic studies clearly indicate that the key to better films is to have higher oxygen pressure. This can be achieved either by actually increasing the pressure, which will eventually lead to a decrease in rate, or by using an activated source of oxygen. We have chosen the latter technique, which has proven successful[39, 43, 96] in producing good samples at lower temperatures for BSCCO and YBCO. Activated oxygen can be provided through the use of ozone (O_3), NO_2, N_2O, oxygen plasma or oxygen activated by ECR (electron cyclotron resonance). We decided to try N_2O, or nitreous oxide, commonly called laughing gas because of its relaxing effect at low concentrations, a welcome side-effect for stressed graduate students; the toxicity at higher doses should be kept in mind, however! This oxidizing agent had the advantage that we could use our system without any modification: both ozone and to a lesser extent NO_2 are dangerous to handle because of their corrosive and unstable character, and ECR and plasma techniques require special equipment.

2.5 Films made with N_2O

Using N_2O instead of O_2 has allowed us to improve the sample quality in a remarkable way. Furthermore, it has also enabled us to produce superconducting samples with sharp transitions as deposited, albeit with a lower transition temperature. The film preparation proceeds exactly as with oxygen, except that about 250 mTorr of N_2O

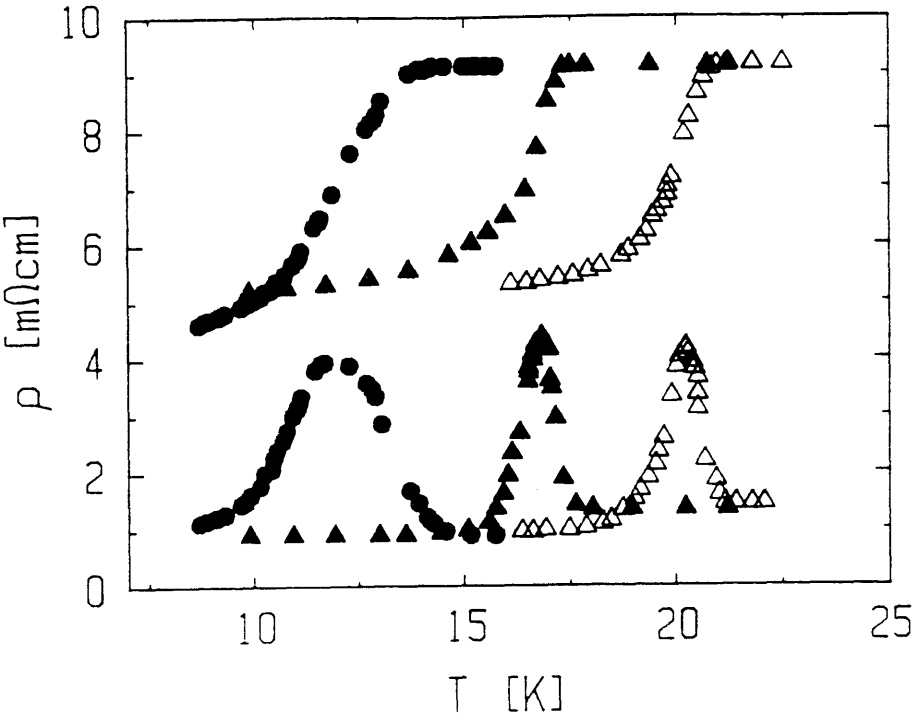

Figure 2-6: Ac-susceptibility traces of three samples. The upper curve is the inductive response, the lower curve the dissipation peak. From left to right, one sees a sample prepared in O_2 with 30 minutes vacuum anneal (circles), a sample prepared in N_2O without anneal (black triangles) and a sample prepared in N_2O followed by 30 minutes vacuum anneal (white triangles). The sample prepared in N_2O without anneal is superconducting at a higher temperature than the sample prepared in O_2 with 30 minutes vacuum anneal. Note also the sharpness of the transition for the non-annealed sample.

are let into the system instead of O_2. Samples are subsequently either cooled in N_2O or vacuum annealed. Figure 2-6 shows the ac-susceptibility traces of three samples: one of the best samples we were able to produce in O_2, one made in N_2O without vacuum anneal, and one made in N_2O with 30 minutes vacuum anneal. The improvement brought about by N_2O is clear. Figure 2-7 shows $R(T)$ of the vacuum annealed film. The best results were obtained for films 1500Å or thicker, which showed sharp transitions above 20K determined by ac-susceptibility. We made films up to 5000Å thick (15000 pulses) which showed sharp transitions above 20K after 30 minutes of vacuum anneal. But films thinner than 1000Å show lower resistive transitions. This could be due to a narrower time window for the annealing, or to the

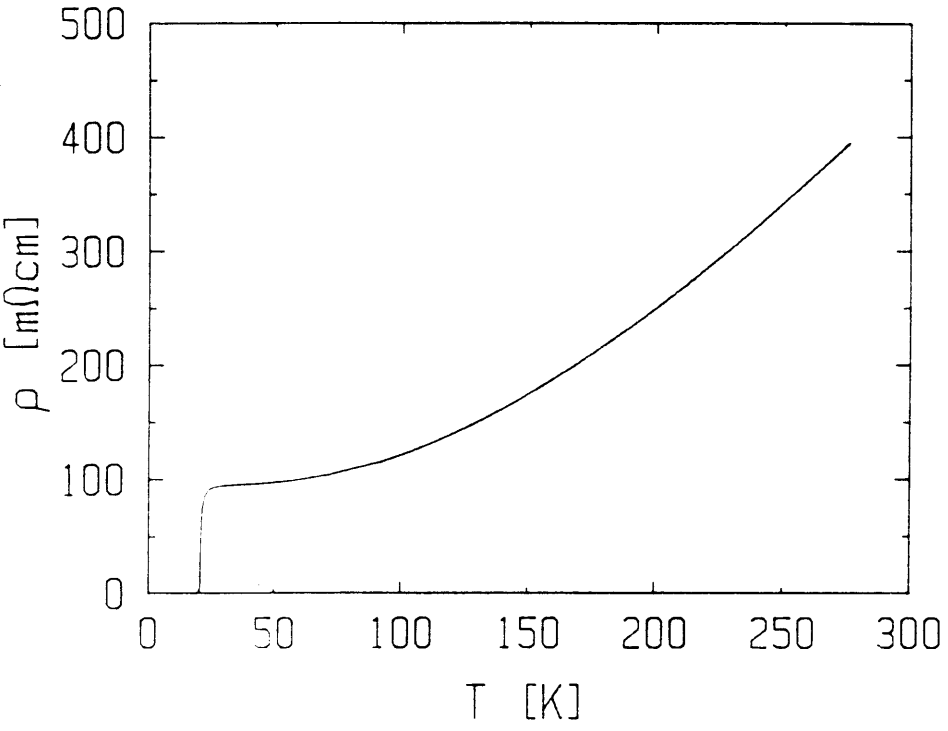

Figure 2-7: Resistance as a function of temperature for a vacuum annealed sample prepared in N_2O. Note the quadratic dependence above T_c and the high ratio (over 4) of the residual resistance to the room-temperature value.

decomposition at the surface that will obviously affect thinner samples more strongly. However, resistance measurements made during deposition suggest that the resistivity for samples thinner than 1000Å is already higher just after the deposition.

Before we turn to the discussion of film characterization, where more differences between films made in N_2O and those made in O_2 will be shown, let us try to understand the role of N_2O. Laughing gas has long been known to chemists as a powerful oxidizer under certain conditions. For instance, if one burns a metal powder in oxygen and then lets in nitreous oxide, the reaction will proceed even more violently. However, if the reaction is slow to start with, nitreous oxide will extinguish it[74]. This can be explained by the presence of a barrier in the oxidation reaction with N_2O. If this barrier is overcome, the reaction will eventually be more exothermic, but in equilibrium, N_2O will have a lower activity (equivalent partial pressure of O_2). During the formation reaction, where activated species with high kinetic energy are present in the plume, it will be a powerful oxidizer. This is consistent with our observation of high crystalline quality (cf. also channeling data below), a proof that there is enough oxygen provided during the reaction. The fact that the samples have a lower oxygen content (they are superconducting as cooled down) is consistent with less oxygen diffusion, or possibly some loss, at subsequent times. We also noted that the plume is bigger and more intense when N_2O was used instead of O_2, indicating an enhanced reaction between the ablated species and the gas environment. These observations clearly suggest that oxygen has a kinetic rather than a thermodynamic (equilibrium) role in the formation of the crystal structure with the process of laser ablation. It is well known, also for other high T_c systems, that once the right phase is formed, it is stable under much lower oxygen pressures (around 10 mTorr should be enough), indicating that the equilibrium properties are not the limiting factor here. Two samples were prepared in a mixture of O_2 and N_2O, one with anneal, one without. The as-deposited sample was not superconducting, as expected. The sample annealed for 30 minutes was superconducting, but with a low T_c and a broad transition. This is a likely indication that diffusion of higher amounts of oxygen into the sample make it difficult to withdraw it later through vacuum annealing.

2.6 Sample characterization

We will now look in more detail at some of the characterization techniques already mentioned earlier.

2.6.1 Resistive Measurements

The resistance as a function of temperature is an important measurement that was carried out on every single film made. It does not only give the T_c of superconducting samples, it also allows to tell how far one is from obtaining superconductivity (by the position of T_m, cf. above). The resistance is always measured by a 4-terminal method which is the only way to eliminate the contact resistance. A large number of samples was patterned with a laser-patterning setup, which allows the fabrication of a 200x30 μm^2 bridge in a few minutes and thus an easy determination of the resistivity (Figure 2-8). The resistance measurement rig used at IBM comprised a flowing gas ^4He cryostat and a sample holder with a thermal diode. The data acquisition was done automatically by a computer program (property of IBM). Room-temperature resistivities of superconducting or near-superconducting samples were of the order of a few hundred $\mu\Omega cm$, with films made in N_2O having a lower resistivity than those made in oxygen. Bridge measurements and macroscopic Van der Pauw measurements yielded values that could be quite different (factors 2 to 5) for the same sample, probably due to inhomogeneities. Samples made on MgO, $LaAlO_3$ and $NdGaO_3$ showed much lower resistances than films on $SrTiO_3$ when measured without patterning (factor 10 lower), but bridge measurements do not show such a large difference. This illustrates the difficulty of measuring the intrinsic resistivity of the samples, which causes some problems when we discuss weak localization and fluctuation effects, where one needs to know the resistivity accurately. For these latter measurements, we have used a more conventional pattern (Fig.3-1).

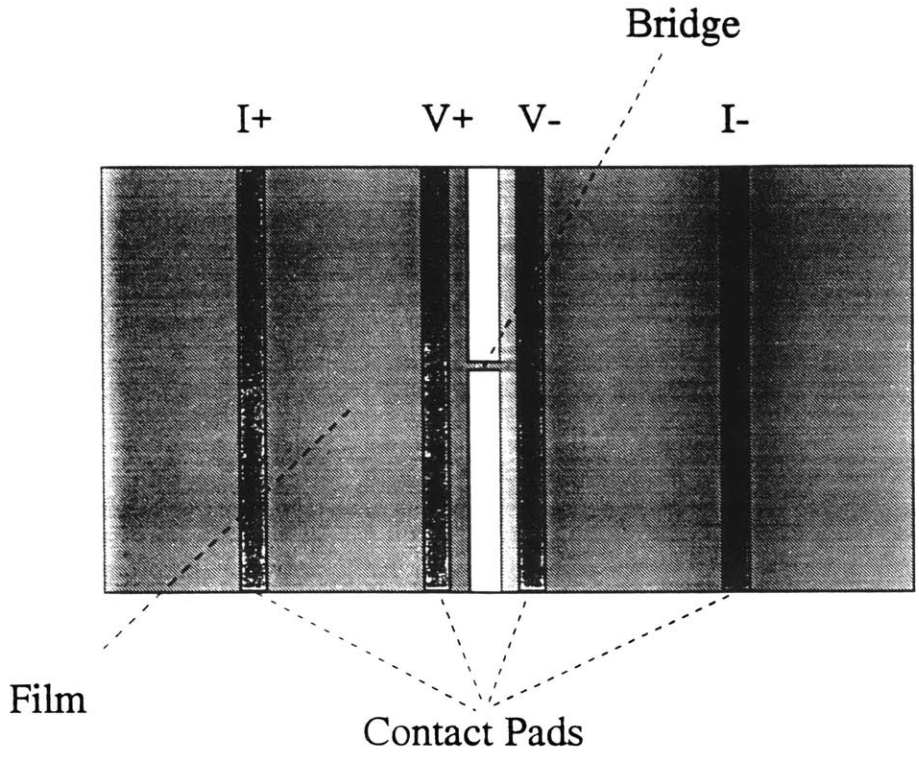

Figure 2-8: Laser-patterned bridge and contact geometry used for the resistivity determination. The bridge was usually $200\mu m$ long and 30 to 60 μm wide. The most important part of the 4-terminal resistance measured through the contacts comes from the bridge, but spreading resistance effects should be taken into account. This method is mainly used as a quick check of the resistivity of films prepared under different conditions.

2.6.2 ac-susceptibility

In the setup used at IBM, put together by Dr. T. Worthington, the sample is attached on top of a coil of diameter 1mm and slowly cooled through the superconducting transition. The resistance and reactance of the coil are recorded as a function of temperature for a frequency of 20MHz. When the sample goes superconducting, the magnetic field lines going through the coil can no longer go through the sample, and this strongly modifies the self-inductance of the coil. In the temperature region close to T_c, where the field produced at the sample surface by the coil is higher than H_{c1}, vortices can form and cause dissipation, detected as a peak in the resistance. The high frequency allows a high enough sensitivity (the signal goes as $L\omega$) to do the measurement with a single coil. One can work in the kHz range if one uses the mutual inductance of two coils with the sample inserted between the two, and two supplementary coils wound in such a way as to cancel the signal in the absence of the sample. The latter method is clearly more complicated. The ac-susceptibility technique has been extensively used to study the penetration depth, i.e., the density of superconducting electrons, and the vortex dynamics in the superconducting phase (through the temperature and field dependence of the dissipation peak). We used it mainly to complement the simple resistive measurement of the transition. It is a more stringent test of sample quality than the resistance: in three dimensions, it is enough to have 15% of the sample superconducting to form a percolating path and completely short the resistance; for the ac-susceptibility, one needs to exclude the flux, which requires superconducting material to cover each part of the coil surface, even though the whole thickness need not be superconducting. We already showed a comparison of the ac-susceptibility of samples made in O_2 and N_2O.

2.6.3 X-ray diffraction

X-ray diffraction is a simple and powerful tool to analyze periodic spatial structures. The elastic scattering of X-rays from the atoms arranged in a periodic array produces an interference pattern that is constructive in a discrete number of spatial directions.

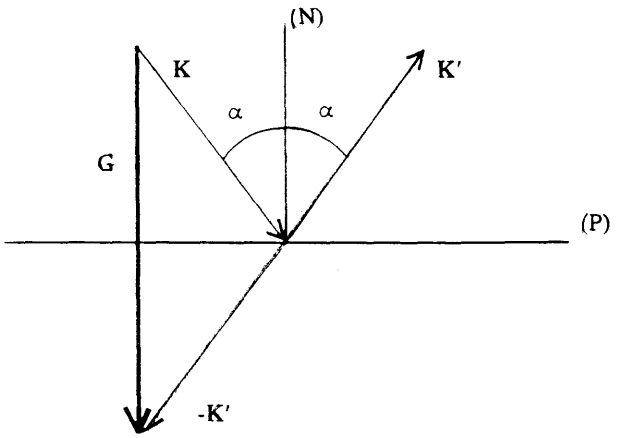

Figure 2-9: Geometry of the $\theta - 2\theta$ scan used to analyze our samples. **K** and (**K'**) are the incoming and outgoing wavevectors respectively, and the Bragg relation is satisfied when there exists a reciprocal lattice vector **G** equal to **K-K'**. Because of the geometrical constraint between the beam, the sample plane and the detector, one can only see planes families parallel to (**P**), the sample holder plane. The angle α shown is the complement of the angle θ used in the Bragg relation. It is important to realise that one only looks for families of planes parallel to the plane (P). A single crystal with a different orientation will in general give no signal.

These directions are points of the reciprocal lattice, and the knowledge of the reciprocal lattice gives important information on the initial lattice. Unfortunately, the transformation is not one-to-one, and the reconstruction of the crystal structure in three dimensions is an extremely difficult problem; so one usually needs to have some idea of the crystal structure to start with. A more detailed description of the different techniques can be found in Ashcroft and Mermin[8]. The most commonly available technique used for the analysis of powder samples is the Bragg-Brentano technique, also called the $\theta - 2\theta$ geometry(Figure 2-9). It requires the sample in form of a powder or a thin film to be attached to a planar holder. The direction of the incoming monochromatic X-ray beam and the direction of the detector are maintained in a plane comprising the normal to the sample, with a further geometrical constraint: the angle between the incoming beam and the detector is equal to twice the angle between the incoming beam and the sample normal. Because of the condition of elas-

tic scattering, this implies that one can only detect families of lattice planes that are parallel to the substrate plane (see Figure 2-9). The relation between the spacings of these planes and the angles at which one detects a response is given by the Bragg relation

$$d = n\lambda/2\sin(\theta)$$

where $\theta = \frac{\pi}{2} - \alpha$ is the angle between the direction of the incoming beam and the plane, which is usually recorded, d is the spacing associated with a family of lattice planes and λ is the wavelength of the radiation used.

For this method to work with single-crystalline films, one needs to have substrates that are well cut, with reasonably parallel faces, and furthermore the film orientation must have a definite relation to the substrate orientation. Our films are c-axis oriented, but we have had problems with $SrTiO_3$ substrates that were sometimes miscut by 2^o. In this case, one has to be patient and try to place the substrate at various angles on the holder until one gets a reasonable response at the substrate peaks (X-rays penetrate a few microns into the samples, so that one always sees the substrate signal for thin films). We often noticed changes in the intensity of more than an order of magnitude by simply rotating the substrate by 90^o in the plane of the holder, which is due to **G** forming a sharp angle with **N** (Figure 2-9) and going through the plane defined by **K** and **K'**. The method is really designed for powder samples where one has an enormous number of microcrystalline grains at random angles, so that one picks up every family of planes of the crystal strucure. For a single crystal or well oriented thin film with random orientation with respect to the beam geometry, one will not get any signal. However, the method is so widespread and simple that most materials-researchers use it.

Our samples were analyzed at the central X-ray diffraction facility at MIT after a thorough introduction by J.Adario. A Rigaku rotating anode generator was used, allowing high power (60kV, 250mA). We used Cu-Kα radiation (λ= 1.54Å). Films made in N_2O without anneal show the best diffraction pattern in that there is no large foreign phase peak (Figure 2-10). Apart from the substrate peaks (here $SrTiO_3$), one

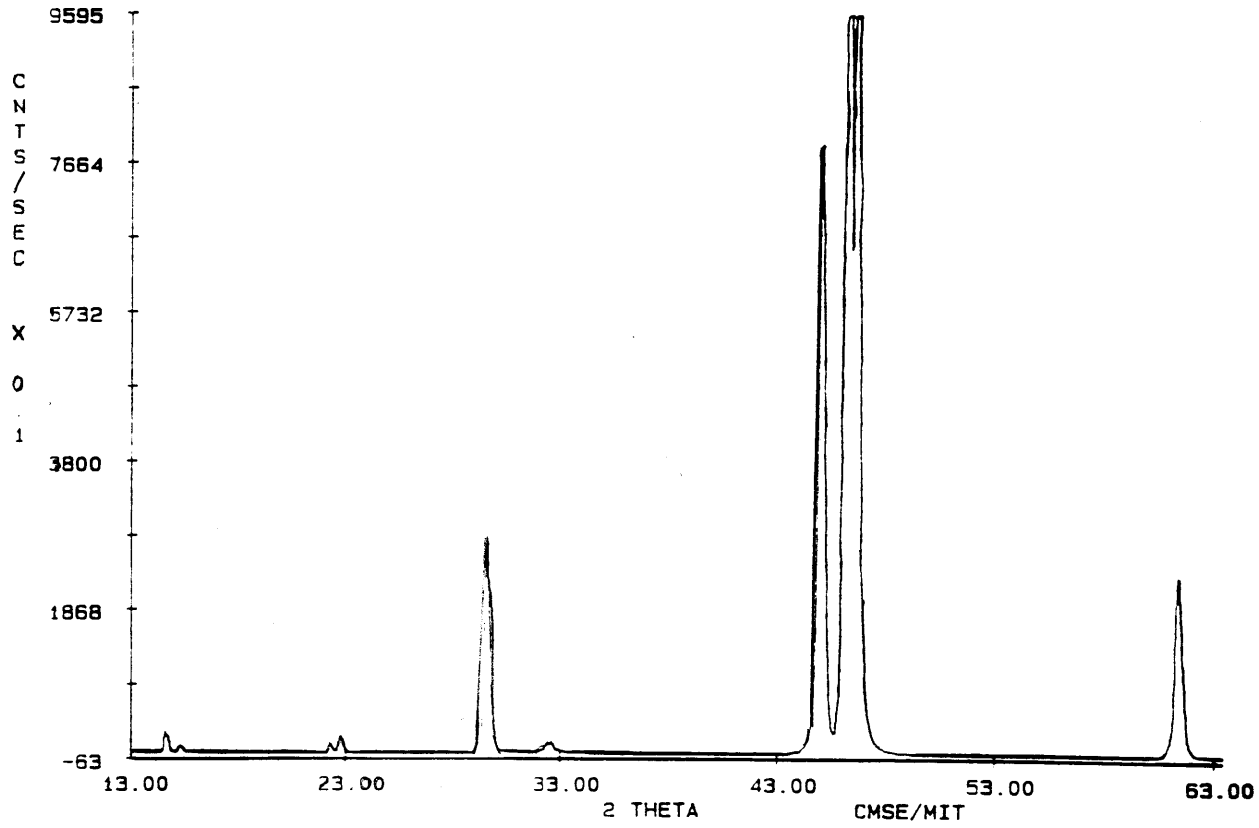

Figure 2-10: X-ray diffraction pattern ($\theta-2\theta$ scan) of a non-annealed sample deposited in N_2O.

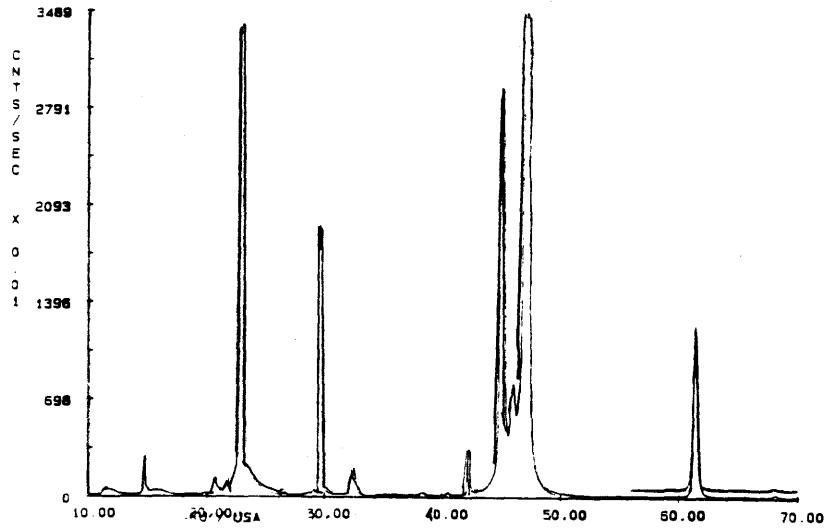

Figure 2-11: X-ray diffraction scan of a film deposited on $NdGaO_3$ in N_2O. The peak at 32.5° is a foreign phase of composition $Nd_{.5}Ce_{.5}O$. However, its intensity is not as high as on vacuum-annealed films made on $SrTiO_3$.

sees the peaks corresponding to c-axis oriented $Nd_{1.85}Ce_{.15}CuO_{4-\delta}$ structure. The lattice constant calculated from the Bragg relation is 12.05Å. Unfortunately, as soon as one does a high temperature vacuum anneal, a peak at 32.5°, which was very weakly present in the non-annealed samples, starts to grow and becomes comparable in intensity to the nearest peak of c-axis oriented NCCO. This peak is also seen in single-crystal work[69], and has been identified as coming from a cubic NdCeO phase. As discussed in the first chapter, reduction is followed by irreversible decomposition of the sample. The preparation through N_2O has the advantage that one can produce superconducting samples without anneal and without decomposition. X-ray diffraction of films made on $NdGaO_3$ and $LaAlO_3$ show a smaller foreign phase peak (Figure 2-11), even for annealed samples.

Future work should explore the potential of these substrates for growing even better films (cf. also channeling data). On the other extreme, samples deposited on MgO show severe degradation.

2.6.4 RBS

Rutherford Backscattering Spectroscopy (RBS) is a powerful, non-destructive method of composition analysis of thin film samples, which can also be used to determine the quality of the crystallinity (through channeling). A very good overview can be found in [63]. The physical principle is the following: a monochromatic beam of alpha-particles generated by a Van de Graaf generator impinges on the sample surface. An energy-sensitive detector is placed at a known angle close to the backscattering direction. The alpha-particles collide with the atoms constituting the sample. According to the laws of classical mechanics (conservation of momentum, and conservation of kinetic energy of the system of two particles in the absence of internal excitations or resonances), the knowledge of the incident energy, the angle with respect to the original direction and the energy of the backscattered He^{++} allow the determination of the mass of the atom involved in the collision. One also knows the cross-sections of the collisions between alpha-particles and elements, so that one can directly determine both the nature of the elements composing the film (by the peak position) and the relative ratios (by renormalising the relative peak heights with the cross-sections). In reality, things are more complicated: because of many near-collisions, the alpha-beam loses energy as it goes through the sample; instead of delta peaks, one gets thicker peaks whose leading edge comes from the particles bouncing off the first layers (thus at the energy predicted by the theory) and whose trailing edge at lower energies comes from particles having gone all the way through the film and back. The availability of powerful computers and good programs that allow the simulation of quite complex structures and stoichiometries has made this technique a powerful analysis tool. It is important to realise that with the knowledge of scattering cross-sections, this is an absolute method of measuring the stoichiometry and does not require standards. We made measurements at the IBM facility and at the Harvard-MIT facility, and used an IBM-program[68] as well as the RUMP program (Cornell, distributed by Computer Graphics Software) for the analysis. Figure 2-12 shows a spectrum taken on an NCCO film and the overlay of a simulation. The (Nd+Ce) to Cu ratio obtained was usually within 10% of the theoretical ratio (i.e., 2). For samples prepared in low

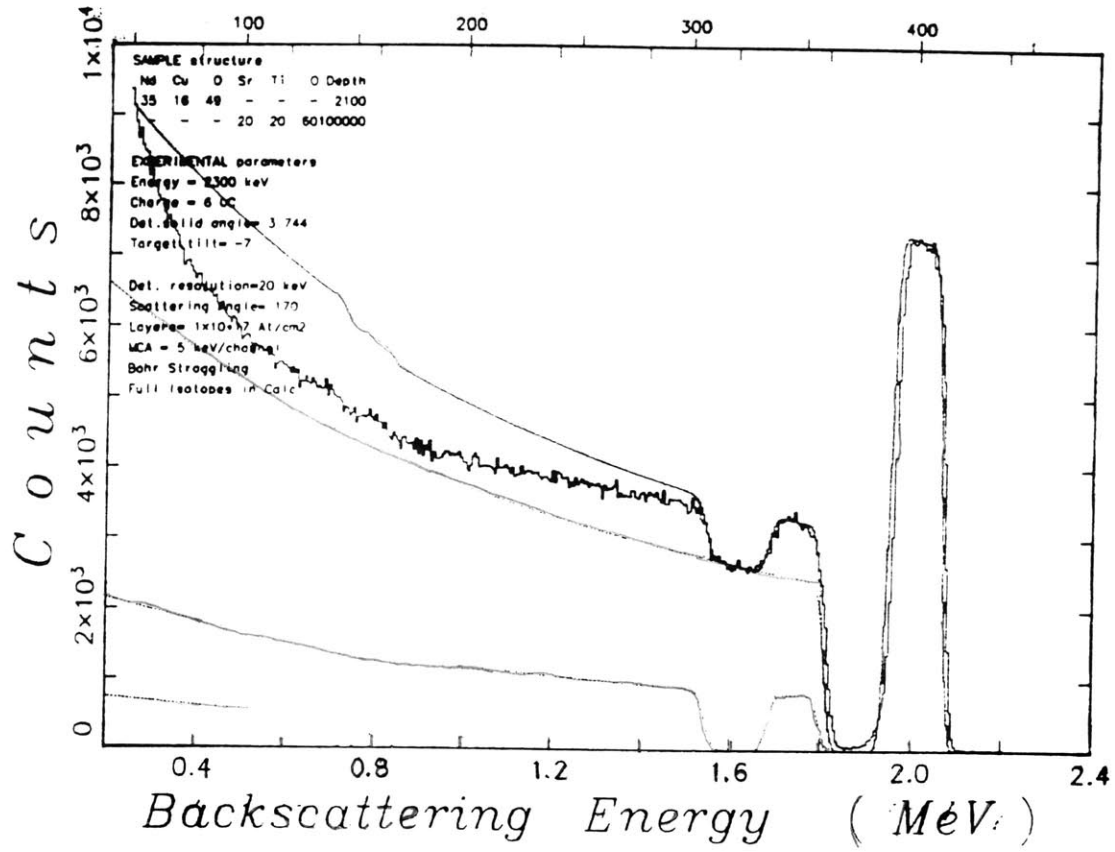

Figure 2-12: RBS spectrum and theoretical simulation. The theoretical parameters are the ratio of the heavy elements ((Nd+Ce)/Cu = 2.2) and the thickness (2100Å). This film was deposited with 6000 pulses in 230 mTorr O_2. Because one can not distinguish Nd and Ce, one has only access to the sum of the two. Oxygen has a small cross-section (because it is light), so that one cannot get quantitative information about its stoichiometry.

oxygen pressures or vacuum annealed for a long time, there were deviations. For the latter samples in particular, the Nd-peak shape changed close to the surface. It is important to take samples with clean surfaces for this measurement; a rough surface or organic residues can produce artefacts in the spectra. Some of the drawbacks of this method are: the low cross-section of light elements such as oxygen, which make a quantitative determination of the oxygen content impossible, the bad resolution at high energies (one cannot distinguish Nd and Ce).

Apart from composition analysis, one can also get an idea of the crystalline order by the channeling technique. Here, the idea is that if a whole row of atoms is exactly aligned with the beam direction, only the first atom can backscatter an alpha particle; the others are hidden. Thus, if the crystalline order is good and if one aligns the beam with the atomic rows, the backscattering yield should go down as compared to the random incidence, except for the first few layers. The ratio of the yields (often called χ_{min}) gives information about the ordering; for state-of-the-art Si wafers, one gets yields of about 2%. Our samples are not quite as good. For the first films made in 150 mTorr O_2 and annealed, we found χ_{min} =.3. Films made in 230 mTorr N_2O on $SrTiO_3$ without anneal have χ_{min}=.1. The best χ_{min} was obtained on films deposited in 230 mTorr N_2O on $LaAlO_3$ substrates, and was close to 6%(Figure 2-13) . Together with the above-mentioned X-ray data, this makes $LaAlO_3$ a promising substrate, and shows the high quality of the films that we can now obtain.

2.6.5 SEM

The scanning electron microscope (SEM) is also a standard analysis tool. It allows the study of the surface morphology down to about 1000Å. By analyzing the spectrum of X-rays emitted by the spot being hit by the electron beam, one can also get a chemical analysis of the sample (microprobe). Unfortunately, it is difficult to make this a quantitative method without good standards, especially for thin films, so that we have mainly used SEM for morphological studies. Figure 2-14 shows an SEM picture of the surface morphology of one of our NCCO films. The only features that one can distinguish are a few particulates that are an inherent feature of the laser

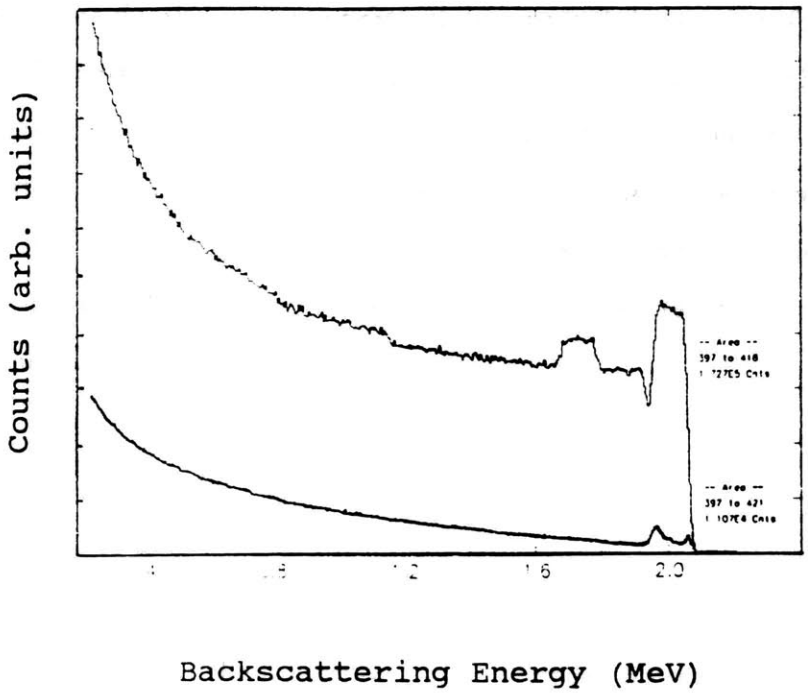

Figure 2-13: Random and channeled spectra for a film deposited on $LaAlO_3$ in N_2O (non-annealed, superconducting). The minimum yield is close to 6%.

Figure 2-14: SEM picture of the surface of a non-annealed sample. One does not see any features except for a few particulates.

ablation process. The density of these particulates is much lower than for YBCO or BSCCO films. The currently accepted explanation for this is that NCCO targets are denser, which reduces the splattering that yields to the formation of at least part of the particulates on the film surface. The reason for the higher density is that this compound can be sintered at higher temperatures (because its melting point is higher), and the resulting higher mobility leads to better reactions at the grain boundaries of the crystallites.

This concludes our chapter on sample preparation and characterization. It took us a long time to understand the importance of the oxygen pressure, and to discover the improvements brought about by the use of nitreous oxide. During that time, we could not do much work on the superconducting properties, for lack of good samples. But the systematic study of the deposition was an absolutely necessary step before we could start to think about the physics. This illustrates the fact that in the field of high temperature superconductivity, the physicist has to understand more than ever before the difficulties involved in sample preparation. This is necessary in order to distinguish the intrinsic effects from artefacts that only a good knowledge of the preparation and characterization techniques can help take into account.

Chapter 3

Experimental methods for transport measurements

3.1 Film preparation

3.1.1 Surface preparation

One of the major obstacles that we had to overcome in order to do the transport measurements was the contact resistance problem that we encountered with our films. The usual way of making contacts with silver paint yielded contact resistances orders of magnitude higher than the film resistance. As a result, transport measurements were very noisy. Although vacuum annealed samples are most affected (presumably because of the Cu loss already mentioned), non-annealed films also display contact problems, especially if left in air for longer periods. We investigated two methods: etching of the surface by ion milling and by acetic acid.

Acid etches have been used successfully on YBCO[32] and yield very low contact resistance, as well as reproducible tunneling curves. A bromine etch has been most successful on YBCO. XPS results on $Nd_{1.85}Ce_{.15}CuO_{4-\delta}$[92] show that acetic acid and hydrochloric acid are better at cleaning the surface and yield better spectra. We mainly used acetic acid for our experiments. The etch was prepared by diluting one part of glacial acetic acid in ten parts of distilled water. Films were left in this

solution for 15 minutes, then rinsed with pure methanol. In our first experiments, we used silver paint to make contacts on the treated surface. There is definitely an improvement compared to untreated samples, but a typical spot size of a few mm^2 yields a contact resistance of about 1 kΩ. For comparison, a typical film resistance between two contacts at a distance of a few mm is about 100-200 Ω. Annealing these contacts in air at 250°C can bring the contact resistance further down to a few hundred Ω, and allows us to measure $R(T)$ without too much background noise. Unfortunately, the quality of the contact degrades in a matter of days, and the adherence of the silver paint to the NCCO film is poor. In many cases, the dot of paint came off without leaving a trace. We found that using gold contacts on top of the freshly etched film surface solved some of these problems. The samples were mounted on a sample holder and masked under flowing nitrogen as soon as the methanol was removed. They were then transferred into the vacuum system as quickly as possible. Exposure to air was therefore limited to a short time of about 2 minutes. The comparison of a two terminal measurement and a four terminal measurement of $R(T)$ using this kind of contact revealed that the contribution due to the contact resistance is comparable to the measured film resistance. At low temperatures, a rise in the two terminal resistance is observed, while the four terminal resistance at the same temperatures shows a plateau. Thus, the rise is due entirely to the contact resistance. This effect is of course undesirable for contacts, and the resistance (a few hundreds of Ω for a typical contact of 1 mm^2) is still high. However, it turned out that these contacts were extremely stable in time, could withstand repeated thermal cycling from room temperature to 1K, and yielded very reproducible dI/dV vs. V curves. Furthermore, annealing the contacts in air at 250°C brings the contact resistance further down. In this manner, we were able to make very clean measurements of the magnetoresistance and Hall effect in our films.

We conclude that the acetic acid removes at least partially the high resistance material that forms on the surface of the films. Our tunneling measurements described in chapter 6 make it clear that there is some kind of barrier at the interface NCCO/Au. It is not clear if this barrier was formed during the short exposure to air, or during

exposure to vacuum, or if it was due to a residue from the etching process. Exposure to air will cause the contact problems to reappear. Similarly, annealing in argon or helium at 400°C after the etching process also causes the surface to become highly resistive. Acetic acid can be used to clean the deteriorated surface and has been of great practical value in our experiments. An important question is whether the bulk of the film is affected by the exposure to acid. $Nd_{1.85}Ce_{.15}CuO_{4-\delta}$ is more resistant to acids than for example YBCO: this is readily seen when it comes to cleaning old substrates for repeated use. A bridge 10 μm wide and 60 μm long was exposed to the etch for various times. No change was seen in the $R(T)$ curve for exposure times of less than 1 hour. The transition became broader only after an exposure of more than 3 hours. The method is thus relatively safe.

In another set of experiments, the NdCeCuO thin films were ion milled in oxygen with a 2kV bias. About 15 nm were removed in 20 min. The chamber was then evacuated and a gold film was evaporated on top of the freshly treated surface. The room temperature resistance of the contact ($1mm^2$) was only a few Ω, thus much lower than the value for acetic acid treated films. The temperature dependence of the resistance is also different: as the temperature is lowered, it shows an extremely fast increase down to about 100K, where it changes to a much slower rise down to low temperatures. This is a strong indication of the existence of a layer of material that has been affected by the ion milling process.

For all of the transport measurements except tunneling, we used the acid etch because of its simplicity. As will be seen later, both methods yielded similar tunneling results.

3.1.2 Patterning

Figure 3-1 shows a pattern used for transport measurements. Measuring the bias directly between 1 and 3 allows the measurement of the sheet resistance, and thus the resistivity; measuring between 2 and the point between the two resistance boxes allows the measurement of the Hall effect. In this case, the ratio of the resistances is adjusted so as to null the bias in zero field. The reason for the nulling is that one thus

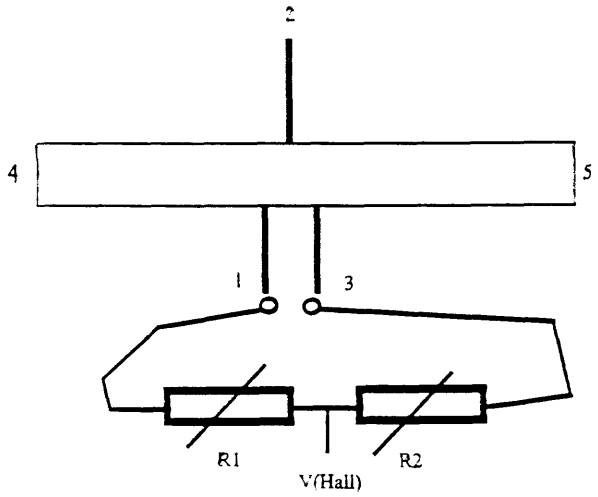

Figure 3-1: Pattern used for transport measurements.

cancels out any longitudinal bias which could be field dependent (magnetoresistance) and appear (wrongly) as a Hall voltage. It is good to invert the field direction if this is possible: this allows one to get the real Hall voltage because the magnetoresistance effect is even in field, whereas the Hall voltage is odd (both are odd in current, so that it does unfortunately not help to reverse the direction of current flow). We have checked the homogeneity of the films by monitoring the ratio of the bias between 1 and 3 to the bias between 2 and 3 in zero field: it was constant up to a few percent between room temperature and 4.2K, indicative of the good lateral homogeneity of the samples on the scale of a few mm^2.

3.2 Transport measurements

The resistance of the films in the ab-plane was measured both as a function of temperature in zero field, and as a function of an applied field of variable orientation with respect to the CuO_2 planes, with the temperature maintained at constant values between 35K and .5K. For the fixed temperature measurements, the sample was attached to a heater and kept in a fridge submerged in a ^4He bath. The heat exchange between sample and bath was reduced to an acceptable level by pumping on

the exchange gas in the jacket. Following the advice of Dr. B.Brandt, we found that one hour pumping with a previously warmed-up diffusion pump was needed in order to be able to work above 20K for several hours. This was critical for the orientation dependent measurements, where the temperature had to be maintained constant for the duration of the run. I found that it was possible to do measurements from 4.2K to 35K in one session, provided that one starts pumping on the jacket as soon as the Helium is transferred: there is still enough exchange gas to do the lowest temperature sweeps, but as one goes up in temperature, the heat transfer gets slower so that one needs to input little current (a few 100mA at most). The temperature was read from a Carbon Glass Resistor (CGR) in zero field, and controlled during the field sweep by a capacitance thermometer to avoid the effect of magnetoresistance in the CGR at the lower temperatures (important especially below 10K). For experiments below 4.2K, a ^{3}He fridge was used, i.e., instead of ^{4}He exchange gas, ^{3}He was used. Above its condensation temperature, the ^{3}He remains in the gaseous state and acts like normal exchange gas, but it condenses at about 1K at the pressure available, at which point the temperature can be lowered further by pumping on it (down to about .5K if one uses a good pump). The temperature is determined first from the pressure above the ^{4}He (4.2K to 1.1K), and then above the ^{3}He (1.1K to .5K). This is a simple and accurate way to measure temperature, and is of course field independent. A diaphragm controls the pressure very precisely to a preset value. The measurements in field were done in the high field facility at the Francis Bitter National Magnet Laboratory, and for the measurements where the temperature control above 4.2K was needed, we used the NUSH (New Universal Sample Holder) available to the users. For the resistance measurements in zero field, the sample was manually lowered into a ^{4}He bath while monitoring R and T. In most of our experiments, the data acquisition was done on a MacIntosh II computer running under the LabView software (National Instruments) configured for the field sweeps by Dr. S.Hannahs. The data were then analysed with the Igor software on the Mac, or transferred via modem to a Unix machine and analysed with the C-plot program (Certified Software).

3.3 Data reduction: extraction of physical quantities

3.3.1 Conductance per CuO_2 plane

In most of our experiments, one puts a known current through the sample and measures a bias, and this is used together with geometric properties of the sample to extract a value of the resistance (or a Hall number). For macroscopic samples, the resistance can usually be expressed as the product of an intensive value (the resistivity) by a certain number of sample dimensions (this is not true for very small sample dimensions where quantum mechanics play an important role, e.g., weak localization on length scales smaller than the thermal length, or mesoscopic phenomena). In 3D, one has $R = \rho l/S$, where l is the length of the sample in the current direction and S is the sample section (thickness by width). It is easy to see that for a fixed thickness t, the resistance of a square is not dependent on the size of the square; this value defines the resistance per square, or sheet resistance, $R_\square$. In 2D, the corresponding formula is $R = \rho l/w$, where l is the length and w the width of the sample defined with repect to the current direction, and if $l = w$ (square sheet), then this value again is size independent. This means that in 2D, resistivity and resistance per square are the same, and resistivity is expressed in the same units as resistance. For a layered compound, one calculates the resistance per layer by assuming that all the layers provide identical and parallel conduction paths: $R_{\square perlayer} = NR_\square$, and N=thickness/interlayer spacing. One can of course also define a 3D resistivity $\rho = R_\square t$. In our case, superconducting samples show a resistance above the transition $R_\square$=10Ω. The sample thickness being 2000Å, and the interlayer spacing 6Å, one gets a resistance per CuO_2 sheet of about 3000Ω. In theory, the conductance is actually the more important value: this is because a current (being a non-equilibrium phenomenon) is always caused by an external perturbation, e.g., an electric field, and one usually relates the current to the perturbation by linear response theory. The natural response coefficient is thus the conductivity $j = \sigma E$, and by virtue of

the fluctuation-dissipation theorem, it is related to the current-current correlation function (Kubo formula). However, in practice, it is of course easier to measure a current going through the sample (div$j$=0 in the stationary state, so it is sufficient to measure the current in the lead going to the sample to know what it is inside). This current is related in the sample to a gradient of the field, which is easy to measure even with bad contacts. There is no way to obtain a true 4-terminal measurement of the conductance, so one gets the conductance by inverting the 4-terminal resistance. Understanding these fundamental differences is very important for tunneling measurements.

3.3.2 Hall effect and carrier densities

By elementary theory[8], if one assumes one kind of carrier (either electrons or holes of same mass), one finds that $V = IB/net$, where V is the lateral bias, I the current, B the magnetic field, e the charge of the charge carriers, t the sample thickness and n the carrier concentration. The sign of the carriers is determined by the sign of the bias. We did two measurements: a non-superconducting sample showed a constant carrier density of 0.4 $10^{28}\mathrm{m}^{-3}$ at 77K and 4.2K. A superconducting sample showed n=0.7 $10^{28}\mathrm{m}^{-3}$ at 300K, 0.2 $10^{28}\mathrm{m}^{-3}$ at 77K and 0.16 $10^{28}\mathrm{m}^{-3}$ in the normal state above H_{c2} at 4.2K. This temperature dependence of the Hall coefficient in superconducting samples is in agreement with observations from other groups[44]. We always observe a sign compatible with negative carriers (it is useful to know that the fields in the Bitter magnets point upwards). The 3D carrier density can be converted to a density per layer by multiplying by the interlayer spacing: we find a carrier density of the order of 2 $10^{18}\mathrm{m}^{-2}$. This allows one to extract an order of magnitude for the Fermi wave vector, assuming a free electron gas[8] in 2D: $n_{2D} = k_F^2/2\pi$, yielding $k_F \approx 0.4$ 10^{10} $\mathrm{m}^{-1} \approx 1.3/a$, where a is the lattice constant in the ab-plane, and the Fermi velocity $v_F \approx 0.4$ 10^6 m/s. Going on, we can estimate the carrier life-time τ from the Drude formula $\sigma = ne^2\tau/m$, giving $\tau \approx 5$ 10^{-15}s assuming a free electron mass. The mean free path is then $l = \tau v_F \approx 20$Å, smaller than the in-plane coherence length $\xi_{ab} \approx 70$Å. This places us in the so-called dirty limit of superconductivity. It is

also useful to estimate the diffusion constant D, which is related to σ by an Einstein relation:

$$D = \sigma / e^2 N(E_F) \tag{3.1}$$

where $N(E_F)$ is the DOS at the Fermi-level in 2D, estimated by the free electron model $N = m/\pi\hbar^2$. One finds $D \approx 4$ cm^2/s.

This concludes the last chapter of "preliminaries". It is time now to start talking about physics!

Chapter 4

Magnetoresistance measurements in the normal state

4.1 Introduction

The motivation of the magnetoresistance (MR) measurements described in this chapter was to understand the reason for the upturn of the resistance at low temperatures. Also, for a long time, no high quality superconducting samples were available, so that the study of non-superconducting samples was forced on us by destiny. However, this turned out to be a blessing, and the amount of information gained was important for the study of superconducting samples, which were obtained later on. Indeed, since the normal state transport properties at low temperatures are hidden in the superconducting samples unless one applies a field higher than H_{c2}, it is necessary to study non-superconducting samples to obtain low-field, low-temperature information concerning the normal state. And from a practical point of view, it is also easier to prepare high quality samples of the latter kind: the reduction step usually necessary to obtain superconducting samples is accompanied by a partial decomposition, making it difficult to make homogeneous superconducting samples.

At 4.2K and for fields perpendicular to the CuO_2 planes, we find a reduction of the resistance by 16% in a field of 13.2T, with no sign of saturation. The effect in parallel fields is much smaller, and the field dependence is different. The perpen-

dicular field data are fit by the theory of weak localization in two dimensions. This provided the answer to the question of the resistance upturn at low temperature: it is a weak localization effect. But it revealed a more interesting fact: the observed MR is consistent with a model in which the films are treated as stacks of non-interacting two-dimensional conductors.

4.2 Experimental Results

4.2.1 Description of the samples

The orientation-dependent magnetoresistance measurements were done on samples deposited in 150 mTorr O_2 and cooled down in the same atmosphere. In other words, these samples would be superconducting if a reducing step were performed after the deposition. The carrier concentration determined by Hall effect measurements, assuming a single carrier model, was found to be 0.4(+/-.05) 10^{22} cm^{-3} and temperature independent between 77K and 4.2K. The carriers are negatively charged. The resistivity, determined by four terminal measurement of a patterned strip, is 5 mΩcm at 300K. This somewhat high value suggests the presence of disorder.

Plotting the conductance of the film (together with that of another film made in 230 mtorr) as a function of $\log(T)$ results in Figure 4-1. The two films were plotted together to show that the correction in both cases is linear and about the same, i.e., independent of the conductance. We used the conductance per CuO_2 layer, in units of $L_{oo}=e^2/\pi h$, on the vertical scale. There is a maximum of conductance followed by a linear decrease from 100K to 30K, and a more gentle decrease at lower temperatures. A least squares fit to a line from 40K to 80K gives a slope of 1. There are experimental uncertainties in the RBS thickness measurement (about 10%), and the assumption that all the planes contribute in the same way is only a first approximation. Nevertheless, the fact that the conductance per plane varies logarithmically with a prefactor close to L_{oo} is a strong indication that two-dimensional (2D) weak localization or electron-electron interaction effects cause the decrease in conductance[51, 14].

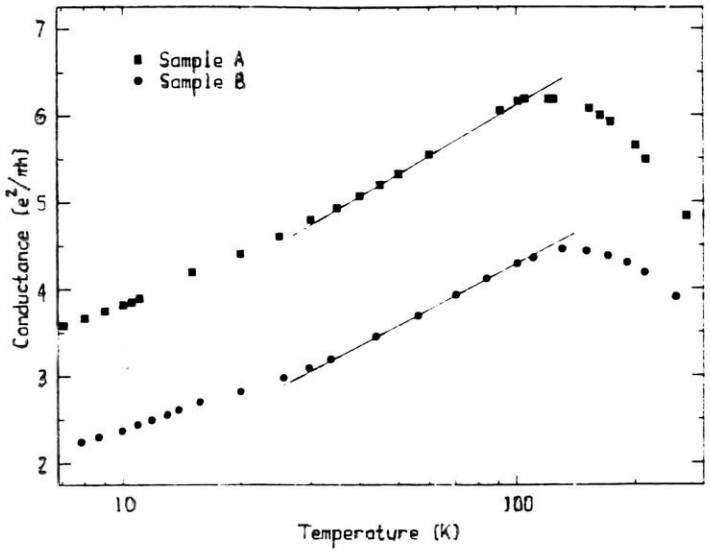

Figure 4-1: Conductance per CuO_2 plane in units of $e^2/\pi h$, as a function of temperature (logarithmic scale), for an as-deposited film made in 150 mTorr O_2 used for the subsequent figures, together with that of a second film made in 230 mTorr O_2 (with higher conductance). The broken line is a linear fit to the data between 30 and 100K.

MR measurements can help distinguish the two effects, and this was the primary motivation for the work presented below.

4.2.2 Magnetoresistance measurements at low temperatures

MR measurements were done at low temperatures in two different field orientations (field H either perpendicular or parallel to the CuO_2 layers, and perpendicular to the current in both cases). Figures 4-2 and 4-3 show the MR at 4.2K and 1.29K. It is strongly anisotropic and negative. The anisotropy is apparent not only in the magnitude of the effect, but also in its temperature dependance. The parallel field curve seems to become flatter at low fields as the temperature is lowered, whereas the perpendicular MR shows just the opposite behavior. The anisotropy clearly reflects the layered nature of the material and is a strong indication of an orbital origin. The negative sign of the MR and its magnitude show that it is a quantum effect. Figure 4-3 shows the MR in a perpendicular field up to 13.2T at 4.2K. It has a parabolic behavior at low fields, but the concavity changes sign and the slope becomes smaller as the field becomes stronger. There is no sign of saturation at 13.2T.

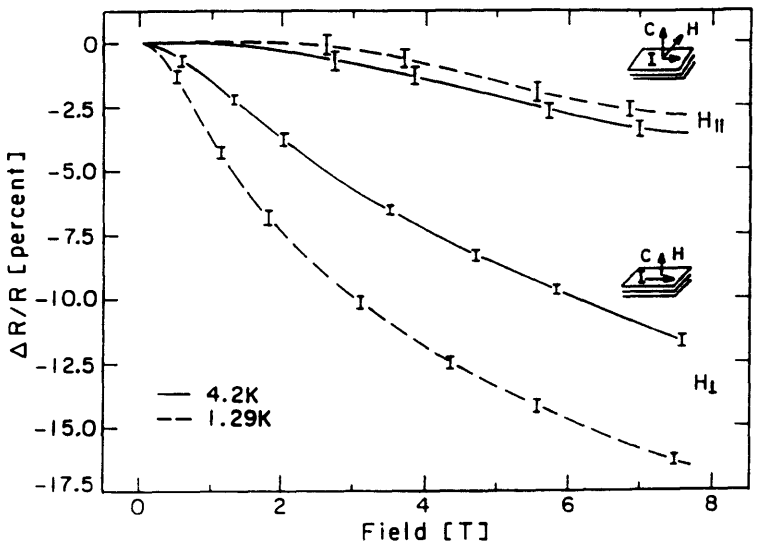

Figure 4-2: Resistance at 4.2K and 1.29K in fields perpendicular and parallel to the CuO_2 layers. The vertical scale represents the percentage change relative to the zero-field value.

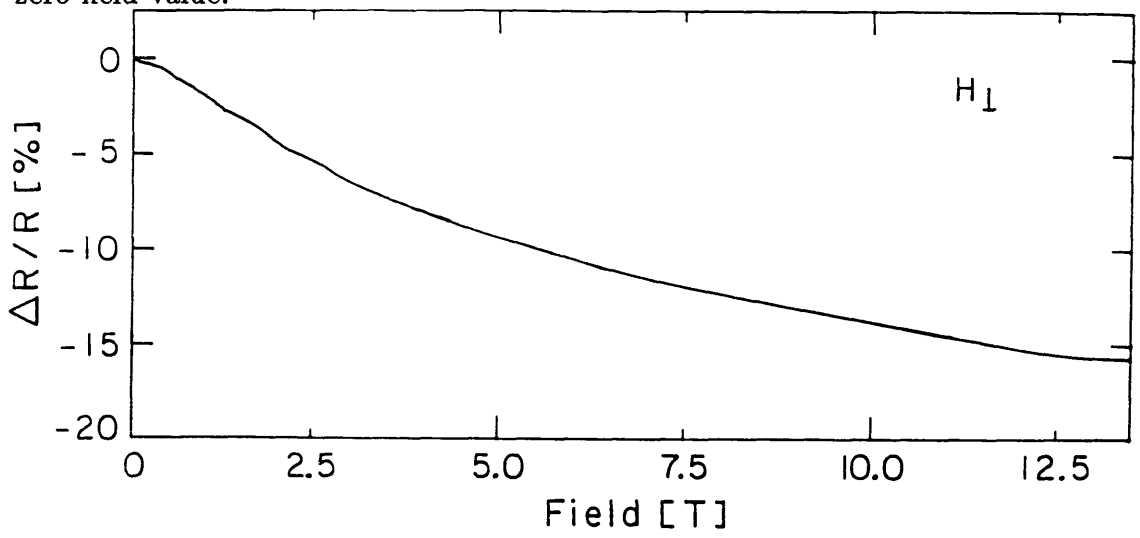

Figure 4-3: Resistance in a field perpendicular to the layers at 4.2K measured up to 13.2K.

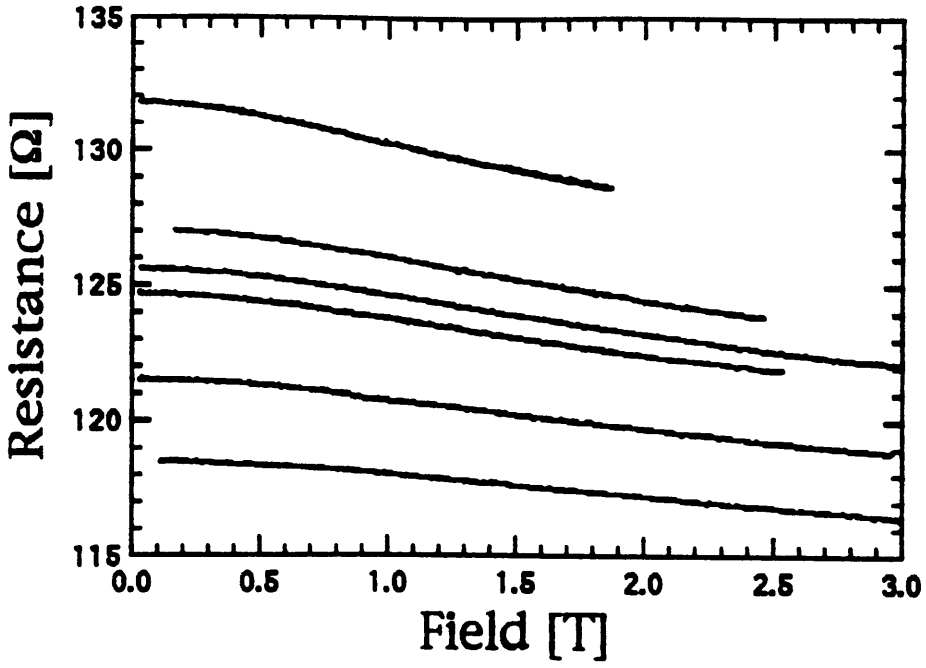

Figure 4-4: MR in perpendicular fields at 14K, 16K, 18K, 20K, 24K and 30K from top to bottom.

4.2.3 Magnetoresistance measurements at higher temperatures

Figure 4-4 shows the magnetoresistance in perpendicular fields between 14K and 36K. It becomes gradually weaker as the temperature is increased. Measurements at 77K (not shown here) revealed that the negative effect has almost disappeared (a fraction of a percent change for 8T).

4.3 Discussion

Before going on with the analysis of the data, it is necessary to present briefly the theory of weak localization, which we believe can explain all of our observations. The reader familiar with that theory can simply skip the next section.

4.3.1 Weak localization

The theory of weak localization was developed in the early 1980s in an attempt to understand how disorder affects the conduction in a metal. Anderson[51] has shown that electrons should be localized if the disorder is strong. The physical reason for this is that the randomness detroys the translational invariance that leads to the existence of extended states; it is difficult to make an extended state from a set of spatially and energetically very different localized states. Weak localization (WL) is a perturbation theory that studies the metallic part of the disorder-driven metal-insulator transition, and evaluates the first-order correction to the classical Boltzmann equation due to quantum-mechanical interference of the electron wave function at the defects. Reviews of the theory can be found[51, 14], and we will only outline briefly the main results that will be used in our analysis.

In a disordered metal, the electrons experience many elastic collisions with the impurity atoms, leading to a diffusive motion, and a certain probability to return to the origin, i.e., make a closed loop. The physical phenomenon that leads to the most important correction is the constructive interference of each closed loop with its time-reversed loop. This enhances the probability of an electron to return to its point of departure by a factor two as compared to the classical probability (simple diffusion equation), and consequently this reduces the conductivity. In theory, one evaluates the conductivity with the Kubo formula and finds that a class of diagrams called the Langer-Neal graphs give the leading correction. The evaluation of these diagrams leads to a correction

$$\Delta\sigma = -\frac{2e^2}{\hbar\pi}\frac{1}{L^d}\sum_Q \frac{1}{Q^2}$$

where the cutoffs for the wave vector Q are $1/L$, where L is the sample size, and $1/l$, where l is the mean-free path for the elastic collisions. This expression diverges for two dimensions if L is infinite, and this accounts for the particular importance of the two dimensional case for weak localization (in addition to the already mentioned fact that conductance and conductivity are identical in 2D, so that the corrections shown

in detail below are universal). However, the interference phenomenon is interupted by inelastic collisions which break the coherence of the electron wave function. So the actual cutoff at finite temperature (the Thouless length, L_{Th}) is related (by the diffusion equation) to the typical time τ_{in} between inelastic collisions

$$L_{Th} = (D\tau_{in})^{1/2}$$

which gives the temperature dependence: if one assumes that $\tau_{in} \propto T^{-p}$, one gets

$$\sigma_{2D}(T) = \sigma_0 + pL_{00}\log(T/T_0) \tag{4.1}$$

where $L_{00} = e^2/\pi h$ as defined above. In other words, one has a universal correction to the conductance. In a similar way, the effect of a magnetic field perpendicular to the 2D metal can be evaluated. Because the change in phase of the electron wave function around a closed loop depends on the flux enclosed with a different sign for the time-reversed path, the coherence is broken for loops that enclose a flux $\phi > h/2e$. This gives a field dependent cut-off $L_H = (eH/\hbar)^{-1/2}$. This explains the negative magnetoresistance: the interference effect that causes the resistance to rise as the temperature is lowered is now cut-off increasingly with higher fields. Interestingly, the presence of spin-orbit scattering will actually cause the magnetoresistance to be positive. The full theoretical expression including inelastic scattering, scattering from localized magnetic impurities and spin-orbit scattering can be written[36, 6, 53]:

$$\sigma(H,T) = \sigma(0,T) + \frac{e^2}{\pi h}[-\frac{3}{2}f(\frac{H}{H_T}) + \frac{1}{2}f(\frac{H}{H_S})] \tag{4.2}$$

where $f(x) = \log(x) + \Psi(1/2 + 1/x)$, Ψ is the digamma function, and $H_S = H_i + 2H_s$, $H_T = H_i + 2/3H_s + 4/3H_{so}$. Here H_i , H_s and H_{so} are related to inelastic, spin-flip and spin-orbit scattering rates by the formula $H_n\tau_n = \hbar/4eD$, where $n = i, s$ or so, τ_n is the corresponding lifetime and D is the electronic diffusion constant.

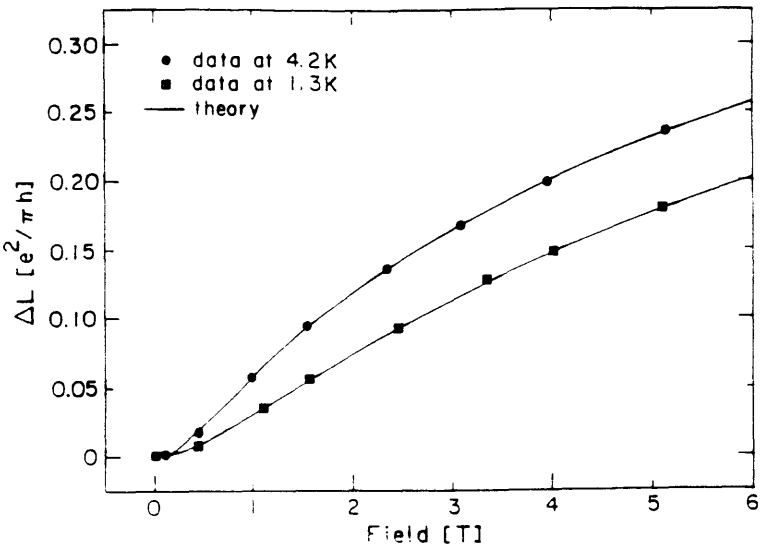

Figure 4-5: Fit of the conductance in perpendicular fields to the functional form predicted for 2D weak localization.

4.3.2 Low temperature data

The observed MR agrees qualitatively with the predictions of 2D weak localization. Electron-electron interactions do not have a strong magnetic field dependence, and it is furthermore usually positive[51, 14]. We will thus use Eq. 4.2 to fit the magnetic field dependence. We note that H_i and H_s enter the expression in a similar fashion, and from magnetoresistance fits alone it is difficult to distinguish them. We will thus use only H_i. H_{so} by itself causes positive magnetoresistance, and we do not take it into account for the time being. Thus, keeping only one parameter H_i, we fit the conductance to the form:

$$\Delta\sigma = cL_{00}f(\frac{H}{H_i}) \tag{4.3}$$

where the magnitude of the correction is allowed to vary freely (through the use of the parameter c which should in theory be equal to 1, but which is usually smaller), and only the shape of the curve is considered. The domain of validity of this equation is $\tau_i >> \tau_0$, where τ_0 is the elastic life time. Figure 4-5 shows the results of these fits. Equation 4.2 is an approximation only valid at low fields, and it neglects spin polarization effects that can become important for $H > k_BT/\mu_B$ (2T for 1.3K). It is quite remarkable that the experimental curves can be fitted so closely by this simple

theoretical expression. The magnitude of the measured correction to the conductance is smaller than the prediction by a factor 4 ($c = 0.25$). This might be due to the simplicity of our assumption that the hundreds of planes that constitute our film are all equivalent and decoupled. One also expects the simple perturbation theory that was used in the derivation of Eq. 4.2 to break down when the predicted corrections become large. A MR of 16% is certainly a large effect, and the temperature correction to the conductance approaches 50% between 100K and 10K. If one extrapolates the logarithmic correction to the conductance, one crosses the zero conductance level at a finite temperature. This is clearly unphysical, and a deviation from this prediction is expected.

Because superconductivity can be achieved by small changes in oxygen stoichiometry, superconducting fluctuations could be present and cause a positive magnetoresistance, thereby reducing the total effect. Since we have not measured any transition down to .5K, it is difficult to make a definite statement on the effects of possible fluctuations. We have seen clear fluctuation effects in superconducting samples (see next chapter) which can be observed even 10K above the transition. Furthermore, it was pointed out by Larkin[49] that even in the absence of a non-zero T_c and with purely repulsive electron-electron interactions, one still expects to see the influence of fluctuations (from the Maki-Thompson diagrams, see below) on the conductance, with a magnetic field dependence identical to the simple WL result. The conductance can then be written:

$$\Delta\sigma = L_{00}(1 - \beta(T))f(\frac{H}{H_i}) \tag{4.4}$$

where $\beta(T)$ is tabulated in his paper, and can take take values of the order of 1 on an appreciable temperature range.

It is not clear yet which scattering process is associated with H_i. In addition to inelastic scattering by phonons or magnetic scattering by local moments (maybe those associated with the Cu antiferromagnetism or the Nd moments), one could think of tunneling between layers[16] as a possible coherence-breaking mechanism revealed by the MR measurement. One can only conclude that spin-orbit scattering is very weak,

since even at lowest temperatures there is no trace of positive MR.

In order to get scattering rates from the magnetic measurements, one has to know the electronic diffusion constant D. Using the value of the conductivity quoted above and the Einstein relation (Eqn. 3.1), we find D=1 cm^2/s for our samples. A calculation of D based on the slope of H_{c2} in superconducting samples will be shown later and yields a similar result (slightly higher D due to the higher conductivity of the superconducting samples). Thus τ extracted from our fits is of the order of 10^{-11} s and increases as the temperature is lowered. Further fits including spin-orbit scattering show that τ_{so} is at least four or five times smaller than τ. Work[79] on furnace annealed films of NCCO published independently of ours shows very similar magnetoresistance data as our in-situ prepared films, showing that the effect is not due to the details of sample preparation. The resistivity at room temperature is lower, the upturn in resistance at low temperature is weaker, and the magnetoresistance is also smaller than in our case (4% change in a 6T field at 4.2K). This simply means that their samples are more metallic; the interpretation of the data in terms of 2D weak localization presented in the paper, including the fit to Equation 4.2, is in total agreement with ours. Work on single crystals[34] published recently is also a nice confirmation of our explanation. The values for τ_i extracted from these measurements are very similar to ours. In our fits, we have assumed from the beginning that $\tau_i >> \tau_0$, where τ_0 is the elastic lifetime, and the parameter c was introduced to take into account possible materials problems; for the fits in Ref [34], the two times were fitted (and c was assumed equal to one), and it was found that $\tau_i \approx 2\tau_0$, which seems quite questionable (many elastic events must take place before the coherence is lost in order for weak localization to become important). In our opinion, this is likely to be an artefact due to a small value of c.

Let us now turn to the measurement in parallel field. For a perfect 2D metal, there is no orbital effect in parallel field. Thus one can look for an explanation in two different directions: looking at a model taking into account the layered nature of the sample, or looking at spin effects to explain the observed negative magnetoresistance in parallel fields.

In a layered compound, one expects electrons to tunnel from one conducting sheet to a neighboring sheet with a certain rate, while the motion within the plane is still governed by a 2D diffusion equation. If the average time spent in a given layer is longer than the time scale set by the in-plane inelastic phenomena, one expects the results of WL to hold without any changes. If this time is of the same order of magnitude or somewhat smaller than the inelastic lifetime, one would expect a decrease in the probability of returning to the origin, and thus a smaller correction to the conductance. This is only true if the average number of tunneling events is very small during the inelastic lifetime. If this last condition is not fulfilled, then one has to describe the movement in the third dimension with a diffusion equation as well, and the overall model will be the anisotropic 3D model, where 3D behavior is expected[51]. In any case, the movement between the planes will yield closed paths that can support a non-zero flux in parallel fields, and can give rise to a negative magnetoresistance. Because of the smaller area of these loops, the characteristic fields are expected to be larger. This agrees with our observations. However, in order to conserve the coherence through the tunneling process, one has to assume elastic tunneling, and thus one does not expect a strong temperature dependence. The only temperature dependence would come from the growth of the typical loop area in the plane, leading to a decrease in the characteristic field scale for the magnetoresistance, which does not seem to be supported by our data.

Negative MR in parallel field has also been seen in hole-doped superconductors. Measurements by Fiory et al.[25] on non-superconducting $Bi_{2+x}Sr_{2-y}CuO_x$ single crystals show anisotropic, negative MR that looks similar to our data, although the magnitude of the effect is much smaller in their case. An interesting possibility is suggested by the results of Preyer et al.,[67] who report an isotropic, negative MR on single crystals of LaSrCuO. Our data might be the superposition of an isotropic part similar to the one observed on LaSrCuO and an anisotropic, perpendicular component due to weak localization.

4.3.3 Temperature dependence

In order to extract the temperature dependence of the scattering time from the data, we adopt the following method: we use only the part of the curve where the correction to the resistance is small and parabolic. One can then write:

$$-\Delta R/R_0^2 = \Delta\sigma = AH^2$$

An expansion of the weak localization formula with one parameter yields for the correction to the conductance for one plane:

$$\Delta\sigma = L_{00}H^2/24H_i^2$$

What we are really interested in is the logarithm of the scattering time, so all constant factors are irrelevant for us, and we calculate:

$$\log(A)/2 = const + \log(\tau_i)$$

since $H_i \propto \tau_i^{-1}$. But from the theory of weak localization, we know that the correction to the conductance goes as $const.' - L_{00}\log(\tau_i)$, where $const.'$ is another, unrelated temperature independent value. So plotting $-\log(\tau_i)$ as a function of $\log(T)$ can be directly compared to the correction to the conductance, and should have a parallel temperature dependence. The two sets of data are shown in Figure 4-6, and the consistency is very good. Between 14K and 30K, the log of the scattering time follows roughly a straight line (a least squares fit gives a slope of .87), but there is again a clear deviation at lower temperatures. The value of the slope shows that the scattering time goes roughly as $1/T$ between 30K and 10K and varies more slowly at lower temperatures. The temperature variation of the conductance is entirely explained by the temperature variation of the scattering time. It should also be mentioned that for this determination of the slope, we do not have to rely on the absolute value of the resistance: a scaling factor will just shift the log by a constant and does not affect the slope. We thus have confidence that the conductance per plane estimated earlier

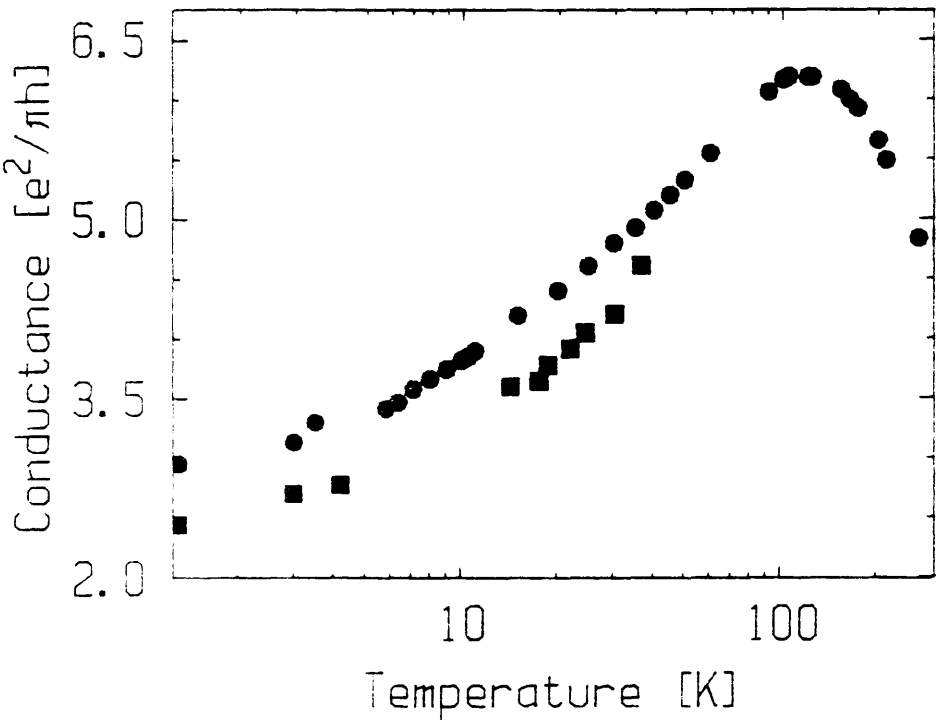

Figure 4-6: Comparison of the logarithm of the scattering time vs. temperature extracted from the parabolic part of the negative MR (squares), and of the conductance in units of L_{00} (circles) on a logarithmic temperature scale. The first curve has been shifted vertically for convenience, since it is only known up to a constant anyway.

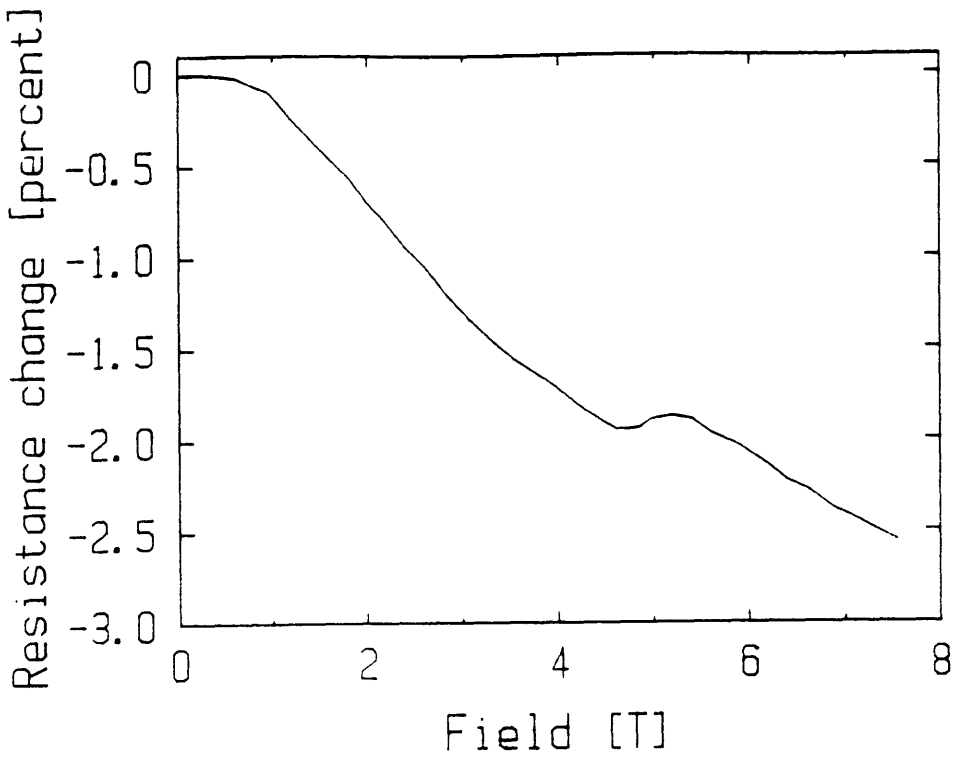

Figure 4-7: MR in perpendicular field at .54K for a more strongly insulating sample.

is not too far off from its real value, and that the deviation of the weak-localization correction in fields from the theory by a factor 4 is real.

4.3.4 Measurements on more strongly insulating samples

We have carried out a MR measurement in perpendicular field at low temperatures on a sample cooled down in 1atm O_2. The sample resistance (same thickness as before) was now of the order of 10kΩ and semiconducting all the way up to room temperature. The results of the measurements are shown in Figure 4-7. The data shown differ from the data for the more metallic samples in two respects: firstly, the negative MR is much smaller, although the theory predicts a stronger correction to the resistance if the resistance is higher (simply because $\Delta R = -R^2 \Delta\sigma$). It thus seems that the more strongly localized samples have a tendency to show weaker corrections. Secondly, there is a prominent bump at about 5T, which had already been visible at 4.2T, although not as sharply. We believe that this bump might be an indication of

a spin-ordering, similar to observations made on other compounds. Because of our interest in superconducting samples, we have not pursued these experiments further, but there is obviously matter for further investigations.

4.4 Conclusion

Our measurements clearly indicate that $Nd_{1.85}Ce_{.15}CuO_{4-\delta}$ can be described as a stack of 2D metallic sheets following very nicely the predictions of weak localization theory: the temperature dependence of the conductance is logarithmic, the slope is close to one; the magnetoresistance is large, negative and strongly anisotropic, and follows the functional form predicted by the theory; the temperature dependence of the scattering time extracted from the low-field part of the curves is also consistent with the temperature dependence of the conductance in the framework of the theory. The magnitude of the correction at low temperature is smaller by a factor 4 than the prediction, and this is attributed to tunneling between planes or break-down of the perturbation theory. One might then ask whether there is a correlation between the existence of localization and the absence of superconductivity. It is well known that an increase of the sheet-resistance in thin films results in a quick suppression of the T_c[33]. The effect is attributed to the increase of the repulsive electron-electron interaction due to the less effective screening by localized electrons. The connection has been made by Tanda et al.[79], who find that samples of $Nd_{1.85}Ce_{.15}CuO_{4-\delta}$ with different O contents change from insulating behavior at $T = 0$ to superconducting behavior at the critical sheet resistance $h/4e^2$. However, we feel that there is no clear evidence that superconductivity disappears because of increasing disorder: we do not see any clear signs of interaction effects in the magnetoresistance, which one would expect to see if interactions were important enough to destroy superconductivity. Also, the inelastic lifetime is long and does not suggest strong interaction effects either.

Another important question is whether the strong 2D character survives in superconducting samples, since it is believed that long-range order does not exist in

two dimensions. One might thus expect a more three dimensional character for the samples as they approach the superconducting state. The study of this question will be the theme of the next two chapters.

It is a pleasure to thank Prof. M. A. Kastner for his encouragement and for enlightening discussions on weak localization. We also acknowledge the helpful comments of Prof. B. L. Altshuler, and discussions with Jari Kinaret.

Chapter 5

Measurements on superconducting samples above T_C

5.1 Introduction

As recognised by Aslamazov and Larkin[9], even above T_c one should see the effect of the imminent formation of pairs as a correction to the conductance. This is because the superconducting transition is of second order: it does not cost much energy to create small volumes where the order parameter is small (but non-zero). This is even more true in reduced dimensionality, where the entropy factor is always more important. They worked out the correction due to the formation of pairs with a finite lifetime, leading to the disappearance of the dissipation that would be expected from the independant electrons forming the pair, and found the following:

$$\sigma_{AL}(T) = \frac{e^2}{16\hbar}\frac{1}{\epsilon} \tag{5.1}$$

where ϵ=(T-T_c)/T_c. Corrections to the conductance obeying this formula were indeed found[30]. To observe these corrections, one must determine what the normal state resistance R_n would be in the absence of fluctuations. In practice, one usually looks at $R(T)$ far above the transition and makes a reasonable extrapolation to the vicinity of the transition (constant or linear extrapolation in most cases). The correction due

to fluctuations is then extracted by calculating:

$$R_{fl} = \sigma_{fl}^{-1} = (R_n R)/(R_n - R) \tag{5.2}$$

and, in the case of 2D, this should be linear in ϵ and reach zero at T_c (as opposed to a square-root like behavior with vertical slope at T_c in 3D). A magnetic field dependence can also be derived[1] by using time-dependent Landau-Ginzburg theory:

$$\sigma_{AL}(T,H) = \frac{e^2}{8\hbar}\{\psi(1/2 + \epsilon/2h) - \psi(1 + \epsilon/2h)\} \tag{5.3}$$

where $h = 2e\xi_{ab}^2 H/\hbar$ (up to a factor of 2π, the field is expressed in units of H_{c2}), and ψ is the digamma function encountered in weak localization. Later, Maki[54] found another important contribution due to the correlations between two electrons of a fluctuating pair that survive even after the pairing has been destroyed. This term is always divergent, and should yield zero-resistance at all temperatures if no mechanism is present to break the surviving correlations; Thompson[88] found a way to rewrite the Maki term in a physical way by introducing the effect of a so-called pair-breaker, which is related to the inelastic lifetime τ_Φ.

$$\sigma_{MT}(T) = \frac{e^2}{8\hbar}\frac{1}{\delta - \epsilon}\log\frac{\delta}{\epsilon} \tag{5.4}$$

$$\sigma_{MT}(T,H) = \frac{e^2}{8\hbar}\frac{1}{\delta - \epsilon}\{\psi(1/2 + \delta/2h) - \psi(1/2 + \epsilon/2h)\} \tag{5.5}$$

where h and ψ have the same meaning as in Eq. 5.3, and $\delta = \pi\hbar/8k_B T\tau_\Phi$. In SI units, $\delta \approx 2.810^{-12}/T\tau_\Phi$, so that the Maki-Thompson (MT) term is only important if $\tau_\Phi \approx 10^{-13}$ s. The MT contribution was clearly seen only in very pure Aluminum films, and is rapidly destroyed by disorder and/or magnetic fields, whereas the Aslamazov-Larkin (AL) term is seen in most cases and represents usually the most important contribution. In addition, the AL term as a function of temperature represents the dominant singularity close to T_c, while the MT(T) term only introduces a slight downward-bending in R_{fl}(T) away from T_c. The expression used for the MT term is

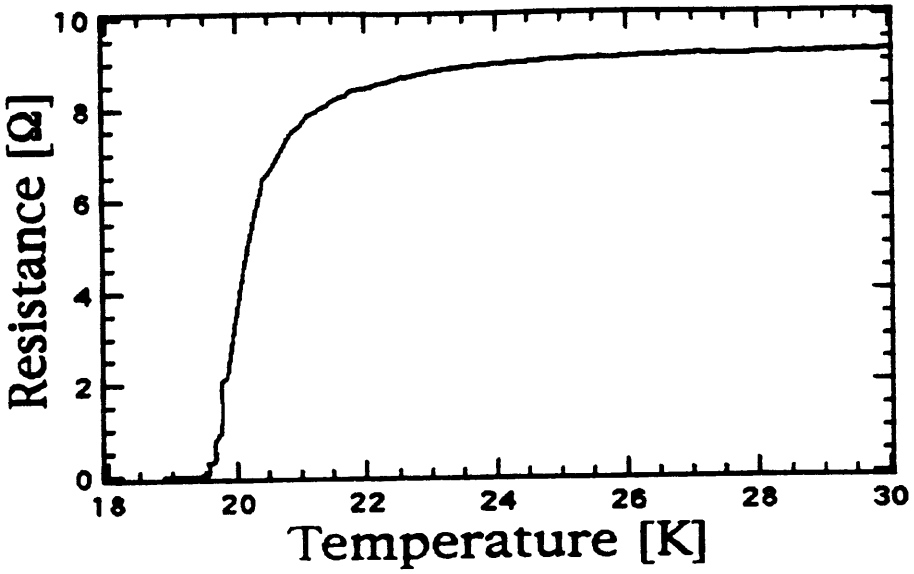

Figure 5-1: $R(T)$ close to the transition.

rigorously valid only close to T_c (within a few degrees)[15], and one of the difficulties of this term is that no closed expression is known to be valid in a large temperature and field range.

5.2 Resistance as a function of temperature in zero field

Figure 5-1 shows the resistance as a function of temperature in the vicinity of the resistive transition. While the lower part of the transition is usually believed to be due to flux flow, the upper part is certainly influenced by fluctuations, the T_c defined by mean-field theory being somewhere in between. We thus tried to apply Equations 5.1 and 5.4 to fit σ_{fl} determined by Equation 5.2. However, other factors influence the resistance and are superposed on the effects of the fluctuations, preventing the saturation of the resistance far away from the transition. In our case, the resistance is proportional to T^2 in a large temperature range[91], but deviations are seen at low temperatures, the exact form of which is not known precisely; the curves in magnetic field are influenced by the effects of weak localization at lower temperatures[47], and although here the functional forms are known, the precise parameters are not known.

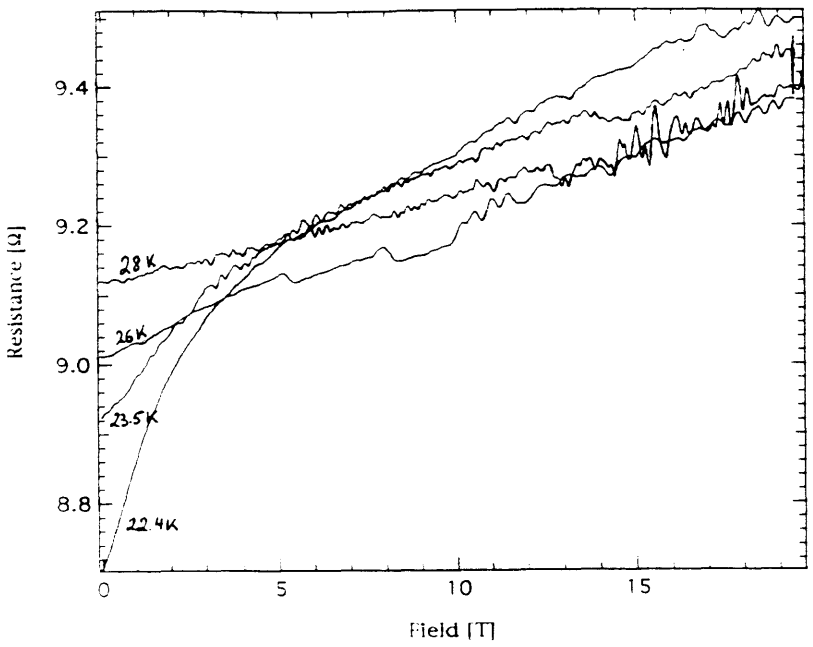

Figure 5-2: Resistance in perpendicular field between 28K and 22.4K.

We thus tried several constant values of R_n for the computation of R_{fl} for every fit. Although it turns out that some important quantities (critical temperature and slope of R_{fl} in its vicinity) are not too sensitive to the exact value used, this is obviously not a very satisfactory way to proceed. Especially, the respective importance of the AL term and the MT term cannot be obtained, since the MT term determines the downward-bending of R_{fl}, which is very sensitive to the exact choice of R_n. We thus started the measurements in magnetic fields above T_c, since the field dependence of R_n due to weak localization is not very important at these temperatures, and one can fit the field dependent part of the fluctuation correction more easily.

5.3 Experimental data above T_c and fit to the theory

Figure 5-2 shows the resistance in a perpendicular field for temperatures ranging from 28K to 22.4K. In the simplest approach, one proceeds as in the case of the fits to weak localization theory: one calculates the sheet-resistance per CuO_2 sheet from

the resistivity and the thickness; this is then inverted to yield the conductance, which is expressed in units of $\sigma_0 = e^2/8\hbar \approx 1/32.9k\Omega$. By subtracting the value in zero field, one obtains the correction due to the magnetic field alone:

$$\Delta\sigma = \sigma(T,H) - \sigma(T,H=0) \tag{5.6}$$

This is fitted to the expression:

$$\Delta\sigma = c\{\psi(1/2+\epsilon/2h) - \psi(1+\epsilon/2h) - \frac{1}{2\epsilon} + \frac{1}{\delta-\epsilon}(\psi(1/2+\delta/2h) - \psi(1/2+\epsilon/2h) - \log\frac{\delta}{\epsilon})\} \tag{5.7}$$

where c (equal to 1 in theory) is again a factor that adjusts for the imperfections of the sample and the inaccuracy of calculating the resistance of the single sheets, as in the case of weak localization. The use an automatic fitting routine did not yield meaningful results, because of the presence of many local minima that made the search algorithm converge to unsatisfactory solutions. We thus decided to try reasonable values for the different parameters and see if there is a given set of parameters that can describe all the curves. Also, our strategy was to start from the smallest possible number of parameters, and see which ones are really necessary. With this in mind, we first tried fits without the MT term, the only parameters being c, T_c, and ξ_{ab}. However, we found very unsatisfactory agreement for low fields: the experimental curves were always sharper than the theoretical prediction. This seemed to indicate the necessity to include the MT term, bringing in the supplementary parameter τ_Φ. The results of these purely 2D fits are shown in Figure 5-3. The parameters are: ξ_{ab}=80Å, c=.19 (close to the value .25 found for the weak localization fits), and the pair-breaking time is found to be $\tau_\Phi = 10^{-13}$s. The pair-breaking rate is thus quite strong. This is surprising in view of the weak localization results, which indicated a low inelastic scattering rate. The two rates are usually assumed to be similar[14], because the coherence between the members of a pair is not lost by elastic scattering. Because the phase-breaking time is measured quite indirectly by the MT term (through the pair-breaker δ), and furthermore the theoretical expression of the MT term is not

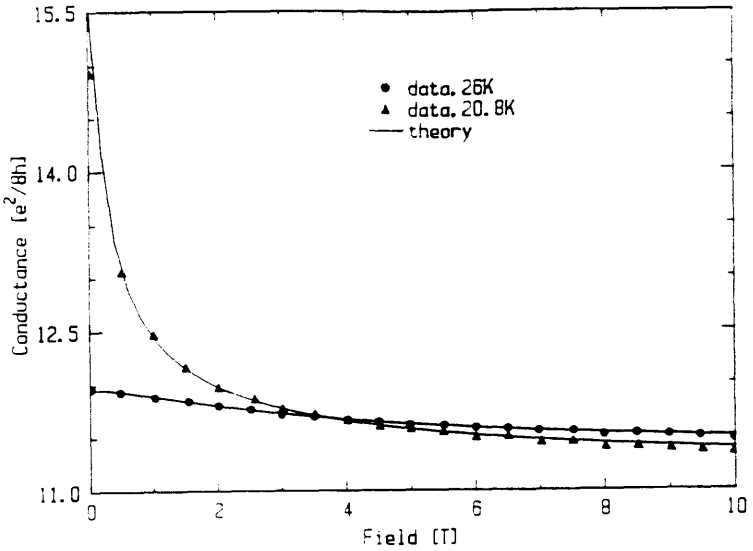

Figure 5-3: Data and fits to 2D Aslamazov-Larkin and Maki-Thomson terms. The vertical axis is the field-induced change in conductance expressed in units of σ_0 per plane. Only the two extreme temperatures are shown; the intermediate fits are as good.

valid in a large range of fields and temperatures, one might question value obtained. It should be pointed out that similar values have been found on $(La,Sr)_2CuO_4$[78] with the same method. Furthermore, the inelastic scattering time determined by the fits to weak localization theory was obtained at 4.2K. It was also found to be temperature dependent, and one can imagine that it may be much stronger at 20K. For this reason, it is difficult to speculate whether the discrepancy between the two values is an artefact or an important clue to the different scattering mechanisms in the superconducting and normal phases; more work will be necessary to completely clarify this point.

The fits allow one to extrapolate with some confidence what the resistance R_n would be in the absence of fluctuations; it is roughly constant in the range from 22.4 to 28K. We now compare the experimental value for R_{fl} obtained from Eq. 5.2 (by replacing R_n with this value) to the theoretical R_{fl} with c, T_c and τ_Φ obtained from these fits (Figure 5-4). In the temperature region where the field data were available,

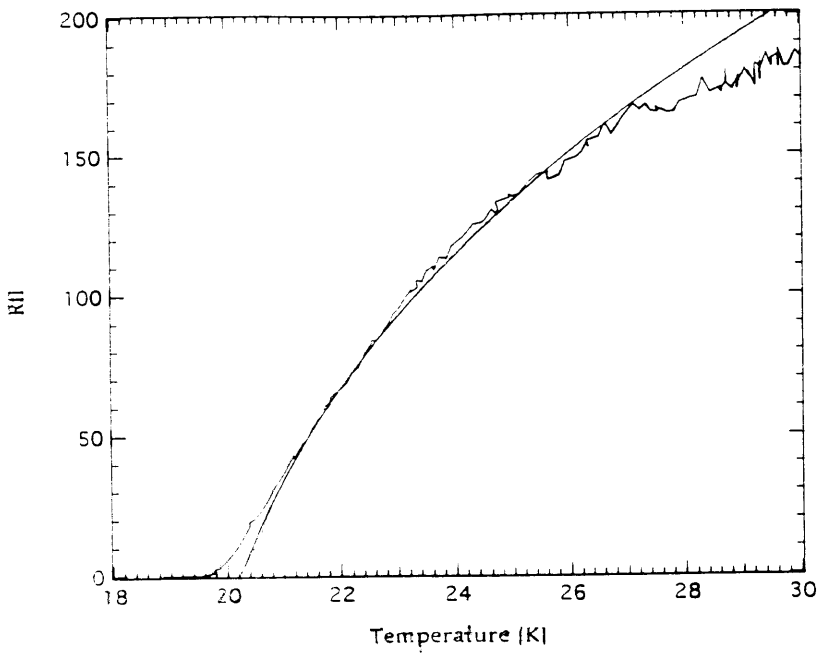

Figure 5-4: Comparison of experimental and theoretical R_{fl}. It should be noted that there is no free parameter here.

the agreement is good, considering that there is no free parameter. The deviation from linear behavior at higher temperatures is due to the influence of the MT term. We can thus conclude that the upper part of the transition is very well described by a purely 2D theory of fluctuations. This is in a way a surprising result because we know that we have a layered compound, not just a single thin film. We will examine next what we can say about the interlayer coupling.

The simplest model for layered superconductors is the phenomenological Lawrence-Doniach model[50], where the free energy of the layer is obtained by taking the usual Landau-Ginzburg free energy and dicretising in the c-direction (perpendicular to the layers). The discrete version of the gradient term can then be interpreted as a Josephson coupling between layers, and the coupling term can be related to the effective mass in the c-direction (M), or to the coherence length ξ_c along the c-axis. The attractive electron-electron interaction is taken to act only within each layer, in the spirit of the BCS model where the interaction is point-like. The model can also be extended to a microscopic theory and one can calculate the critical field for fields parallel or perpendicular to the layers[40]. It is also possible to generalize the results obtained

for fluctuations, and the results have been reviewed in [37]. These models are all based on mean-field theory, and one concludes that there is a single transition temperture where long-range order sets in in all three spatial directions, regardless of the actual strength of the coupling. Close to T_c, $\xi_c(T)$ diverges (in $1/\epsilon$) and will always become larger than the interlayer distance at some temperature close enough to T_c, at which point the layered superconductor becomes effectively three-dimensional. So one expects a smooth crossover from 2D behavior to 3D behavior. We know that close to T_c, the AL term is the most important, and we will ignore the MT term in what follows. For a layered superconductor, the AL term is

$$\sigma = \frac{e^2}{16\hbar} \frac{1}{\epsilon\sqrt{1 + 4\xi_c(0)^2/s^2\epsilon}} \tag{5.8}$$

where s is the interlayer spacing (6Å). The crossover from 2D behavior to 3D behavior as $\epsilon \rightarrow 0$ is clearly seen. We have tried to fit the temperature dependence of R_{fl}, using the same R_n obtained from the magnetic field dependence. We have not obtained a good fit with the value ξ_c =3 Å commonly found in the litterature (and obtained from extrapolation of the critical field measured by the onset of resistance in the parallel direction). The cross-over to 3D behavior produces a faster-than-linear divergence at the transition (i.e., a vertical slope for R_{fl}), which is not seen in the data. For ξ_c=1Å, we get the curve shown in Fig 5-5, which is still too curved. We conclude that the pure 2D theory gives the best fit to the data, which implies that the coupling between the planes is smaller than previously estimated.

Note: The distinction between 2D and 3D behavior is not obvious from the magnitude of the corrections alone, as it was in the case of weak localization. If we look at the temperature dependence, the fluctuations in 3D give a correction to the conductivity

$$\sigma_{AL}^{3D} = \frac{e^2}{32\hbar} \frac{\epsilon^{-1/2}}{\xi(0)} \tag{5.9}$$

Here the relevant coherence length is in the c-direction. For a single CuO_2 layer, one would thus predict a correction to the conductance (i.e., conductivity multiplied by

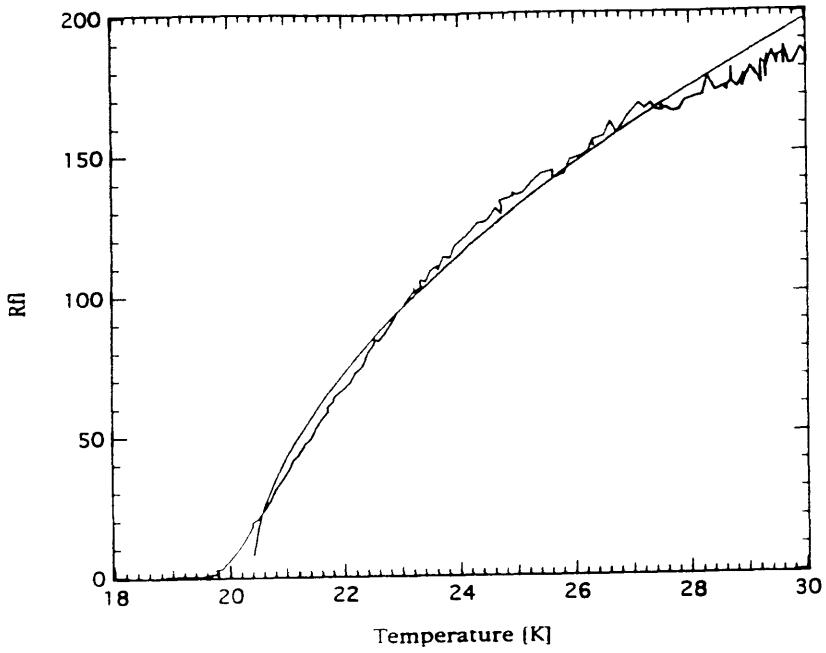

Figure 5-5: Comparison of R_{fl} to a model taking into account a dimensional crossover. We assume ξ_{ab}=1Å.

layer thickness) $\sigma = \frac{e^2}{32\hbar}\frac{s}{\xi_c(0)}\epsilon^{-1/2}$, which can be of the same order of magnitude as the 2D result because $\xi_c(0) \approx s$. However, in our case, it did actually turn out that the prediction of the 3D theory produces a smaller correction than what we observe.

5.4 Conclusions

The resistance as a function of temperature and field is well described by the purely 2D theory of conductance fluctuations above T_c. From the fits, we find it necessary to include both the AL term and the MT term. We find that the set of parameters ξ_{ab}=80Å, c=.2, and τ_Φ=10^{-13}s gives a good agreement to the theory. The value of the inelastic scattering time is very different from the estimate gotten from weak localization (10^{-11}s). It is not clear what this discrepancy is due to. Of the two methods, the Maki-Thompson result is likely to be the less reliable, mainly due to difficulties in the theory.

Chapter 6

The resistive transition in fields

6.1 Introduction

The motivation of the study of the resistance as a function of magnetic field was to extract the temperature dependence of the upper critical field H_{c2}, which allows in principle the evaluation of many physical parameters related to the conduction and to the superconducting properties: anisotropy, spin-orbit scattering rate, coherence lengths, etc. However, the determination of H_{c2} by a transport measurement is made difficult by the presence of fluctuations above and below T_c (vortices are topological excitations of the superconducting phase, and can thus be called fluctuations) causing a broad transition. Work published by other groups[35] has not taken this difficulty into accout, and the results obtained (such as the coherence length, or the observation of an upward bending of $H_{c2}(T)$) cannot be trusted blindly. We thus tried to apply the knowledge of fluctuations above T_c gained in the previous chapter to extract the values of the critical field in the perpendicular direction by extrapolation. We were also interested in exploring the 2D properties of $Nd_{1.85}Ce_{.15}CuO_{4-\delta}$ further by looking at the angular dependence of the critical fields (or, rather, the resistive transition in fields, since the determination of the parallel critical field turned out to be out of the range of the magnet used for the orientation-dependence measurements).

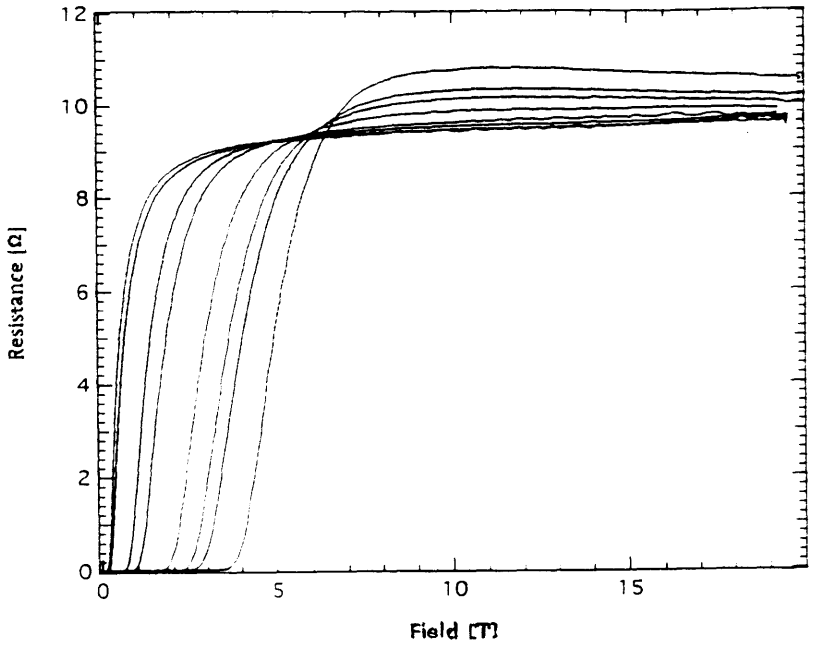

Figure 6-1: Resistive transitions in field at fixed temperatures. From left to right, the curves were taken at 19, 18, 17, 15, 13, 10, 8 and 5K.

6.2 Resistive transition in perpendicular fields

6.2.1 4.2K to T_c

Figure 6-1 shows the resistive transitions as a function of field at various temperatures between T_c and 4.2K. Close to T_c, the curves show a striking similarity to the resistive transition as a function of temperature, in that there is a fast initial rise followed by a rounded top. The curves broaden as the temperature is lowered, and the critical field becomes larger. Clearly, three regions can be recognized on each curve: at very low values of the resistance $R(H)$ compared to the normal state resistance (R_n), $R(H)$ varies over several orders of magnitude in a small field range. The detailed behavior in this region is not the focus of this work, and has been studied close to T_c elsewhere [97]. It was found that the $I(V)$ curves are non-linear for small currents and the dissipation is believed to be due to the motion of flux becoming unpinned, although the detailed mechanism is still a subject of great interest and controversy. We will

be interested in the resistance at higher fields, where $I(V)$ is linear, which happens roughly at about $R(H)/R_n$=.1. The second part of the curve is linear with field until one reaches a "knee" and changes over to a region of much slower increase of $R(H)$. The slope of the linear part of the curve decreases as the temperature falls, until about 4-5K, at which point it starts increasing again. In fact, the transition as a whole sharpens at these low temperatures, which means that most of the broadening is not caused by inhomogeneities. At high values of the field, the resistance decreases; this behavior has been explained by the effects of weak-localization.

Similar broadening of the transitions has been observed in YBCO[59, 13, 18]. The breadth of the transition (about 2T to go from 10% to 90% of R_n at 4.2K in our case, which represents 40% of the field where the resistance reaches half its normal state value) makes the determination of H_{c2} problematic. The use of criteria based on certain levels of R_n (50% or 90% usually) could lead to artefacts in the temperature dependence of the values inferred for the critical field[87], and can clearly only be used for very rough estimates. In early studies[35], the broadening had seemed less of a problem for $Nd_{1.85}Ce_{.15}CuO_{4-\delta}$, for the following reason: if one looks at the resistance as a function of temperature in a fixed field, the curves merely seem to fan out in the case of YBCO, with the upper part of the transition staying at a fixed point and only the "tail" shifting to lower temperatures [87]. In the case of $Nd_{1.85}Ce_{.15}CuO_{4-\delta}$[97, 35], the curves broaden but also show a clear shift to lower temperatures. This means that at least part of the temperature variation of H_{c2} obtained by the R/R_n criterion is real. But when one looks at the curves as a function of field, it is apparent that the error bars on H_{c2} at low temperature are still large. Figure 6-2 demonstrates the differences in the values and temperature dependences of H_{c2} that one gets from using different resistive criteria. This motivates our efforts to analyse the resistive transition in more detail, which we will do in the next section.

6.2.2 Fluctuations above H_{c2}

The complete theoretical expressions for the fluctuation conductance above H_{c2} are quite complicated. However, not too far from H_{c2}, the Aslamazov-Larkin expression

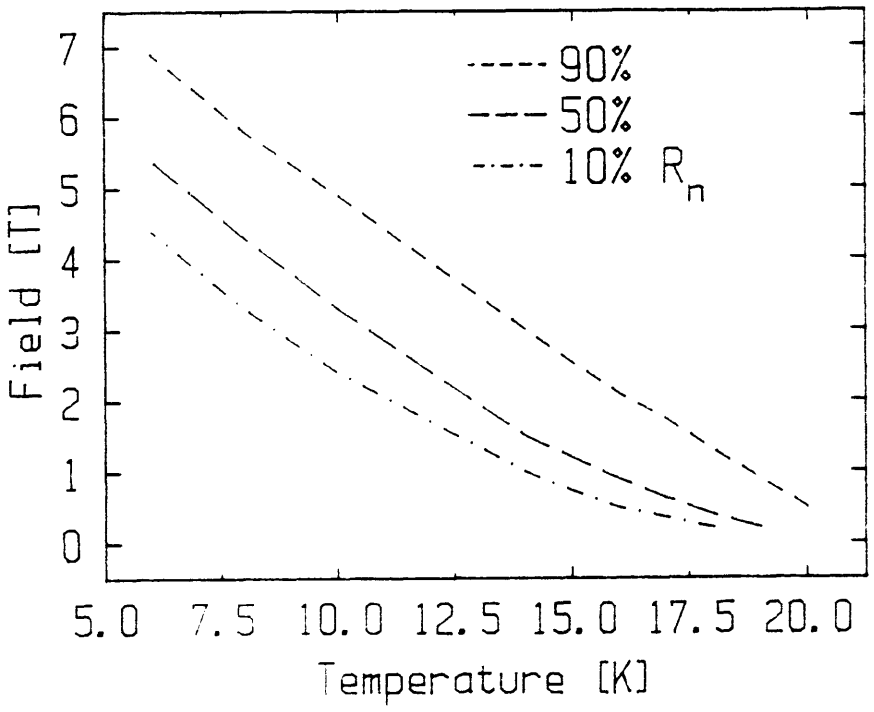

Figure 6-2: Comparison of three H_{c2} curves obtained by applying respectively the 90%, the 50% and the 10%R_n criterion.

can be written[5]:

$$\sigma_{fl} = \frac{e^2}{16\hbar} \frac{k_B T}{\frac{\pi De}{4}(H - H_{c2})} \tag{6.1}$$

where D is the electronic diffusion constant, which is related to the conductance through the Einstein relation 3.1. The Maki-Thompson term is more complicated, and should not be important because of the pair-breaking due to the field[19]. These equations are valid only in the case of a dirty superconductor ($\xi_{ab} > l$, where l is the mean free path), which will be assumed to hold in our case (we will come back to this at the end of the chapter). Close to T_c (down to about 15K) we took the value of R_n extracted in the previous section from the field dependent fluctuations above T_c. Figure 6-3 shows the values of R_{fl} extracted from the data from 19K to 13K. From the data, it is clear that as one goes down in temperature, R_{fl} deviates from the straight line at low values of the resistance (tail of the transition). But according to Eq. 6.1, the magnitude of the fluctuations does not depend on the value of H_{c2}, only on T, and thus the effect of fluctuations alone should result in a sharpening

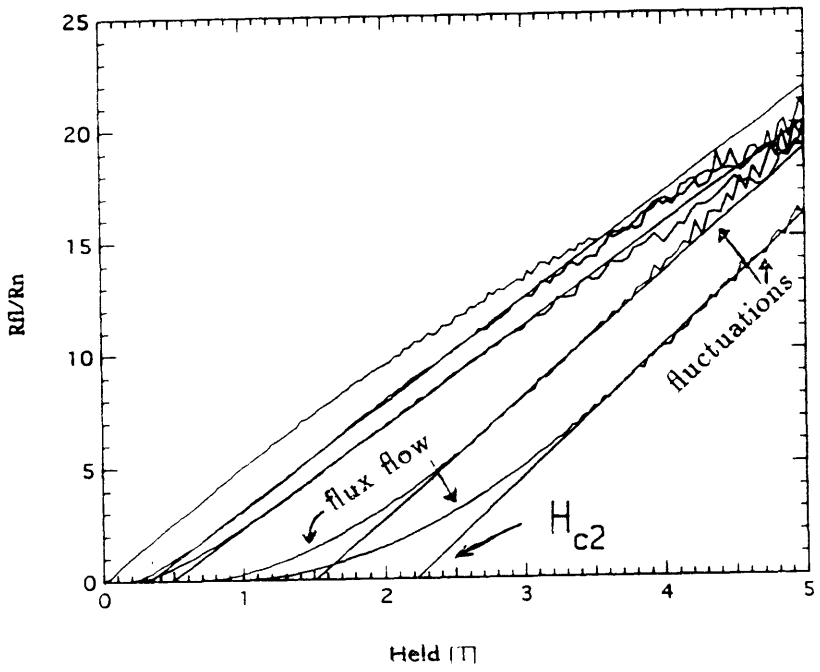

Figure 6-3: R_{fl}/R_n calculated from the data by keeping R_n = const, determined from the fits above T_c. From left to right, the curves are taken at 19K, 18K, 17.3K, 15K and 13K. Also shown are the straight lines fit to the data at higher fields. The slope of these lines is compared to the theoretical prediction in the text.

of the transition. The observed broadening together with the increasing deviation from fluctuation theory confirms the importance of other mechanisms in causing the broadening of the transition as the critical fields get higher. Thus it is clear that one can only hope to fit the high part of the curve to fluctuation theory. We will thus use the linear part of R_{fl} and determine H_{c2} by extrapolation to R_{fl}=0. As a consistency check, we use the slope to estimate D through the use of Equ. 6.1. We find a value of D= 4 cm^2 /s within 5% for the four curves shown, the same value as obtained from the conductivity through Eq. 3.1. It should be noted that an underestimate of the conductance per layer (expressed by a factor $c < 1$) will have exactly the same effect on the diffusion constant calculated by the Einstein relation and from the slope. Below 13K, the value of R_n becomes strongly temperature and field dependent, due to the effects of weak localization. Because the resistance at high fields turns downward, one does not get a straight line for R_{fl} if one assumes a constant R_n, but rather a linear part followed by a maximum and a downturn. So one does not expect an agreement to Equation 6.1 over a field range of more than a few T if one does not know the field dependence of the normal state resistance very precisely. In order to proceed, we decided to do the following: assuming a constant D equal to its value close to T_c where R_{fl} is very linear, we calculate the slope of R_{fl} at lower temperatures as predicted by the theory (i.e., the slope is assumed proportional to T). We then adjust R_n (field independent) so that the extracted R_{fl} has the right slope in its linear part. We then extrapolate the linear part to R_{fl}=0 to obtain H_{c2}. The critical fields obtained in this manner are all found in the upper part of the $R(H)$ curve. At 13K, R=.75R_n at H_{c2}, and their positions move to higher fractions of the normal state resistance as the temperature is lowered; this illustrates the danger of using a constant resistance criterion, or even worse, using the field where the resistance starts to deviate from zero as an estimate of H_{c2}.

Figure 6-4 shows H_{c2} as a function of temperature determined in this way. It is difficult to put error bars on the values obtained by our procedure, especially at low temperature. Above 13K, the $R_{fl}(H)$ curves are linear over a large field range, and the error due to the extrapolation (i.e., the choice of the interval where one chooses

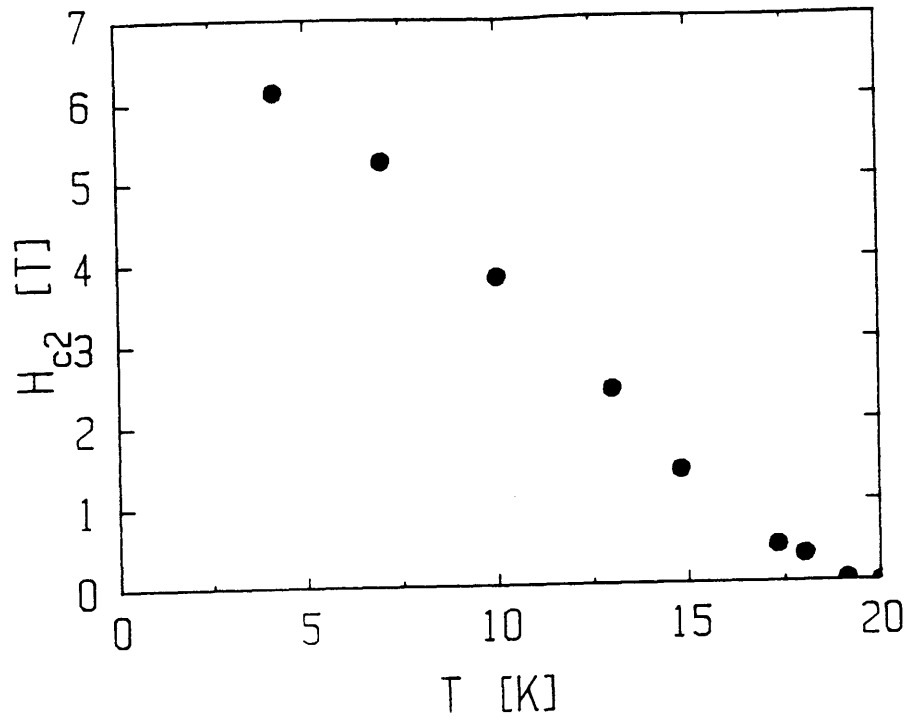

Figure 6-4: $H_{c2}(T)$ determined from extrapolation of the fluctuations. Note the upward curvature close to T_c.

to do the least-squares fit) should be lower than 10%. Of course, we assume that the AL theory describes our data well, but the beautiful straight line obtained close to T_c is very reassuring in this respect. At low temperature, the shape of R_{fl} and the extrapolated H_{c2} are extremely sensitive to the choice of R_n. If one knows the expected value for the slope of the linear part, the uncertainty is reduced to less than 10% due to the extrapolation alone. However, it is clear that the procedure rests on the assumption that the slope of R_{fl} is directly proportional to T. We will come back to this assumption later when we fit the critical field to the theory. Fortunately, the curves at lower temperature do get narrower, and if one assumes that the critical field is in the upper 80-90% and below the knee, one can reduce the error on H_{c2} considerably.

It should be noted that there is a slight upward-curvature in the temperature dependence of H_{c2} close to T_c, whereas the theory predicts a linear behavior. This can also be seen from the fact that at 19K, about 1K below the T_c extrapolated from

fluctuations, H_{c2} is still zero. Although an upward curvature is seen in the parallel critical fields of layered superconductors[40], there should be no such effect in the perpendicular field. The reason for this curvature is not well understood, but our analysis reveals that it is not an artefact due to the broadening of the transition. But it should be noted that the effect is much weaker than the upward-curvature observed when the H_{c2} curve is obtained by a resistive criterion. We will come back to this problem at the end of the chapter when we compare the $H_{c2}(T)$ curve to the theoretical predictions.

6.2.3 Extrapolation of the flux flow resistance

One would like to have another way of determining H_{c2}. It is inviting to try to extrapolate from the properties in the superconducting state. As already mentioned, it is believed that most of the broadening of the transition in fields is due to dissipation associated with the movement of flux (vortices)[87]. The idea of the extrapolation is the following: in the simple Bardeen-Stephen[12] model of flux flow, any current going through the sample will exert a Lorentz force on the flux lattice, causing a motion of flux perpendicular to the current and a dissipation due to the electric field induced by the moving flux. The expression for the resistance below H_{c2} is

$$R = R_n(1 - H/H_{c2}) \tag{6.2}$$

The prefactor is R_n because the dissipation really takes place in the normal cores of the vortices, and the linear increase is due to the ratio of material that becomes normal as the field is increased. At H_{c2}, where the whole sample goes normal, one smoothly goes over to the normal state resistance. Another model of the flux flow resistivity in dirty superconductors was proposed by Larkin and Ovchinnikov[48] and predicts a behavior

$$R = \frac{R_n}{(1 + \frac{f(b)}{b(1-t)^{1/2}})^{-1}} \tag{6.3}$$

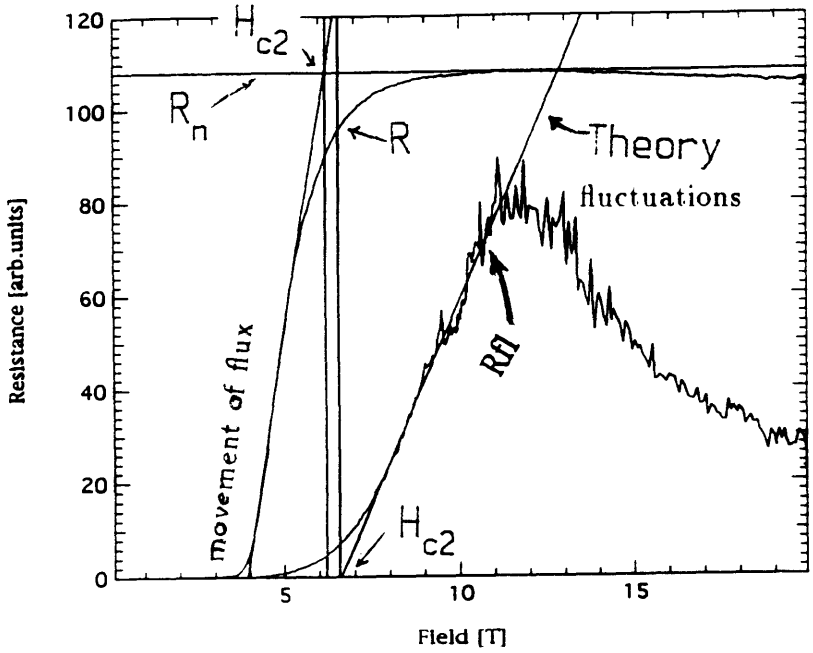

Figure 6-5: Comparison of H_{c2} values obtained by the two different methods described in the text. The data is taken at 4.2K.

where $b = H/H_{c2}$, $t = T/T_c$, and $f(b)$ is a function equal to 4.04 when b is small and equal to $0.43(1-b)^{3/2}$ when b is close to 1. This can in practice be approximated by

$$R/R_n \approx 1 - \alpha(T)(1-b) \tag{6.4}$$

where $\alpha(T)$ is between 2 and 4. Again, one finds a linear part close to H_{c2} and the extrapolation of $R(H)$ to R_n yields H_{c2}. Both models are valid in the absence of pinning, i.e., the resistance increases immediately in the field, whereas in our case it is zero until it reaches the region of activated behavior. Unfortunately, no reliable theory including the influence of pinning is available to this day. However, we will assume that once the barrier is overcome, the flux behaves similarly to unpinned flux, and that the resistance is again proportional to the amount of normal material. One thus gets H_{c2} by extrapolating the linear part to the value R_n. Figure 6-5 compares the two extrapolations at 4.2K. The extrapolation of the flux flow resistance yields H_{c2}=6.1T, compared to 6.6T for the fluctuations. The two values are within 10% of each other, which is all one can hope for. We also find $\alpha(T)$ within the right

Sample description	H_{c2}	$\Delta H/H$	T_c
LAF73 standard	6.8T	.4	20T
LAF79 standard	6.1 T	.6	21K
LAF73b standard	6.2 T	.4	19K
LAF76 no v.a.	5.6T	.7	17.5
LAF75 15" v.a.	6.9T	.4	19K
LAF95 standard	6.2T	.4	19.5K
LAF95-MGO on MgO	7.1T	.45	19K
LAF90 NGO(110)	7.5T	.45	<17K

Table 6.1: Values for H_{c2} , breadth of transition at 4.2K ($\Delta H = H_{50\%} - H_{10\%}$) and T_c measured on various samples.

boundaries. This good agreement gives us confidence in the validity of our method. It is clear that the measurement of H_{c2} is very difficult, and that one cannot expect to get an accurate value out of transport measurements. The fluctuation analysis is useful in providing at least some clue as to which part of the resistive transition one should look at. It shows that at low temperatures, one can use the $90\%R_n$ criterion or extrapolation of the flux flow part to get a reasonable approximation of H_{c2}. We will use these criteria for the remainder of this work.

6.2.4 H_{c2} at 4.2K

We have measured the resistive transitions at 4.2K of more than 10 samples prepared under various conditions. Table 1 summarizes the results of these measurements. There is some spread in T_c and H_{c2} for "standard samples" (i.e., prepared in N_2O, on $SrTiO_3$, and annealed for 30 minutes). The T_c's are between slightly above 19K and slightly below 21K, the H_{c2}'s are between 6.1T and 6.8T, thus a spread of about 10% on both parameters. To characterize the breadth of the transition, we show

$\Delta H_{90\%-10\%}/H_{50\%}$, and this value is 0.4 in all the samples, except for the sample with highest T_c, which has a broader transition. The same sample also has the lowest H_{c2}, which we will try to understand below. The sample without vacuum anneal has a lower T_c, a broader transition and a lower H_{c2}. The effect of the anneal is to give a sharper transition, which can be due to stronger pinning or to a homogenization of the oxygen stoichiometry through the sample. Samples prepared on $NdGaO_3$ and MgO substrates (all the other conditions being standard) do not show very different behavior from standard samples. Especially, the breadth is about the same although the channeling results suggest a better crystalline order for samples on $NdGaO_3$. This points to the interesting conclusion that crystalline disorder does not provide good pinning in $Nd_{1.85}Ce_{.15}CuO_{4-\delta}$. The sample LAF1090-NGO(110) was prepared on a $NdGaO_3$ substrate cut in the (110) direction. The X-ray diffraction pattern revealed a c-axis oriented film, but the resistivity was about an order of magnitude higher, and T_c was depressed to less than 17K. This is suggestive of a "dirty" sample. This film has the highest H_{c2} which is in agreement with the theory for dirty superconductors: a small diffusion constant means a high slope dH_{c2}/dT , and a correspondingly high $H_{c2}(0)$. For instance, in Nb_3Ge, with T_c=23.2K, one has $H_{c2}(0)$=36T. This might also explain why the sample with the highest T_c has the lowest H_{c2}.

6.2.5 Measurements below 4.2K

Only a few samples were checked down to .5K. Figure 6-6 shows the resistive transition below 4.2K for a sample prepared under standard conditions. The transition becomes sharper again, which is expected[87] since the temperature is lowered and the upper critical field is saturating, so that both flux flow and fluctuation broadening should decrease. However, the transition does not sharpen quite as fast as one would expect from the decrease in temperature. This might be due to sample inhomogeneity, which one expects from the sample to sample variations: it is unlikely that the breadth will decrease below 10% of H_{c2}. Figure 6-7 shows the resistive transitions at 4.2K, 1.2K and .5K for a sample deposited on MgO (left) and the sample deposited on (110)$NdGaO_3$(right). The curves at the two lower temperatures tend to similar values

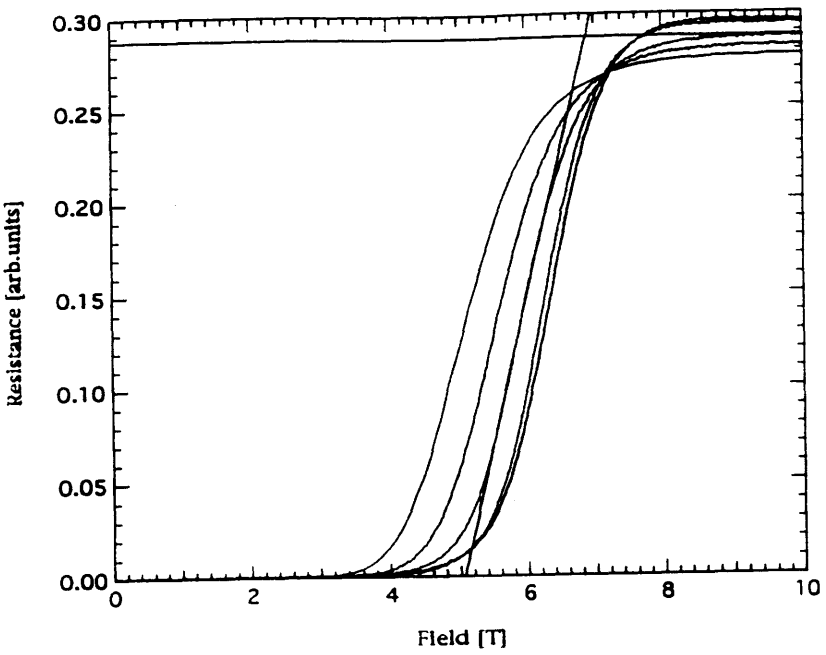

Figure 6-6: Transitions in field at 4.2K, 3K, 2K, .8K and .5K resp. from left to right.

at high fields, but cross each other close to H_{c2}. This is reminescent of the strong sharpening of the resistive transition at low temperatures that has been observed in thin Al films[82], where it was interpreted as a change in the order of the transition (from second order at high temperature to first order at low temperature). This change is due to the competition between the paired state and the Pauli paramagnetic state where the electron spins are aligned by the external field. As the critical fields grow, they pass a limit H_P called the Chandrasekhar-Clogston field above which the paramagnetic state becomes energetically favorable. The phase transition becomes a first order transition. In practice, spin-orbit scattering will push the limit to higher fields, but our weak localization experiments showed that the corresponding rate is very low, so that we are in a favorable case. The usual sign of the change in order is that $R(H)$ at lower temperature rises faster and crosses the curves at higher temperature. Because of the combined effect of increasing R_n and decreasing R(H) at low temperature, it is very difficult to judge if the crossing that we see is real or an artefact. Also, $H_P \approx 40T$ in our case, which is much higher than the perpendicular H_{c2}. Of course, this gives us strong incentive to measure H_{c2} in the parallel direction

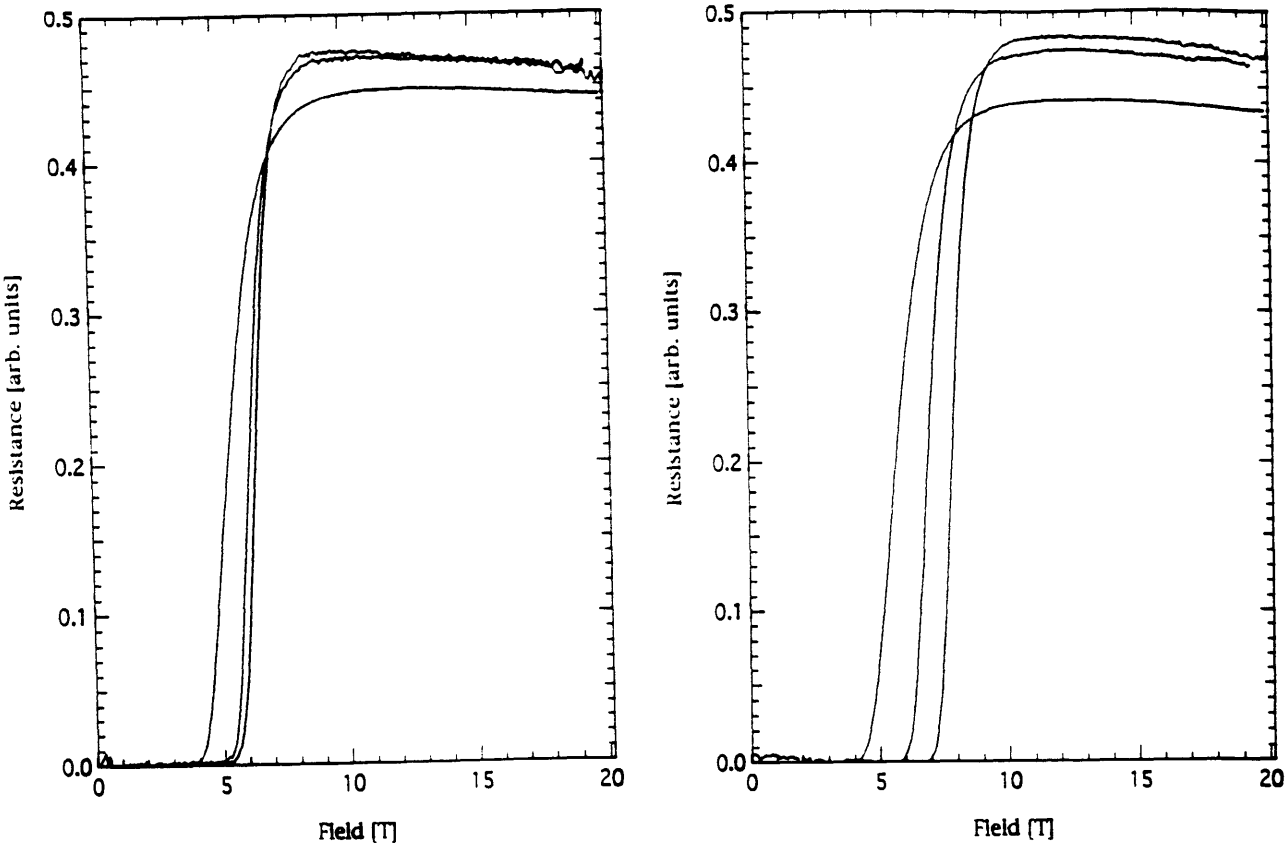

Figure 6-7: Resistive transitions in field for a film deposited on MgO(left) and a film deposited on a $NdGaO_3$ substrate cut in the (110) direction (right). The temperatures are 4.2K, 1.2K and .5K from left to right.

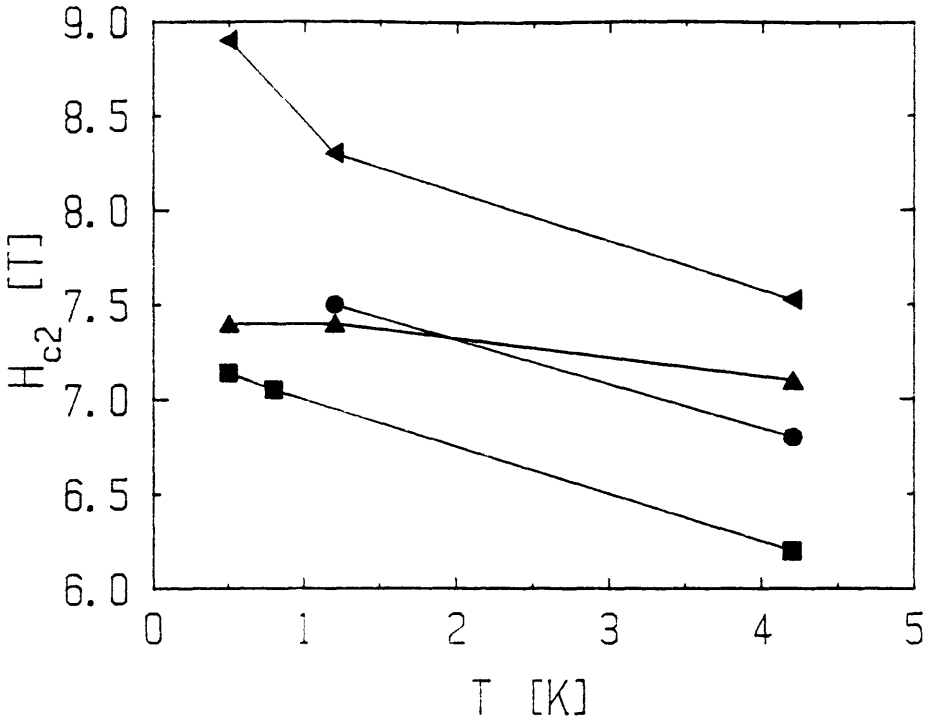

Figure 6-8: Recapitulation of H_{c2} at low T for several samples: ■, ●: standard conditions, on $SrTiO_3$, ▲ on MgO;◂ on $NdGaO_3(110)$.

in the new hybrid (35T) which should be available soon.

The right part of figure 6-7 shows the transitions for the high-resistivity sample made on (110) $NdGaO_3$. Unlike the two previous samples, the critical field is clearly still increasing considerably at the lowest temperatures. It is higher than on any other samples measured, reaching 9T at .5K, indicating a smaller coherence length (ξ_{ab}=60 Å). Here, the effects of weak localization (increase of R_n as T is lowered) are also much stronger.

Figure 6-8 recapitulates the temperature dependence of various samples measured below 4.2K. Except for the sample on MgO where H_{c2} has saturated, there is a clear upward slope which is not expected for such small values of the reduced temperature. The more disordered sample is clearly out of line, and shows an upward curvature. For the other samples, $H_{c2}(0) \approx$ 7.4- 8T, or $\xi_{ab} = 64 \pm 1$Å. This is shorter than the value obtained from the fits above T_c by 20%, but considering the difference in temperature at which the two estimates were done, this is actually a sign of good

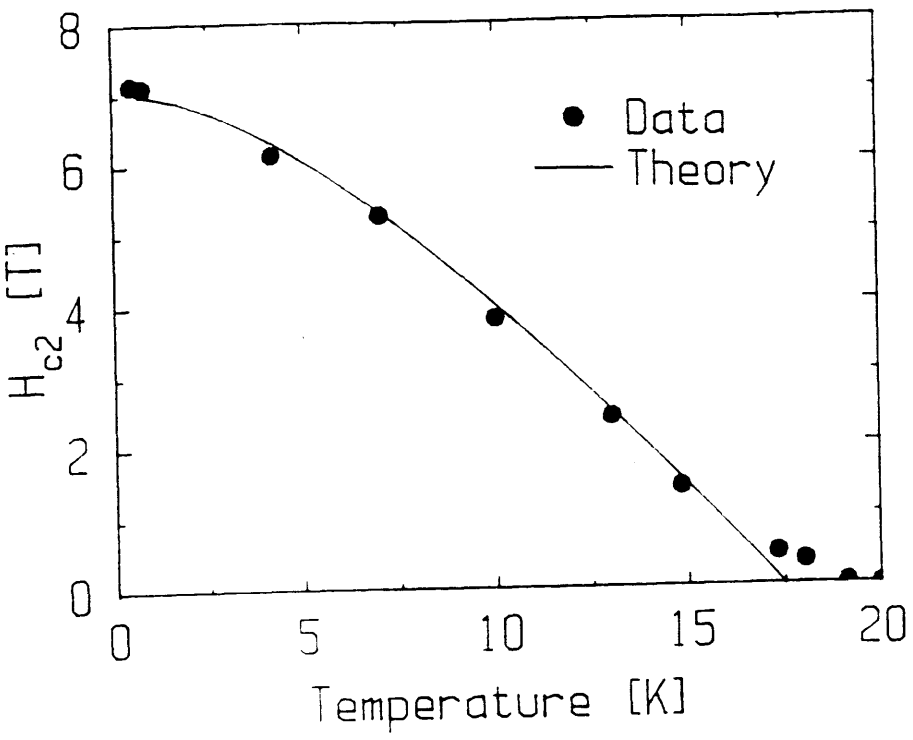

Figure 6-9: Fit of H_{c2} data to the WHH theory.

consistency.

6.2.6 Fit of $H_{c2}(T)$ to the theory

The WHH theory[94] predicts a linear variation of $H_{c2}(T)$ close to T_c whereas our data is somewhat upward-bent. It is thus clear that one cannot hope to fit the data close to T_c. It turns out that the upward curvature is often observed in conventional superconductors[85], and the usual procedure is to ignore the data close to T_c. Figure 6-9 shows the comparison of our experimental data to the WHH theory. It turns out that for values of D of the order of a few cm^2/s, the influence of Zeeman effects is negligible; this is consistent with the fact that $H_{c2}(0)$ is much smaller than H_P. We thus used the simple WHH formula with only two parameters (T_c and D), ignoring the spin terms. Below 15K, the agreement is excellent, better than our estimate of the error bars would suggest. The value of D extracted from the fit is D=2cm^2/s. This is a factor two lower than our estimate from fluctuation theory and conductance (which

both agreed). But as noted, the two previous estimates are affected by the knowledge of the absolute conductance per plane, whereas the estimate from the critical field curve is independent of that value. The disagreement is thus not to be taken too seriously.

Despite the good agreement, a doubt remains about the upward curvature of $H_{c2}(T)$, and the discrepancy for T_c: the value obtained from this fit is 17.5K, obviously lower than the value suggested by the transition (20.2K). Our explanation for this difference is the following: the ac-susceptibility shows a transition width of 1-2K, but the real spread in T_c might be even higher. We showed, both from theory and from experimental observations, that samples with high T_c have low H_{c2}, and vice-versa. As one goes down in temperature, regions with lower T_c become superconducting, and remain superconducting in higher fields. This can explain the upward curvature that we observe. But if one looks at the transition from above, one will see the strongest fluctuations from the regions with higher T_c which also have longer coherence length (and higher diffusion constants). This model can thus explain the few inconsistencies that we observe between the measurements at low temperature and close to T_c. It brings up again the question about the validity of choosing a constant diffusion constant for the extrapolation of H_{c2} from fluctuations, since the low-temperature behavior might be influenced by the parts of the sample with lower D. We went back to the extraction of H_{c2} at 4.2K, assuming D=2cm^2/s, rather than the value of 4 cm^2/s used previously. We found H_{c2}=6T, compared to 6.6T with the old value of D. This is only a 10% change, and it is closer to the value extrapolated from the flux flow assumption. As long as one assumes a slope of R_{fl} corresponding to a diffusion constant of the order of a few cm^2/s, the value of H_{c2} obtained will not vary much.

6.2.7 Summary of the measurements in perpendicular fields

We have used the knowledge gained from the study of the fluctuations above T_c to pin down the value of H_{c2} on the broad resistive transition. The effect of fluctuations on the transition is more and more hidden at temperatures below 13K by other effects

(possibly flux flow), which make the use of this method difficult at lower temperatures. We showed that one should look for H_{c2} in the higher part of the transition (90% of R_n). If one assumes a simple model for the flux flow resistance, one can get another extrapolation for H_{c2} giving values in good agreement with the fluctuation extrapolation on samples where both methods were used. From the fluctuation resistance, we extracted $D \approx 4$ cm^2/s, in good agreement with the value extracted from the conductance by the Einstein relation. The temperature dependence of H_{c2} follows the prediction of the WHH theory from 15K down to .8K. The upward curvature close to T_c is likely to be due to inhomogeneities. The diffusion constant obtained from the fit is D=2cm^2/s. From $H_{c2}(0)$, we obtain $\xi_{ab} \approx 64$ Å, also slightly different from the value obtained from the fluctuations (80Å), but this variation is consistent with our assumption that the "dirtier" parts of the sample influence the properties at low temperature. We conclude that the overall agreement to the theory is good, suggesting that we are in the presence of a not too unconventional superconductor in the dirty limit.

6.3 Measurement of the angular dependence of $R(H)$and H_{c2}

For a thin film ($d \ll \xi$), the effects of a perpendicular field and of a parallel field are quite different: a perpendicular field forces the electrons into Landau levels (ie cyclotron orbits), making the pairing more difficult and destroying superconductivity (orbital effect), whereas a parallel field can only act through the spin of the electrons (Zeeman effect). Parallel critical fields are thus usually much higher than parallel fields. Similar effects are expected for layered samples. However, there is a difference between a real 2D case and a very anisotropic 3D case. In the 2D case, one expects the critical field as a function of angle to follow Tinkham's law[86]

$$\frac{H(\theta)sin\theta}{H_{c2}^{\perp}} + (\frac{H(\theta)cos\theta}{H_{c2}^{\parallel}})^2 = 1 \qquad (6.5)$$

where $H_{c2}^{\perp}$ and $H_{c2}^{||}$ are the upper critical fields in the perpendicular and parallel direction, and $H(\theta)$ is the critical field measured for the angle θ. The anisotropic 3D case should follow the relation:

$$(\frac{H(\theta)sin\theta}{H_{c2}^{\perp}})^2 + (\frac{H(\theta)cos\theta}{H_{c2}^{||}})^2 = 1 \tag{6.6}$$

In particular, Tinkham's law predicts a cusp close to the parallel direction, whereas the anisotropic 3D behavior is smooth. This kind of measurement was done[62, 23] on YBCO and BSCCO samples, and it was found that BSCCO follows the 2D law whereas YBCO is anisotropic 3D. The criterion used for the determination of the critical field was the $10\%R_n$ criterion, so there is always a doubt as to what one is exactly measuring: dissipation due to moving flux, or true thermodynamic quantities? We are convinced now that the true H_{c2} lies somewhere in the upper part of the curve, just below or slightly inside the "knee" of the transition. Unfortunately, as shown in Figure 6-10, the 8T field available in the radial access magnet used for the orientation dependent measurements is barely sufficient to obtain 20% of R_n at 17K. It is surprising how broad the transition becomes in parallel fields. The curve is linear for a while, then curves away as in the perpendicular case, but the field scale is much higher. Since we do not have the whole curve in parallel field, it is difficult to even estimate the anisotropy. A conservative estimate based on the 30% criterion is a value of about 10 at 18.8K. If one extrapolates the linear part of the curve to the normal state value, one gets a field of about 10T. The perpendicular field is certainly smaller than .5T, so that the actual anisotropy might be closer to 20 at this temperature. The anisotropy increases further as the temperature is lowered. At 17K, a resistive criterion gives an anisotropy of about 20. The best thing we can do is to use a resistive criterion and compare the angular dependence of the fields thus extracted with the 2D and 3D behavior. We can then look back at the work done on BSCCO and YBCO (where the fields were extracted in the same manner), and see which one comes closer to NCCO. Figure 6-11 shows the angular dependence of the field at which the resistance reaches 30% of its normal state value for the run at

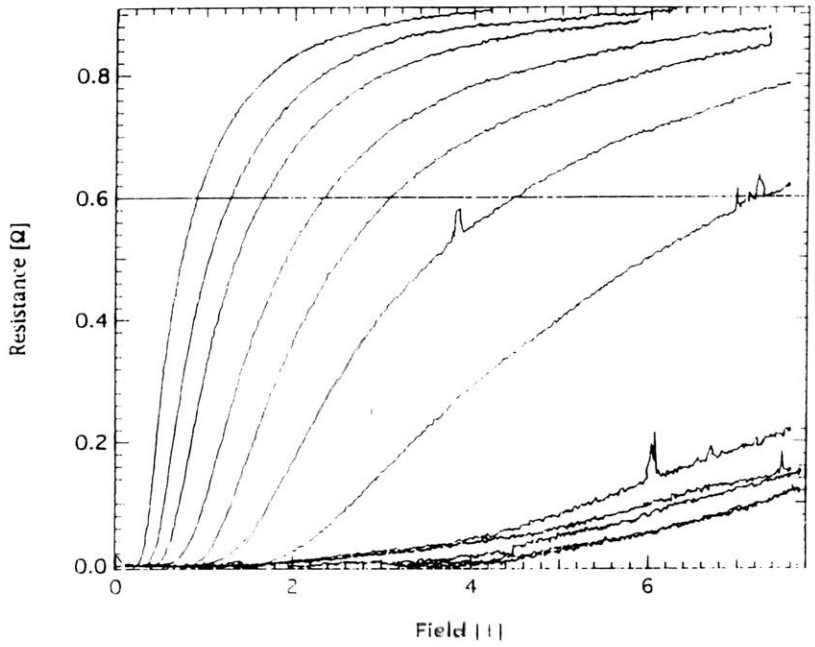

Figure 6-10: $R(H)$ at 17K for various angles between perpendicular field orientation at left and parallel at right.

18.8K, together with the two theoretical predictions. The two equations have as only parameters the parallel and perpendicular fields which one extracts from the data, and merely predict the behavior between these two values. The angular dependence is somewhat sharper than the 3D behavior. It is quite difficult to tell the two kinds of behavior apart when the anisotropy is high (10 or more), and one has to have very precise measurements close to parallel field. A further problem is that in order to see the resistance in parallel field, one has to be close to T_c; but there, one might expect more three-dimensional behavior (although the fluctuations above T_c do not show such a cross-over). The interpretation of the experiment is thus difficult; however, it looks like NCCO has a behavior intermediate between that of YBCO and that of BSCCO[62] if one applies similar criteria. This observation is quite important by itself and has not been made by other groups to the best of our knowledge.

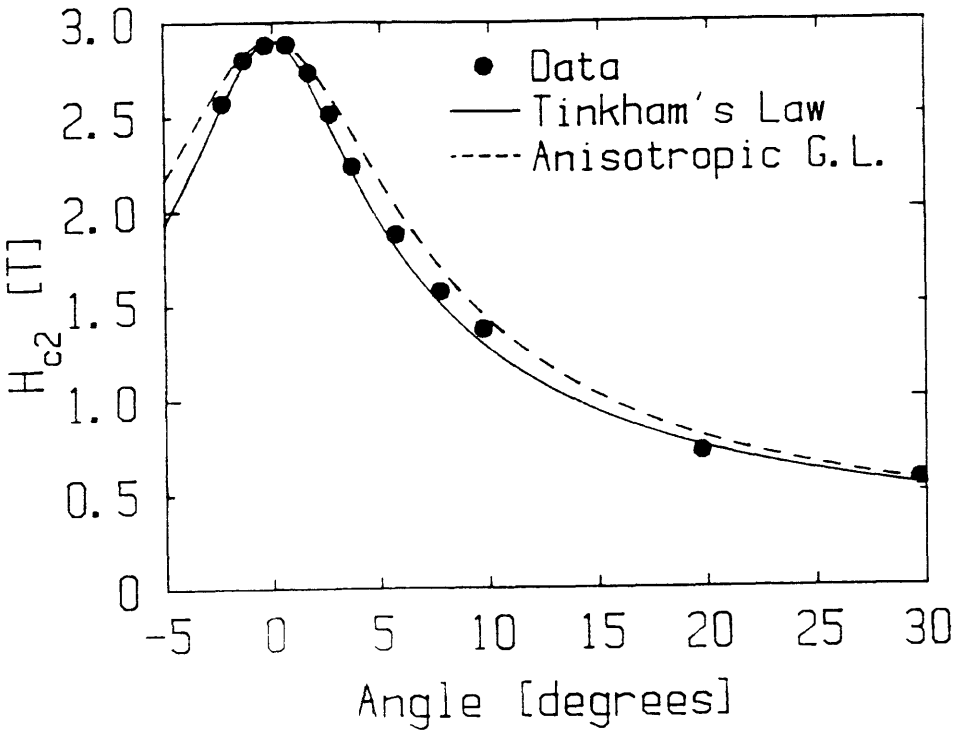

Figure 6-11: Angular dependence of the field where the resistance reaches 30% of the normal state value, together with the two theoretical predictions. Data taken at 18.8K. The error bar on H corresponds roughly to the point size.

6.4 Conclusion of the critical field work

We feel that we have made some progress in the problem of the determination of the critical field from transport measurements. The values that we get from the extrapolation of the conductance fluctuations are in good agreement with the WHH theory, and the extracted parameters are consistent with values obtained by fitting the fluctuations above T_c. We have shown that the critical field is to be found in the upper part of the resistive transition. If the parallel field case is similar, this means that much higher fields are required to get reliable information on the critical field in the parallel direction. This has rendered our initial idea to check the two-dimensionality of $Nd_{1.85}Ce_{.15}CuO_{4-\delta}$ by the angular dependence of H_{c2} more difficult to pursue. Using a resistive criterion to define a field at each angle, we found that this field follows a narrower angular dependence than the three-dimensional theory predicts. However, the fit to Tinkham's 2D law is not very satisfactory either, suggesting that the behavior $Nd_{1.85}Ce_{.15}CuO_{4-\delta}$ lies between that of YBCO (very 3D) and that of

BSCCO (2D, cusp-like).

Chapter 7

Tunneling on BSCCO and NCCO thin films

7.1 Introduction

Significant effort has been made to produce tunnel junctions based on high-T_c materials. Tunnel junctions made on conventional superconductors[75, 95] have allowed measurements of the energy gap[28] and the quasiparticle density of states, the phonon density of states[57], and many other important physical parameters like spin orbit scattering rates[81, 83] and Fermi liquid parameters [84, 29].Thus, tunneling experiments on high-T_c superconductors may give information about the mechanisms leading to superconductivity in these compounds. Tunneling has always been the ultimate goal of our film-making, and this explains why we chose to study BSCCO and NCCO in particular: it became clear in 1988 that it was extremely difficult to tunnel into YBCO, and it was believed that this was a result of the degradation of the sample surface in vacuum (oxygen loss). Although reproducible junctions can be made on YBCO films with a chemical etch[32], the observed structures do not look intrinsic to superconductivity. Because both BSCCO and NCCO have the highest T_c when they are slightly reduced, and especially NCCO has a much more stable surface when exposed to air[92], one hopes for a more successful junction preparation.

Before our results on BSCCO published in 1990[45] (reported in more detail be-

low), some bulk work had been done on this compound by various groups (cf[45] for a review of some earlier results), especially by Ekino *et al.*[22], who found gap values in the c-direction of 25 mV and 20 mV respectively for the 110K and the 85K phase. To our knowledge, we were the first group to report a thin film result. Some more recent work has confirmed our results since then[58].

The work available on NCCO(bulk)[21, 80, 98] suggests a gap around 3.5mV, and a reduced gap $2\Delta/k_BT_c \approx 3.5 - 4$[98]. Except for the work shown in [98], the gap-structure is always very broad, making a accurate determination of the gap value difficult. Only Ref.[98] sees a BCS-like density of states, by inserting a tunneling tip deep into the material. Because it is well known that point-contact measurements are prone to artefacts related to single-particle charging effects of the tunneling tip, these results should be viewed with caution.

We start by presenting a brief introduction to tunneling spectroscopy, followed by our work on BSCCO thin films. We then talk about NCCO, where we have tried both out of plane (c-axis) and in-plane tunnel structures, the latter through the use of bi-crystals.

7.2 Principles of tunneling spectroscopy

We will call tunnel junction a structure constituted by two conductors (at least one of which is superconducting in our experiments), separated by a thin insulating barrier in the ideal case (a thick, semiconducting barrier is sometimes the only practical solution). In the case of two superconductors, the quasiparticle part of the tunneling current can be written as[75, 95]:

$$J \propto \int_0^{+\infty} dE \rho_L(E)\rho_R(E - eV) \mid T \mid^2 [f(E) - f(E - eV)] \tag{7.1}$$

where E is the quasiparticle energy, ρ_R and ρ_L are the quasiparticle densities of states in the two electrodes called right and left, V is the bias, $\mid T \mid^2$ is the square of the modulus of the tunneling amplitude, and f is the Fermi function. This expression is

very intuitive and is most simply understood with the semiconductor model, where the two densities of states are shifted with respect to one another by the bias voltage and the current is just proportional to the number of filled states facing empty states. The derivation of the expression is not trivial[95] because one has to take the coherence factors into account. It is also worth noting that only the total energy enters the expression, not the term associated with the k_z component of the electron motion. We will use this expression for the case where one of the electrodes is normal(SIN), where it reduces to Giaever's discovery[28].

The influence of different terms on the conductivity as a function of bias is well known. When $\mid T \mid^2$ is independent of E and V, the densities of states are the only bias-dependent factors and their influence on the conductivity is then easy to evaluate (we will discuss the energy dependence of the barrier transmission below). Let us briefly recapitulate the main results in the $T = 0$ case; here $f(E) = 1$ for $E < E_F$ and 0 otherwise. One then has:

$$I \propto -\int_{E_F}^{E_F+eV} \rho_L(E)\rho_R(E - eV)dE$$

(we changed from current density to current) and

$$G = dI/dV \propto -\int_{E_F}^{E_F+eV} \rho_L(E)\frac{d}{dE}\rho_R(E - eV)dE \; + \; \rho_L(E)\rho_R(E - eV)$$

In the SIN case, one then takes ρ_L to be a BCS density of states

$$\rho_L(E) = \frac{E - E_F}{\sqrt{(E - E_F)^2 - \Delta^2}} \text{when}(E - E_F > \Delta)$$

(and there are no states below the gap Δ) and $\rho_R = \rho_N(E_F)$ (the normal metal does not have any features in its DOS within a few Δ of E_F, since gaps of known superconductors are much smaller than Fermi energies). In this case, the first term does not contribute and $[dI/dV](V)$ is proportional to $\rho_S(eV)$. The SIS case is similar: both DOS are of the BCS form with two different gaps Δ_1(right) and Δ_2 (left, and assumed to be larger). This time, the second term is always zero because there are

no states at E_F. It is clear that one will have peaks (singularities) when both E and $E - eV$ hit the singularities of their respective functions, which leads to $eV_{peak} = \Delta_2 \pm \Delta_1$. The peak associated with the minus sign is not observed at $T = 0$ because the energy Δ_2 needed in the DOS is out of the bounds imposed by the rigorous cut-off of the Fermi function, since $eV = \Delta_2 - \Delta_1 < \Delta_2$. So one sees a strong peak at the sum of the gaps, with an enhanced singularity due to the derivative of the BCS square-root singularity, and a much weaker, temperature dependent peak at the difference. However, it is important to realise that this conclusion is based on two assumptions: the total absence of states in the gap, cancelling the second term in the expression of the derivative, and a strong singularity for the derivative at the gap value. If these assumptions do not hold, as we suspect may be the case for high-T_c superconductors as we will see below, one does not necessarily expect much to happen at the sum or the difference of the gaps. Another problem already hinted at earlier is the introduction of structure from the barrier, which we will discuss below in connection with the parabolic conductance at high bias observed in our BSCCO junctions.

7.3 Results on BSCCO

We measured the conductance of a tunnel junction made on a thin film of Pb-BSCCO containing both the 110 K and the 85 K phase, using a conventional superconductor, Al, as a counter electrode. We found

$$2\Delta/k_B T_c = 5.5 \pm 0.6$$

We explain the observed asymmetry and parabolic background of the differential conductance curves in the framework of conventional normal metal-insulator-normal metal (NIN) and superconductor-insulator-normal metal (SIN) junction theory at zero temperature. This procedure leads to a simple approximate method of separating the density-of-states contribution to the tunneling current from the contribution due to

the dependence of the barrier height on the applied bias.

7.3.1 Junction Preparation

Our thin films were sputtered from a pressed, non reacted powder target, containing Pb_3O_4, Bi_2O_3, $CaCO_3$, $SrCO_3$, CuO, with Pb:Bi:Sr:Ca:Cu in the ratios .3:1.7:2:2:3. The sputtering gas was Ar with about 20% O_2. Cleaved MgO crystals were resistively heated in a Pt foil to 860°C (evaluated by pyrometer) during deposition. The films were annealed for a short time (furnace heat-up to 860°C, then 10 minutes at that temperature, followed by quenching to room temperature), and X-ray diffraction patterns showed mostly the peaks corresponding to a c-axis oriented film of the 85K material(1112). The resistive transition (Figure 7-1, insert) shows the presence of the 110K (2223) phase, and the resistance was zero by 78 K. We conclude that our films contained 110K material, 85K material, and other material driven into the superconducting state by proximity effect, thus decreasing the transition temperature. There is some uncertainty in choosing the right value of T_c for calculating $2\Delta/k_BT_c$. We decided to take the midpoints of the transitions for this purpose: 84K and 105K. XPS measurements showed that Pb was almost completely gone after the anneal.

An artificial barrier of aluminum oxide was sputtered onto the annealed films. The thickness, evaluated by a previous calibration, was on the order of 20Å. The cross-strips were evaporated aluminum(1000Å).

7.3.2 Experimental results

Figures 7-1 and 7-2 show the differential conductance as a function of the bias at different temperatures. As the temperature falls, we see several features appearing and becoming sharper. At 4.2K and below, there is a region of very low conductivity (in comparison to the background), with two pairs of peaks. At 0.9K, below the T_c of Al, the peaks further sharpened, as expected for conventional SIS tunneling.

These peaks can be seen as two pairs at nearly equal positive and negative biases, although there is a slight asymmetry in the tunneling conductance. If we consider

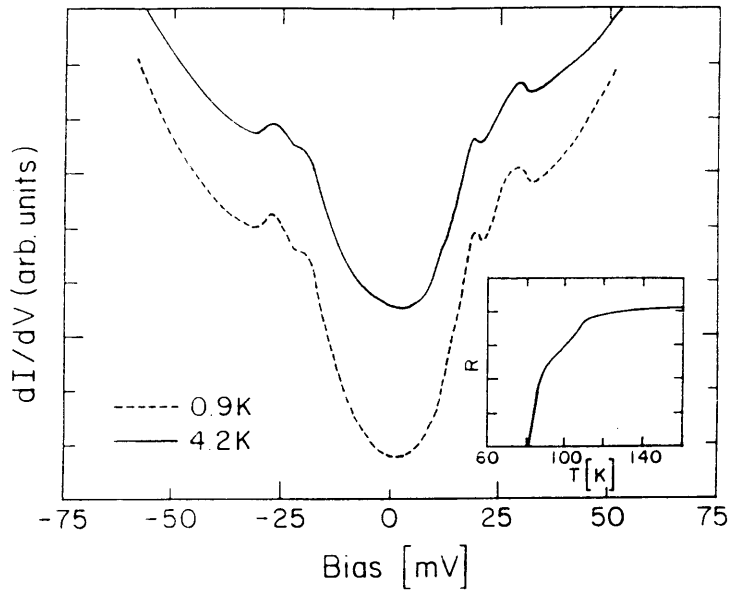

Figure 7-1: Plot of low temperature dI/dV as a function of V. The curve taken at .9K was shifted down vertically by one division (as shown) for clarity. The same bias convention is used in all the figures. Inset: Resistive transition of the film used for tunneling.

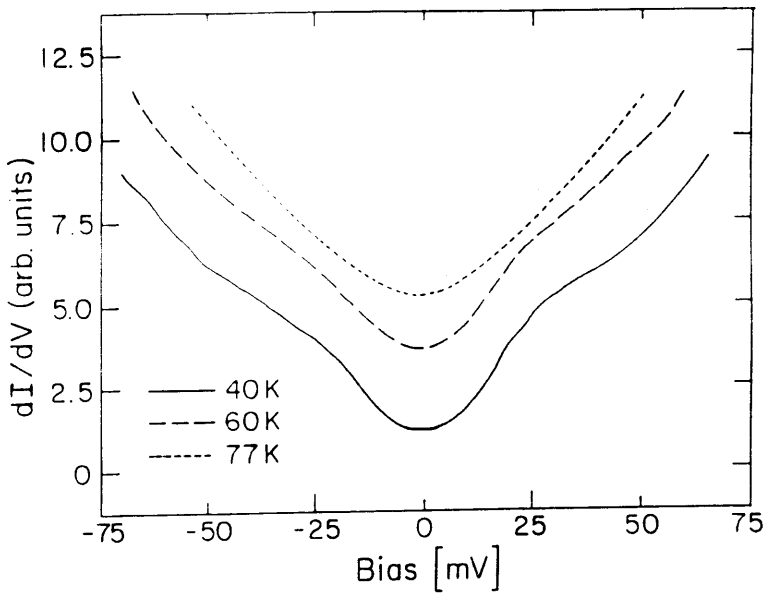

Figure 7-2: Measured dI/dV at higher temperatures. These data were taken on the same junction as the previous figure. The zero of conductance corresponds to the curve taken at 77K.

the junction as consisting of many parallel junctions formed between the Al film and the grains of various phases of Bi-Sr-Ca-Cu-O, we can relate these peaks to the gaps of the two superconducting phases seen on the resistive transition, obtaining

$$\Delta_1 = 18 - 21 \text{ mV for the } (2:2:1:2) \text{ phase,}$$

$$\Delta_2 = 25 - 28\text{mV for the } (2:2:2:3) \text{ phase,}$$

and

$$2\Delta/k_B T_c = 5.5 \pm 0.6$$

for both phases. The agreement of the presumed reduced gap parameters is supportive of the association of the observed features and the superconducting energy gaps of the phases. The reduced parameters are higher than the BCS weak-coupling value of 3.5, but not extraordinary in comparison to strong coupling superconductors, such as Pb and amorphous Ga which have shown values up to 4.5.

Various characteristics of the measured data obstructed our efforts to interpret conductance directly in terms of the quasi-particle density-of-states (DOS). There was some leakage conductance at low temperatures, probably due to normal regions in the BSCCO surface. Although this level of leakage would be intolerable in conventional junctions, it is more than respectable for high-T_c work. Tunneling from superconducting Al (T_c =1.2K for 1000Å films) into another superconductor should split the gap peaks into sum and difference peaks. But as mentioned earlier, this holds only if both sides of the junction have very sharp (singular) DOS. In any case it is reasonable to assume that if there is a superconductor with a gap of several tens of mV on the other side of the barrier, the opening of the Al gap will not have an effect big enough to be detected under the conditions of this experiment.

We were not easily able to follow the gap to temperatures higher than 60K, because the background became too strong compared with the interesting features. But, as we explain below, when the parabolic background was divided out, structure in the dI/dV curve related to the gap could be seen. Unfortunately, the thermal broadening at this temperature is high, and it is difficult to extract the numerical value of the

gap. Although it is possible to deconvolve this broadening in many cases, we were not able to do it with our experimental curves, presumably because even the dI/dV curves at very low temperature lack sharp features. This makes a deconvolution difficult to perform in practice. We note that the suppression of sharp features at the gap voltage has been observed in conventional superconducting junctions using semiconductor barriers such as amorphous silicon. The very low barrier and electron traps in these barriers cause rounding of the features. The surface layer of the Bi-Sr-Ca-Cu-O may have caused this effect in the present experiment.

7.3.3 Elimination of the parabolic shape

The high bias part of our conductance curves can be well fitted by second degree polynomials $G = G_0(1 + bV + cV^2)$, where b=0.0025 and c=0.00025 when V is given in mV. In our data the linear term always gives a contribution of less than 10% to the total conductivity in the bias range between 0 and 60 mV. For physical reasons, even powers of V should not contribute much to the current, which entails that odd powers of V should be small in the derivative dI/dV.

It has been observed previously, with conventional superconductors, that tunnel junctions show a parabolic conductance, although in most cases the V^2 term only becomes important at biases of the order of 100mV, far away from the gap of conventional superconductors. There is also very often a slight asymmetry, due to a small linear correction. Both effects are usually attributed to the influence of the barrier. We have so far assumed that the $\mid T \mid^2$ term has no energy dependence. The usual WKB expression for the barrier transmission is

$$\mid T \mid^2 \propto e^{-2\int_{t_1}^{t_2} \sqrt{2m(\phi(t)-E_z)/\hbar^2}dx}$$

where ϕ is the barrier height, $t = t_2 - t_1$ the thickness, x a parameter varying between T_1 and t_2, and $E_z = \hbar^2 k_z^2/2m$. The application of the bias will cause an additional term to the barrier height, and one has $\phi(x, V) = \phi + eV(x - t_1)/t$. The influence of this bias dependent term been studied by Stratton[76] on planar NIN junctions. He

finds a current of the form:

$$J \propto V + aV^2 + bV^3,$$

where a is zero for a symmetric barrier, and b is of order $\frac{1}{6}\alpha^2 t^2/\phi$, where and α=1.025eV$^{-1/2}$Å^{-1}. In most experiments, one observes both kinds of behavior: The rapid variations due to the densities of states, and a slowly rising parabolic background due to $\mid T \mid^2$. It is clear that this effect is especially strong for low barriers (low compared to typical values of eV).

For the case of a typical Al/Al_2O_3/Al junction with ϕ=1V and t=10 Å, the coefficient of V^2 is close to 50V^{-2}. Our curves can be fitted with coefficients of the order of 300V^{-2}. To see if this is reasonable, we assume a barrier composed of two sections: between 0 and t_1, the barrier height is ϕ_1, and between t_1 and t_2, it is ϕ_2. This incorporates the effect of a bad surface in addition to the artificial barrier. We assume that the artificial barrier has a thickness of 15Å and a height of 1 eV. Then an additional 5Å of a barrier of height 0.5 eV give the desired curvature, while the linear term associated with the asymmetry remains very small.

7.3.4 Application to our data

There are at least three contributions to the total conductivity: a contribution from superconducting regions with a T_c close to 80K; a second contribution from regions containing the 110K phase; and a third contribution called a leakage current, which we assume to be due to non-superconducting regions in the thin film. We assume that these conductances add up as for parallel circuits. The current through a tunnel barrier being an exponential function of $-t\sqrt{\phi}$, variations in the barrier thickness of a few Å, or variations in the barrier height of a few tenths of a volt, change it by several orders of magnitude. Thus, if different regions give contributions to the current which are comparable in magnitude, then the barrier characteristics associated with these contributions must be almost identical. It is then reasonable to assume that the curvature of the differential conductance, which is a much smoother function of the barrier parameters, is the same. Fig. 7-3 and 7-4 show the result of dividing out

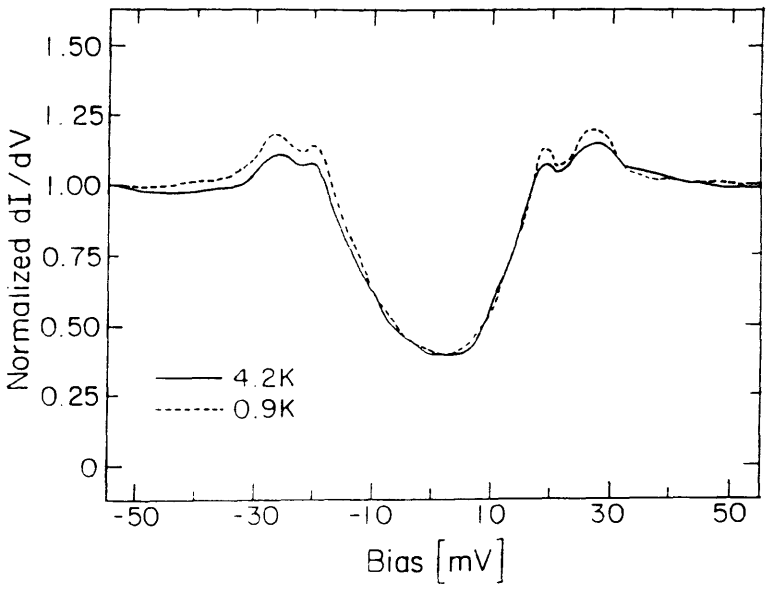

Figure 7-3: Low-temperature dI/dV after dividing out the parabolic background.

the parabolic dependence. Because of the various assumptions and approximations we made, these curves can probably not be directly interpreted as being (thermally broadened) densities of states, but they show several features that one would expect from the quasi particle DOS of a superconductor: a region of low conductance, which looks like the indication of a gap although there is a slow and continuous rise, followed by a peak, which is not quite as high as would be a BCS peak. All of these features were already visible in the original data, but they become much clearer after this numerical treatment. The upper and lower bounds given for Δ stay valid.

7.3.5 Conclusion

The tunneling conductance of our BSCCO/Al_2O_3/Al junction displays features all of which have been seen before in conventional superconducting tunnel junctions. At low temperature, the conductance curves display peaks which can be interpreted as arising from the gaps of the two superconducting phases present. The voltage at which these peaks appear are in the ratio of the T_c's of the two phases and give a reduced gap of 5.5. The parabolic behavior of the conductance is consistent with tunneling theory and

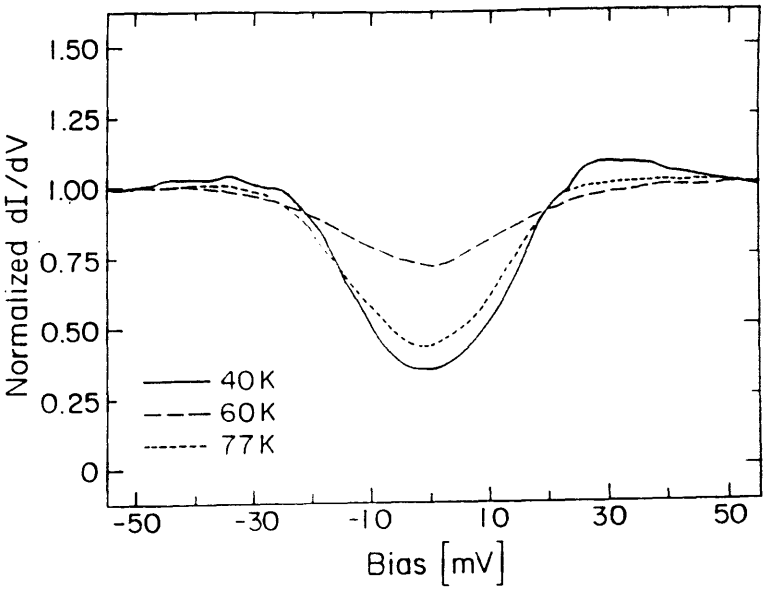

Figure 7-4: dI/dV at higher temperatures after parabolic background was divided out.

can be understood by assuming that a surface layer of the superconducting material is semiconducting and gives an additional barrier. The rounding and attenuation of the peaks is reminiscent of similar structure seen in tunneling conductances of conventional superconducting junctions with semiconducting barriers. The non-zero conductance at low temperature and small bias is also likely to be the result of poor surface quality. We therefore feel these conductance data demonstrate the existence and magnitude of the energy gap in BSCCO.

Some very recent results[58] have confirmed our interpretation. Various groups are now able to grow BSCCO in a much more controlled way, and can artificially reproduce the layered structure of the various phases on a sub-monolayer basis, using in-situ RHEED monitoring of the growth. It is thus possible to cleave a crystal of BSCCO(2212), check the surface quality, and then deposit epitaxially a layer of the semiconducting (2201) phase. Because of the semiconducting nature of the barrier, one needs quite thick barriers (usually a few 100Å). A 2212/2201(300Å)/Au junction fabricated in this manner yielded Δ=18mV, or a reduced gap of 4.7. The temperature dependence of the gap appeared to be BCS-like.

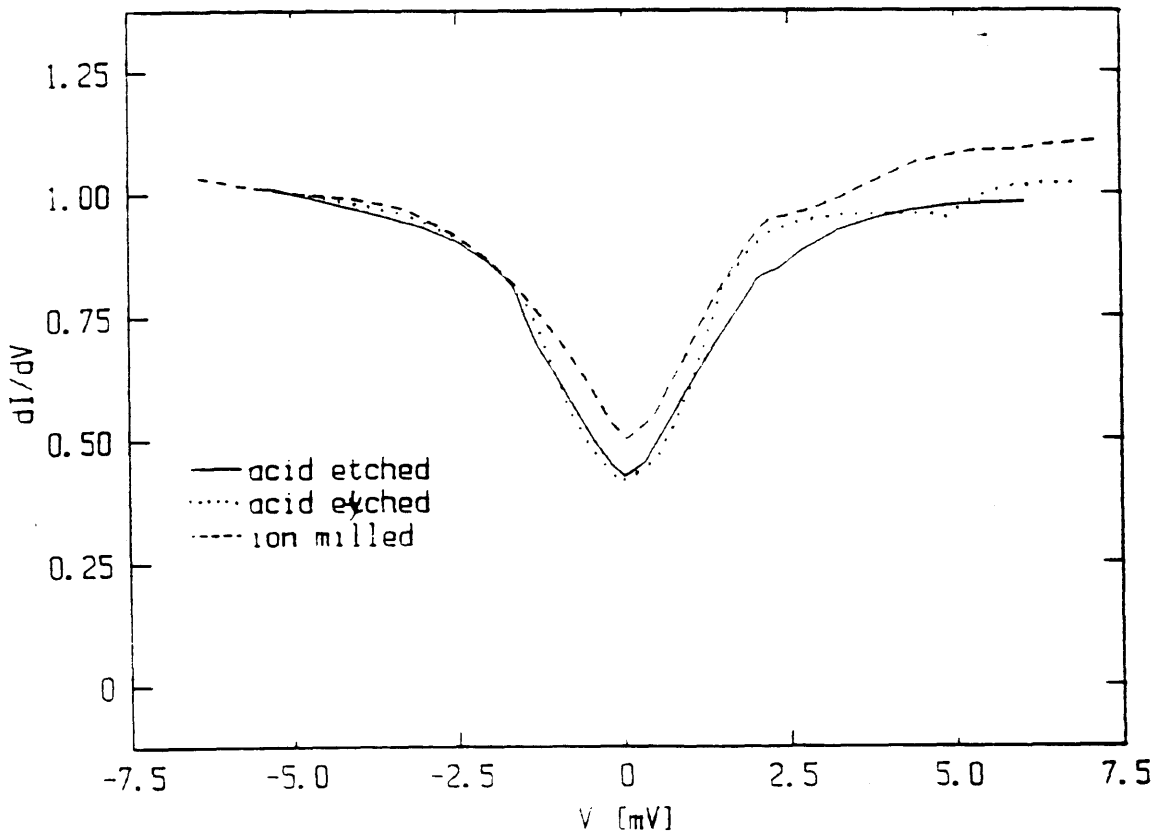

Figure 7-5: Tunneling conductances for acid etched and ion-milled surfaces with Au counter-electrodes at 1.35K. The horizontal axis is V(NCCO)-V(Au).

7.4 Work on $Nd_{1.85}Ce_{.15}CuO_{4-\delta}$

7.4.1 c-axis oriented films

As mentioned earlier, the bad surface found on vacuum annealed films made it very difficult to even make good contacts on the samples. Our first tunneling results were thus very irreproducible. Progress was made with the use of the surface treatments described above. Figure 7-5 shows the differential conductance (dI/dV) as a function of junction bias at low temperature(1.35K) for two contacts made with the two different methods described above.

We used a film with a resistive transition temperature of 8K; but films with higher T_c studied subsequently showed similar structure (whic means that either the stucture is not related to the gap, or that films with low resistive T_c have regions

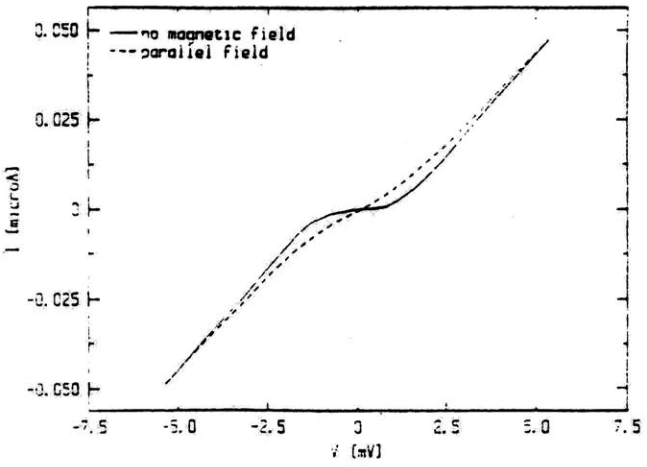

Figure 7-6: $I(V)$ for a Pb contact on an acid etched film, with and without magnetic field.

with higher T_c that can be seen by tunneling). Despite the different nature of the barrier (revealed through the temperature dependence of the junction resistance[46]), the tunneling curves look very similar. The region of low conductance near zero bias starts appearing at the superconducting transition of the film. As the temperature is lowered, this dip in the dI/dV becomes deeper, but the width seems to be constant and close to 5mV. We believe that this is an indication of a superconducting gap of about 2.5mV. A NdCeCuO film with a metallic R(T) but without superconducting transition (because of the oxygen doping) was studied in the same way. In this case, there was no dip in the dI/dV even at 1.35K. To establish that the current at 1.35K is due mostly to elastic tunneling, we prepared a Pb counter-electrode on top of the same film after cleaning the surface with acetic acid. Fig. 7-6 shows the $I(V)$ of this junction with and without magnetic field. When the Pb is superconducting, the curve has a very strong non-linearity around zero bias. The slope at 0mV is 10 times smaller than the slope at 2.5mV, and this is directly related to the depth of the dip in the dI/dV. When the Pb electrode is driven normal by an applied parallel field of 2T, the curve changes dramatically. In fact, the derivative of the curve in magnetic field is very similar to the curves obtained with Au contacts. The comparison of the two curves is a convincing indication of quasiparticle tunneling being the major mechanism of current transfer between the film and the counter-electrode.

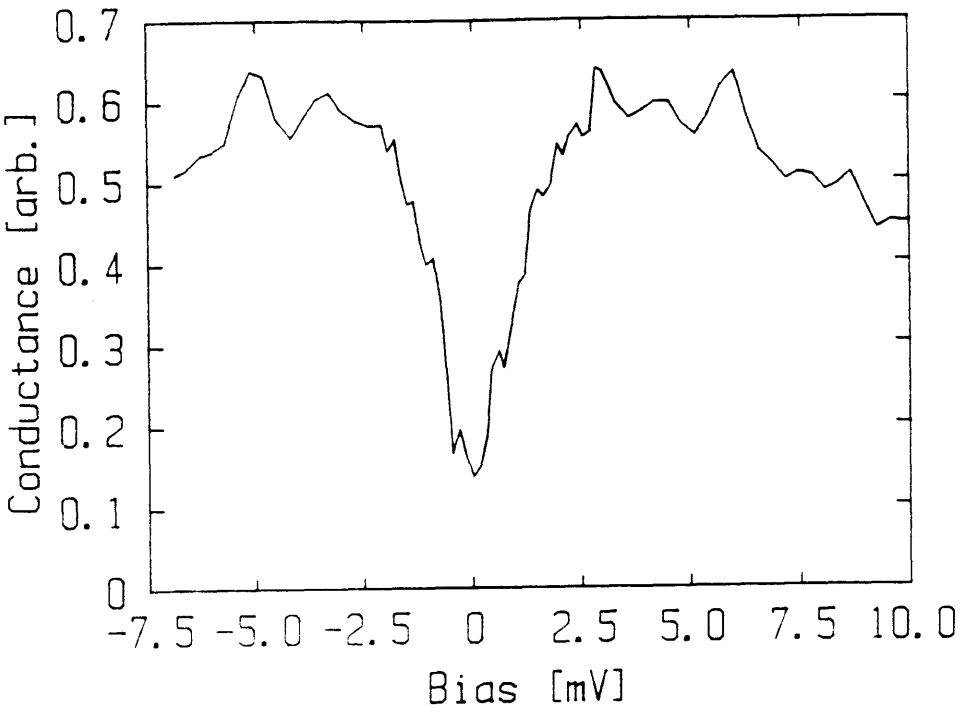

Figure 7-7: dI/dV at .5K of an artificial grain-boundary of $Nd_{1.85}Ce_{.15}CuO_{4-\delta}$. We used a bi-crystal with 25° misorientation.

7.4.2 Work on bi-crystals

The idea of using an artifial bi-crystal substrate to produce an artificial grain-boundary in the film was initially used by P.Chaudhari to find the dependence of the critical current of this artificial weak link on the grain misalignment. One simply sinters together two pieces of $SrTiO_3$ with a controlled misorientation. For films of $Nd_{1.85}Ce_{.15}CuO_{4-\delta}$ deposited on such substrates, it was found that the critical current rapidly went to zero as a function of grain misalignment. Misorientation angles higher than 10° produced no detectable Josephson current. Our current interpretation of this phenomenon is that the oxygen leaves the grain boundary region more easily with higher misorientation, resulting in faster loss and stronger barriers and suppression of the Josephson current. But this might produce just the right kind of barrier for quasiparticle tunneling. We thus looked more carefully at the differential conductance of a 25° misoriented grain-boundary, shown in Figure 7-7.

Again, one sees some broad structure in the region around 5mV (note that 2Δ for

a BCS superconductor of this T_c is 5.6mV). A perpendicular magnetic field of a few T broadens this structure even more, filling in the "gap".

The technique of using bi-crystals to make tunnel structures in the direction of the planes appears to be very promising. The difficulty of obtaining the bi-crystals has limited our experiments to the one shown here so far, but more work is planned in the future.

A vary recent report on TlCaBaCuO step-edge Josephson junctions[55] reports the observation of quasiparticle tunneling through a grain boundary.

7.4.3 Conclusions

The results on $Nd_{1.85}Ce_{.15}CuO_{4-\delta}$ suggest that there is a broad "gap" structure between 3 and 5mV, which is quite reproducible. We feel much less confident about calling this the energy gap than in the case of BSCCO, because of the absence of a clear peak structure that normally follows the gap. We feel, especially in view of the point-contact results[98], that this is still a surface quality problem, made worse by the short coherence length in the c-axis direction. The use of artificial bi-crystal structures taking advantage of the longer in-plan coherence length looks quite promising, but this is only based on one experiment so far. More work is required, but the rewards of a good junction are worth the effort.

Chapter 8

Conclusion

We will now recapitulate the main findings described in the previous chapters.

We have systematically studied the influence of various deposition parameters (such as temperature, reactive environment, nature of substrate) on the quality of thin films of $Nd_{1.85}Ce_{.15}CuO_{4-\delta}$ prepared by laser ablation. We succeeded in considerably improving the quality of our films by using a more reactive N_2O ambient during the deposition. This allows us to reproducibly obtain samples with T_cs of the order of 20K. To our knowledge, no other groups have obtained samples of this quality by a purely in-situ method.

The study of oxygen rich, non-superconducting samples has revealed the importance of weak localization phenomena in the normal state. The experimental observations (temperature and field dependence) point to the strongly two-dimensional character of the conduction in this compound. The fit to the theory has allowed us to extract the value of the inelastic scattering time at low temperatures (4.2K and below), $\tau_i \approx$ 10ps. It was also found that the spin-orbit scattering is weak. The temperature dependence of τ_i is linear down to about 10K, below which it varies more slowly. It is also found that the magnitude of the measured correction to the conductance in fields is about a factor four smaller than what one would expect from the theory. Possible explanations are the inadequacy of the perturbation theory used, the role of interlayer tunneling, or a partial cancellation by a positive term due to fluctuations; but the observation of a similar effect in the fits to fluctuation theory

suggests that the effect might simply be due to sample imperfections.

In the superconducting samples, conductance fluctuations above T_c are observed. Their field and temperature dependence are fitted by the Aslamazov-Larkin and the Maki-Thompson terms in two dimensions. The parameters used are ξ_{ab}=80Å, and a pair-breaking time $\tau_\Phi = 10^{-13}$s. Again, the field dependence was found to be smaller (by a factor five) than the theoretical prediction. However, the reasonable fit of the temperature dependence of the conductance fluctuations with the theoretical prediction using the parameters extracted from the field dependence is a reassuring sign of the validity of the model. Just below T_c (about 20K), the fluctuation resistance in a perpendicular field is found to follow the linear behavior characteristic of the Aslamazov-Larkin contribution in two dimensions. We can use this behavior to extract the critical field down to about 13K, at which point other effects give the major contribution to the breadth of the transition. In order to extract the critical fields below this temperature, one then has to assume that the Aslamazov-Larkin term will follow the simple theoretical expression with the diffusion constant obtained from the data at higher temperature. Fortunately, the values of H_{c2} obtained in this way are not too sensitive to the value of D chosen. The critical field curve shows an upward curvature close to T_c that cannot be accounted for by the theory, as often observed in conventional superconductors. If one ignores this region, one gets a good fit to the theory of dirty superconductors, and the value of the diffusion constant obtained from the fit is in fair agreement with the value obtained from the fluctuation fits. The value of ξ_{ab}= 64Å inferred from $H_{c2}(0)$ is actually slightly smaller than the value obtained at higher temperature. A model based on a distribution of regions with different degrees of impurities can accout for most of the observations in a qualitative way. The position of the critical field is in the upper part of the H_{c2} curve, going upwards as the temperature is lowered. At 4.2K, it is at about 90% of R_n. One has to be careful about conclusions drawn from field values extracted from the lower part of the curve.

The 2D behavior is seen in both the normal state properties (through weak localization) and the superconducting properties (fluctuations), and this is a remarkable

observation. We have also looked for signs of two-dimensionality in the angular dependence of the upper critical field. The fields available for this experiment (8 T) were not sufficient to saturate the resistance in parallel field. Using a somewhat suspect resistive criterion, we find that the corresponding field follows a narrower angular dependence than the three dimensional theory; however, the interpretation of this experiment is not straightforward. We can at best conclude that the behavior of $Nd_{1.85}Ce_{.15}CuO_{4-\delta}$ lies between that of YBCO (3D) and that of BSCCO (2D).

Tunneling on $Nd_{1.85}Ce_{.15}CuO_{4-\delta}$ has proven difficult. We find reproducible structures at biases of a few mV, but their relation to the gap is not clear. Recent exp[eriments on bi-crystals are promising. A good tunnel junction would allow an independent determination of H_{c2} based on the disappearance of the gap. Our results on BSCCO are more convincing, and yield a reduced gap value of 5.5 ± 0.6 for the two phases with T_cs of 85K and 110K.

How do these observations help us in the understanding of the issue of electron-hole symmetry? It is clear that transport measurements on their own cannot answer these questions, but only provide a basis for comparison with other spectroscopies. Because of the big differences among the hole superconductors (YBCO and BSCCO have very different tunneling behavior, and YBCO is likely to be more three-dimensional than BSCCO), it is furthermore difficult to distinguish fundamental differences from more incidental ones. We have seen that observations of negative magnetoresistance related to weak localization have been made on BSCCO by Fiory *et al.*[25]. The effect is smaller than with $Nd_{1.85}Ce_{.15}CuO_{4-\delta}$, but this can simply mean that in the range of temperatures and fields accessible, and for the samples that one can make, the conditions for the observation of these effects are better in $Nd_{1.85}Ce_{.15}CuO_{4-\delta}$. The same might hold for the measurements on LSCO by Preyer *et al.*[67], where an isotropic negative magnetoresistance is observed: their samples are less metallic, and we have seen that the weak localization effects are not as clean in more insulating samples of $Nd_{1.85}Ce_{.15}CuO_{4-\delta}$. It should be noted that LSCO and BSCCO show logarithmic corrections to the conductance at low temperatures as one goes away from the superconducting compositions. It thus seems that, at this point, one sees

more analogies than differences between hole-doped and electron-doped compounds.

It is clear that many interesting physics questions can still be explored with our $Nd_{1.85}Ce_{.15}CuO_{4-\delta}$ films. The most obvious continuation of the work presented here would be a series of measurements in parallel fields in the new hybrid magnet, whose maximum field of 35T comes close to the Chandrasekhar-Clogston limit of $Nd_{1.85}Ce_{.15}CuO_{4-\delta}$ (35-40T). The low value of spin-orbit scattering found from the weak-localization results suggests a rich behavior in this range of fields. The bi-crystal tunnel junctions should also be further investigated.

Bibliography

[1] E. Abrahams, R. E. Prange, and M. J. Stephen, Physica **55**, 230 (1971).

[2] P. A. van Aken, and W. F. Mueller, Physica C **174**, 63 (1991).

[3] J. W. Allen, C. G. Olsen, M. B. Maple, J. -S. Kang, L. Z. Liu, J. -H. Park, R. O. Anderson, W. P. Ellis, J. T. Markert, Y. Dalichaouch, and R. Liu, Phys. Rev. Lett. **64**, 595 (1990).

[4] M. Von Allmen, J. Appl. Phys. **47**, 5460 (1976).

[5] K. Aoi, R. Meservey and P. M. Tedrow, Phys. Rev. B **9**, 875 (1974).

[6] B. L. Alt'shuler, D. Khmel'nitskii, A. I. Larkin, and P. A. Lee, Phys. Rev. B **22**, 5142 (1980).

[7] B. L. Altshuler, A. G. Aronov, Zh. Eksp. Teor. Fiz. Pis'ma **33**, 515 (1981) [JETP Lett. **33**, 499 (1981)].

[8] N. W. Ashcroft, N. D. Mermin, *Solid State Physics*, Saunders College Philadelphia, PA, 1976, HRW.

[9] L. G. Aslamazov and A. I. Larkin, Phys. Lett. **26A**, 238, (1968); Fiz. Tverd. Tela **10**, 1104(1968) [Sov. Phys. Solid State **10** 875 (1968)].

[10] N. Y. Ayoub, Physica C **165**, 469 (1990).

[11] J. Bardeen, Phys. Rev. Lett. **6**, 57 (1961).

[12] J. Bardeen and J. M. Stephen, Phys. Rev.**140**, A1197 (1965).

[13] P. Berghuis, S. Q. Guo, A. L. F. Van der Sloot, B. Dam, G. M. Stollman and P. H. Kes, Physica C **162-164**, 1169, (1989).

[14] G. Bergmann, Phys. Rep. **107**, 1 (1984).

[15] G. Bergmann, Phys. Rev. B **29**, 6114 (1984).

[16] G. Bergmann, Phys. Rev. B **39**, 11280 (1989).

[17] B. N. Chapman, *Glow discharge processes*, N.Y.Wiley, N.Y., 1980.

[18] T. R. Chien, T. W. Jing, N. P. Ong and Z. Z. Wang, preprint.

[19] J. E. Crow, R. S. Thompson, M. A. Klenin, and A. K. Bhatnagar, Phys. Rev. Lett. **24**, 371 (1970).

[20] D. Dijjkamp, T. Venkatesan, X. D. Wu, S. A. Shaheen, N. Jisrawi, Y. H. Min-Lee, W. L. McLean, and M. Croft, Appl. Phys. Lett. **51**, 619 (1987).

[21] T. Ekino, J. Akimitsu, Phys. Rev. B **40**, 6902 (1989).

[22] T. Ekino, J. Akimitsu, Phys. Rev. B **40**, 7364 (1989).

[23] R. Fastampa, A. Giura, R. Marcon, and E. Silva, Phys. Rev. Lett. **67**, 1795 (1991).

[24] A. T. Fiory, A. Hebard, Phys. Rev. Lett **44**, 291 (1980).

[25] A. T. Fiory, S. Martin, R. M. Fleming, L. F. Schneemeyer,and J. V. Waszczak, Phys. Rev. B **41**, 2627 (1990).

[26] A. Fujimori, Y. Tokura, H. Eisaki, H. Takagi, S. Uchida, and E. Takayama-Muromachi, Phys. Rev. B **42**, 325 (1990).

[27] J. Geerk, G. Linker, O. Meyer, Kernforschungszentrum Karlsruhe, KfK4601 (int. publication).

[28] I. Giaever, Phys. Rev. Lett. **5**, 147 (1960).

[29] G. Gibson, P. M. Tedrow, and R. H. Meservey, Phys. Rev. B **40**, 137 (1989).

[30] R. E. Glover, Phys. Letters **25A**, 542 (1967)

[31] G. Y. Guo, Z. Szolek, and W. M. Temmerman, Physica C **162-164** , 1351 (1989).

[32] M. Gurvitch, J. M. Valles, Jr., A. M. Cucolo, R. C. Dynes, J. P. Garno, L. F. Schneemeyer, and J. V. Waszczak, Phys. Rev. Lett. **63**, 9, (1989).

[33] J. M. Graybeal, Physica **135B**, 113 (1985).

[34] S. J. Hagen, X. Q. Xu, W. Jiang, J. L. Peng, Z. Y. Li, R. L. Greene, Phys. Rev. B, to appear.

[35] Y. Hidaka, M. Suzuki, Nature**338**, 635 (1989).

[36] S. Hikami, A. I. Larkin, and Y. Nagaoka, Prog. Theor. Phys. **63**, 707 (1980).

[37] S. Hikami, and A. I. Larkin, Mod. Phys. Lett. B **2**, 693 (1988).

[38] J. D. Jorgensen *et al.*, Physica B **165-166**, 1509, (1990).

[39] M. Kanai, K. Horiuchi, T. Kawai, and S. Kawai, Appl. Phys. Lett. **57**, 2715 (1990).

[40] R. A. Klemm, A. Luther, and M. R. Beasley, Phys. Rev. B **12**, 877 (1975).

[41] S. Kohiki, J. Kawai, T. Kamada, S. Hayashi, H. Adachi, K. Setsune, and K. Wasa, Physica C **166**, 437 (1990).

[42] A. Gupta, G. Koren, C. C. Tsuei, A. Segmueller, and T. R. McGuire, Appl. Phys. Lett. **55**, 1795 (1989).

[43] G. Koren, A. Gupta, and R. J. Baseman, Appl. Phys. Lett. **54**, 1920 (1989).

[44] S. Kubo, and M. Suzuki, Physica C **185-189**, 1251 (1991).

[45] A. Kussmaul, G. M. Roesler, Jr., and P. M. Tedrow, Phys. Rev. B **41**, 842 (1990).

[46] A. Kussmaul, J. S. Moodera, P. M. Tedrow, A. Gupta, and C. C. Tsuei, IEEE Trans. Mag. **27**, 1325 (1991).

[47] A. Kussmaul, J. S. Moodera, P. M. Tedrow, and A. Gupta, Physica C **177**, 415 (1991).

[48] A. I. Larkin and Y. N. Ovchinnikov, J. Low Temp. Phys. **34**, 409 (1979).

[49] A. I. Larkin, Pis'ma Zh. Exp. Teor. Fiz. **31**, 239 (1980) [JETP Lett. **31**, 219 (1980)].

[50] W. E. Lawrence and S. Doniach in *Proceedings of the Twelvth International Conference on Low Temperature Physics, Kyoto, 1970* , edited by E. Kanda (Keigaku, Tokyo, 1971), p.361.

[51] P. A. Lee and T. V. Ramakrishnan, Rev. Mod. Phys. **57**, 287 (1985).

[52] G. M. Luke, B. J. Sternlieb, Y. J. Uemura, J. H. Brewer, R. Kadono, R. F. Kiefl, S. R. Kreitzman, T. M. Riseman, J. Gopalakrishnan, A. W. Sleight, M. A. Subramanian, S. Uchida, H. Takagi, and Y. Tokura, Nature **338**, 49 (1989).

[53] S. Maekawa and H. Fukuyama, J. Phys. Soc. Jpn. **50**, 2516 (1981).

[54] K. Maki, Prog. Theor. Phys. **40**, 193 (1968).

[55] J. S. Martens, V. M. Hietala, T. E. Zipperian, G. A. Vawter, D. S. Ginley, C. P. Tigges, T. A. Plut, and G. K. G. Hohenwarter, Appl. Phys. Lett. **60**, 1013 (1992).

[56] S. Massidda, N. Hamada, J. Yu, and A. J. Freemen, Physica C **157**, 571 (1989).

[57] W. L. McMillan, and J. M. Rowell, Phys. Rev. Lett. **14**, 108 (1965).

[58] T. Matsumoto, T. Kawai, K. Kitahama, and S. Kawai, preprint.

[59] J. S. Moodera, P. M. Tedrow, and J. E. Tkaczyk, Phys.Rev.B **36**, 8329 (1987).

[60] MRS Bulletin **XVII**, 2, 30(1992).

[61] H. Mueller-Buschbaum, Angew. Chem. Int. Ed. Eng. **16**, 674 (1977).

[62] M. J. Naughton, R. C. Yu, P. K. Davies, J. E. Fisher, R. V. Chamberlin, Z. Z. Wang, T. W. Jing, N. P. Ong and P. M. Chaikin, Phys. Rev. B **38**, 9280 (1988).

[63] W. J. Chu, J. W. Mayer, and M. -A. Nicolet, Backscattering Spectrometry, (Academic Press, New York, 1976).

[64] N. S. Nogar, R. C. Dye, R. C. Estler, S. R. Foltyn, R. E. Muenchausen, and X. D. Wu, in *Proceedings of Laser Ablation Workshop*, Oak Ridge, (1990), to be published.

[65] C. E. Otis and R. W Dreyfus, Phys. Rev. Lett. **67**, 2102 (1991).

[66] J. L. Peng, Z. Y. Li, and R. L. Greene, Physica C **177**, 79 (1991).

[67] N. W. Preyer, M. A. Kastner, C. Y. Chen, R. J. Birgeneau and Y. Hidaka, Phys. Rev. B **44**, 407 (1991).

[68] P. A. Saunders, J. F. Ziegler, Nucl. Inst. Meth. Phys. Res. **218**, 67 (1983).

[69] W. Sadowski, M. Affronte, M. Francois, E. Koller, and E. Walker, J. of Less Comm. Met. **164-165**, 824 (1990).

[70] Y. Sakisaka, T. Maruyama, Y. Morikawa, H. Kato, K. Edamoto, M. Okusawa, Y. Aiura, H. Yanashima, T. Terashima, Y. Bando, K. Iijima, K. Yamamoto, and K. Hirata, Phys. Rev. B **42**, 4189 (1990).

[71] H. Sawa, S. Suzuki, M. Watanabe, J. Akimitsu,H. Matsubara, H. Watabe, S. Uchida, K. Kokusho, H. Asano, I. Izumi, and E. Takayama-Muromachi Nature **337**, 347 (1989).

[72] R. Singh and J. Narayan, Phys. Rev. B **41**, 8843 (1990).

[73] H. M. Smith and A. F. Turner, Appl. Opt. **4**, 147 (1965).

[74] Sneed-Brasted, *Comprehensive Inorganic Chemistry* **V**, D. Van Nostrand Co., Inc., Princeton, N.J., 1956.

[75] L. Solymar, Superconductive Tunnelling and Applications, Wiley Interscience, 1972.

[76] R. Stratton, J. Phys. Chem. Solids **23**, 1177 (1962).

[77] S. Sugai, Y. Hidaka, Phys. Rev. B **44**, 2 (1991).

[78] M. Suzuki, amd M. Hikita, Phys. Rev. B **44**, 249 (1991).

[79] S. Tanda, M. Honma, and T. Nakayama, Phys. Rev. B **43**, 8725 (1991).

[80] I. Takeuchi, J. S. Tsai, T. Manako, and Y. Kubo, Phys. Rev. B **40**, 9286 (1989).

[81] P. M. Tedrow, and R. H. Meservey, Phys. Rev. Lett. **27**, 919 (1971).

[82] P. M. Tedrow, R. H. Meservey, Phys. Rev. B **8**, 5098 (1973).

[83] P. M. Tedrow, and R. H. Meservey, Phys. Rev. B. **25**, 171 (1982).

[84] P. M. Tedrow, J. T. Kucera, D. Rainer, T. P. Orlando, Phys. Rev. Lett. **52**, 1637 (1984).

[85] P. M. Tedrow, private communication.

[86] M. Tinkham, Phys. Rev. **129**, 2413 (1963).

[87] M.Tinkham, Phys.Rev.Lett. **61**, 1658 (1988).

[88] R. S. Thompson, Phys. Rev. B**1**,327(1970).

[89] Y. Tokura, H. Takagi, and S. Uchida, Nature **337**, 345 (1989).

[90] J. M. Tranquada, S. M. Heald, A. R. Moodenbaugh, G. Liang, and M. Croft, Nature **337**, 720 (1989).

[91] C. C. Tsuei, Physica C **161**, 415 (1989).

[92] R. P. Vasquez, A. Gupta, and A. Kussmaul, Sol. St. Comm. **78**, 303 (1991).

[93] G. F. Virshup, M. E. Klausmeier-Brown, I. Bozovic andJ. N .Eckstein, preprint.

[94] N. R. Werthamer, E. Helfand, and P. C. Hohenberg, Phys. Rev.**147**, 295 (1966).

[95] E. L. Wolf, *Principles of Electron Tunneling Spectroscopy*, Oxford University Press, 1985.

[96] S. Yang, P. Wu, Z. Ji, Z. Sun, R. Zhang, Y. Li, S. Zhang, H. Zhang, H. Liu, J. Appl. Phys. **68**, 2308 (1990).

[97] N. C. Yeh, Phys. Rev. B**45**, 5710, (1992).

[98] J. F. Zasadzinski, N. Tralshawala, Q. Huang, K. E. Gray, and D. G. Hinks, IEEE Trans.Magn.**27**, 833 (1990).